SYNTHESIS, CHARACTERISATION AND CATALYTIC PROPERTIES OF SELECTED MESOPOROUS SOLIDS

A THESIS

submitted by

CHALLAPALLI SUBRAHMANYAM

for the award of the degree

of

DOCTOR OF PHILOSOPHY

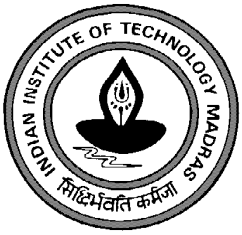

DEPARTMENT OF CHEMISTRY

INDIAN INSTITUTE OF TECHNOLOGY MADRAS

CHENNAI-600 036

MARCH 2003

TABLE OF CONTENTS

Page

Figure captions

Chapter 1

Schemes

Abbreviations

BET	: Brunauer-Emmett-Teller
BJH	: Barrett-Joyner-Halenda
Calc.	: Calcined
Conv.	: Conversion
CTAB	: Cetyltrimethylammonium bromide
IR	: Infrared spectroscopy
CG-MS	: Gas chromatography- Mass spectroscopy
ICPAES	: Inductively coupled plasma atomic emission spectroscopy
EPR	: Electron paramagnetic resonance
SAPO	: Silicoaluminophosphate
SEM	: Scanning electron microscopy
TEOS	: Tetraethylorthosilicate
TGA	: Thermogravimetric analysis
TEM	: Transmission electron microscopy
TMAOH	: Tetramethylammonium hydroxide
TPD	: Temperature programmed desorption
TPR	: Temperature programmed reduction
XRD	: X-ray diffraction
XPS	: X-ray photoelectron spectroscopy

Notations

Å	: Angstrom
θ	: Bragg angle
λ	: Wave number
g	: Grame
h	: hour
K	: Degree Kelvin
R	: Gas constant
T	: Temperature
p_o	: Saturated vapour pressure
v	: Volume
A	: Absorbance
kJ	: Kilo Joule

List of Publications

Referred Journals

(1). **Ch. Subrahmayam, B. Viswanathan and T.K. Varadarajan (2000)** Mesoporous architecture of solids-How are they designed and exploited ?, Bull. Cat. Soc. Ind., 10(6) 1-24

(2). **Ch. Subrahmanyam, B. Louis, B. Viswanathan, A. Renken and T.K. Varadarajan** (2001) Hydroxylation of phenol over transition metal substituted MCM-48, Eurasian Chem Tech journal 3, 59-63

(3). **Ch. Subrahmanyam, B. Louis, F. Rainone, B. Viswanathan, A. Renken and T.K. Varadarajan** (2002) Partial oxidation of toluene by molecular oxygen over mesoporous Cr- AlPO, Catal. Commun., 3 , 45-50

(4). **B. Louis, Ch. Subrahmanyam, L. Kiwi-Minsker, B. Viswanathan, P.A. Buffet. and A. Renken (2002)** Synthesis and characterization of MCM-41 coatings on stainless steel grids, Catal. Commun., 3 , 159-163

(5). **Ch. Subrahmayam, B. Viswanathan and T.K. Varadarajan** (2002), Mesoporous Cr-AlPO- A selective catalyst for oxidation of side chain aromatic substrates, Bull. Catal. Soc. Ind., **1**, 52-57

(6). **Ch. Subrahmanyam, B. Louis, B. Viswanathan, A. Renken and T.K. Varadarajan** Catalytic oxidation of toluene with molecular oxygen over Cr-substituted mesoporous materials, Appl. Catal.A: General, **241**, 205-215.

(7). **Ch. Subrahmanyam, B. Viswanathan and T.K. Varadarajan** Mesoporous V-AlPO- New partial oxidation catalyst, Eurasian ChemTech Journal, 4, 169-173.

(8) **Ch. Subrahmanyam, B. Louis, B. Viswanathan, A. Renken and T.K. Varadarajan** Synthesis, Characterization and catalytic properties of vanadium substituted mesoporous aluminophosphates, Micro.Meso.Mater., (Under revision)

(9). **Ch. Subrahmanyam, B. Louis, B. Viswanathan, A. Renken and T.K. Varadarajan ,** Synthesis and characterization of MCM-48 coatings on stainless steel grids (to be communicated)

(10) **Ch. Subrahmayam, B. Viswanathan and T.K. Varadarajan**, Aerial oxidation of cyclohexane over mesoporous Fe-AlPO (To be communicated)

Papers Accepted/Presented in sympoisa/conferences

1. **Subrahmanaym Challapalli, B. Viswanathan and T.K. Varadarajan** Alkylation of naphthalene with n-butanol over MCM-48, presented in National Seminar Trends in Industrial Catalysis, September 10-11,1999, IPCL India.

P.S. Received best poster presentation award for the above presentation

2. **Subrahmayam Challapalli, B. Viswanathan and T.K. Varadarajan**, Alkylation of naphthalene by alcohols over mesoporous MCM-48, presented in

National Work shop on catalysis, Forays in to Non-traditional areas, Jan 7-8th 2000, IICT Hyderabad

3. **Subrahmanyam Challapalli, S. Shanmugam, B. Viswanathan and T.K. Varadarajan** , Synthesis and characterization of transition metal incorporated MCM-48, presented in CATSYMP-15 & IPCAT-2, Jan 23-25th 2001, pune, India.
4. **B. Viswanathan, Ch. Subrahmanyam and T.K. Varadarajan** , Mesoporous solids- a new generation catalysts , presented in Singapore International Chemical Conference-II, Dec. 18-20th 2001, Singapore.
5. **Ch. Subrahmanyam, B. Louis , B. Viswanathan, A. Renken and T.K. Varadarajan,** preparation and characterization of MCM-48 on stainless steel grids for possible industrial applications, presented in National workshop on catalysis (Catwork-2002), March 8-10th 2002, Gauwhati, India.
6. **Ch. Subrahmanyam, B. Louis , B. Viswanathan, A. Renken and T.K. Varadarajan**, Liquid Phase Oxidation of Ethyl benzene and Benzyl alcohol over mesoporous CrAlPO, Accepted for the presentation in 3rd International Mesostructured Materials Symposium (IMMS 2002) July 8-11 2002, Jeju, Korea.
7. **Ch. Subrahmanyam, B. Viswanathan and T.K. Varadarajan ,** Aerial oxidation of cyclohexane over mesoporous Fe-AlPO, to be presented in IPCAT-3 & TSCRE-2003 to be held at Taipai, Taiwan, 15-17th June, 2003.

Curriculum Vitae

Name	: Subrahmanyam Challapalli
Place of Birth	: Vijayawada, Andhra Pradesh
Education	
B.Sc.(Mathematics, Physics and Chemistry)	
(1993-1996)	: S.R.R & C.V.R Govt. college, Vijayawada
M..Sc (chemistry)	
1996-1998	: Andhra University, Visakhapatnam
Ph.D (Chemistry)	: Indian Institute of Technology-Madras

Abstract

Key words: Mesoporous solids, MCM-48, AlPOs, Alkylation, Oxidation, MCM Coatings and Mesoporous Titania.

The syntheses of mesoporous zeolitic materials of the type MCM-48 and AlPO with incorporation of heteroatoms in the framework have been carried out using CTAB as structure-directing agent under hydrothermal conditions. All the materials synthesized in the present study were found to have mesoporous texture with an average pore size of 28 Å. The acidity of Al or Fe incorporated system was found to be less compared to the conventional zeolites. However, these systems can be suitably employed for reactions where moderate acidity is the driving force for the formation of products. For example, alkylation of naphthalene with alcohols over mesoporous MCM-48 results in monoalkylated naphthalenes. In a similar manner, transition metal incorporated MCM-48s have been examined for phenol oxidation and the results indicate that Ti-incorporated system shows higher activity and selectivity for diphenol formation. A relatively easier approach to synthesize mesoporous aluminophosphates has been achieved and transition elements like V, Cr and Fe have been incorporated into the framework. Various physico-chemical studies confirmed the formation of mesophase as well as the presence of heteroatom within the framework of mesoporous aluminophosphates. Even though the thermal stability of aluminophosphates is less when compared to that of aluminosilicate analogous materials, aluminophosphates exhibit higher activity for the selective side chain oxidation of aromatics like toluene, ethylbenzene and benzyl alcohol. It has been established that less expensive and readily available oxidants like molecular oxygen/air can also be employed as an oxidizing agent

for the oxidation of toluene and cyclohexane. The observed activity of these systems can be attributed to the site isolation of the desecrate redox centers. Mesoporous solids have been successfully supported on unconventional supports like stainless steel, which probably eliminate the mass transfer limitations experienced in actual industrial processes. The successful synthesis of thermally stable titania has also been carried out using CTAB as template.

It is with pleasure, I express my deep sense of gratitude to **Prof. T.K. Varadarajan** for his advice, suggestions, thought provoking discussions and constant encouragement thought out the course of this investigation. He is really a sense of my guide, philosopher and more than a friend. Also I profusely thank him for the opportunity that he gave me to work with him. I deem it a binding obligation on my part to extend my boundless tributes of gratitude and warmth of affection to him. He kept his cool and his valuable suggestions really helped me to complete this task in an easier manner.

I am also beholden to **Prof. B. Viswanathan**, for his enlightening discussions and unfailing guidance at every stage of the research programme. I am really grateful to him for introducing the quintessence of science. I sincerely thank him for orienting me into a logical line of thinking and rationalizing during the course of present investigation. He demonstrated to us how easily one could handle the problems. The way in which he correlates science to the daily life through simple and lively examples is very impressive. He is like an ocean of science; one can get benefited up to his capacity.

I also express my thanks to **Prof. M.S. Gopinathan** (former Head, Chemistry Department) and **Head, RSIC** for providing all necessary infrastructural facilities during my research tenure.

I am also thankful to **Prof. Albert Renken**, EPFL, Switzerland for accommodating me for a short period in his group that really helped me carry out part of my thesis work. At the same time I would like to express my sincere thanks to **Dr. Kiwi-Minsker**, for constructive criticism, which really gave a chance to carryout some interesting research at EPFL.

I sincerely thank **Prof. U.V. Varadaraju, Dr. K. Vidyasagar, Dr. M.S. Subramanian, Dr. R.P. Viswanath, Prof. S. Vancheesan, Prof. G. Rangarao, Prof. D.V. Ramana, Prof. K.K. Balasubramanian, Prof. N. Balasubramanian, Prof. DVS. Murthy and Prof. M.S. Ananth** for their suggestions at every stage of research I would to express my sincere gratitude to **Mr. A. Narayanan, Mr. Ramkumar and Mr. Balgunan, Mr.**

Suryaprgasan, Mr. Sivaramakrishanan and Mrs. Bhavani Kumar, Mr. Mohan for their help at various stages of my research.

It is indeed great pleasure to have been associated with **Mr. Shanmugam, Mr. R. Ganesan, Mr. Kishore and Mr. Chidambaram**, who have been very cooperative to me all the time and helped me throughout my doctoral programme.

My heartfelt thanks go to **Dr. Benoit Louis**, who has been very co-operative ever since he visited our labs and also at EPFL. I must appreciate his encouragement. Also **Dr. Fabio Rainone**, who helped me to carryout reactions at EPFL, Switzerland.

Thanks are also due to 1998-99 batch mates, especially, **Dr. Ramakrishan, Dr. Patra, Mr. Sudhakar, Mr. Raja, Mr. Vijayakrishna, Mr. Angappan and Mr. Mani** who made my stay memorable in IIT Madras. I also wish to express my sincere thanks to my colleagues **Mr. Shankaran, Mr. Sathish, Mr. Meialagan, (Mrs) Dr. Bindu, Dr. Aulice, Mrs. Chandra, Mr. Murugan, Mr. Suresh, Mr. Navalidian, Mr. R. Jothiramalingam, Miss. Poonkodi and also Mr. Brajagopal Mishra, Mr. Vijayashankar, Alok and Rashmi** for their friendly behavior.

I would like to place my sincere thanks on record to my senior lab mates, **Dr. Basab, Dr. Rajesh, Dr. Raghuveer, Dr. Rana, Dr. Srinivasan, Dr. Babu, Dr. Sahoo, Dr. Krishnan, Dr. Kanmani, Dr. Sobhanababu, Dr. Manivannan, Dr. Prabhakarn, Dr. Jayaprakesh, Dr. Srinivasan and Dr. Jesuduri** for their timely help and encouragement.

I am also thankful to **Mr. Ramprasad, Mr. Ramana, Mr. Himakumar, Mr. Venkat, Mr. Indraneel, Mr. Prabhkararao, Mr. P.S. Kishore and Mr. Krishan** for their friendly manner.

I wish to convey my sincere gratitude to **Dr. Suja, Dr. MRK Prasad, Dr. Subba Rao and Dr. Radhakrishanan** of IICT for their timely help in characterizing the

samples. I also thank the timely help offered by **Mr. Viswanath, Mr. Srikanth, Mr. Vijay, Mr. Ravi and Mr. Phan**i for their co-operation and timely help.

Finally I am extremely grateful to my Parents whose unfailing courage and counsel nurtured and motivated me to pursue this research, especially my **Mother**, who didn't remain in this world to see the fruition of my efforts. I am more than indebted to my elder brother, **Mr. Ramakrisha**, whose sacrificial love and affection made me to stand at this juncture. Though he is my elder brother, he is more than every thing to me. I also owe a deep sense of thanks to my sister-in-law, **Mrs. Padma Ramakrishana** and younger brother **Mr. Srinivas** for their boundless and unconditional support throughout my doctoral programme.

Last but not the least, I bow my head in front of the **Almighty** for providing such an opportunity to work in science.

Finally, I apologize for the omissions I made in my attempt to enumerate those who have contributed.

Subrahmanyam Challapalli

CHAPTER 1

INTRODUCTION

1.1 INTRODUCTION TO ZEOLITES

Heterogeneous catalysis plays a dominant role in the production of fine chemicals as well as in petroleum refining. Hydroprocessing catalysts of the type used in the refining processes are dual function catalysts, where hydrogenation reaction takes place at the impregnated metal centers and hydrogenolysis reaction at the acid sites (Holderich et al., 1991). The acidity function can be provided either by alumina, zeolites or amorphous aluminosilicates, which are the catalyst supports generally used. A proper channel geometry combined with high surface area is the prerequisite for an acidic catalyst so that the catalyst can provide appropriate sites for the desired activity and selectivity (Breck, 1974). Site accessibility of a catalyst is controlled by pore size, based on which porous solid materials are classified as a function of pore diameter in the following way: microporous materials ($d < 20$ Å), mesoporous materials ($20 < d < 500$ Å) and macroporous materials ($d > 500$ Å). Construction of a porous solid not only involves chemical synthetic techniques for tailoring microscopic properties such as pore size, channel shape, pore connectivity and pore surface reactivity, but also materials processing techniques such as tailoring the channels which are of molecular dimensions. Zeolites are termed as molecular sieves (Holderich et al., 1991) because they can selectively sieve the substrates.

1.2 STRUCTURAL BUILDING UNITS

The structure of the zeolite is composed of finite tetrahedral units TO_4 (T= Si or Al) (Behrens et al., 1993; Davis, 1991). These units are called secondary building units (SBU), the primary unit being the TO_4 individual tetrahedron (Szostak, 1989). At present, it is possible to visualize all possible existing structures of zeolites with nine such building units; these are given in Fig. 1.1. Zeolites are often classified on the basis of the SBU, as small pore zeolites with 8 membered rings like MTN, NU-l; medium pore zeolites, MFI, MEL; large pore zeolites FAU, MTW and extra large pore zeolites-UDT (Meir et al., 1992). When AI^{3+} substitutes Si^{4+} one excess negative charge per aluminium atom is introduced. This negative charge can be compensated either by a proton or extra framework cation, which is exchangeable that makes zeolites as ion-exchangers. If the charge compensation occurs through proton, Bronsted acidity results that make zeolites suitable for acid catalyzed reactions. Moreover, incorporation of aluminium also results in the generation of Lewis acidity (Jacobs et al., 1974; Ward, 1970; Davis et al., 1988)

1.3 CLASSIFICATION OF ZEOLITES

Compositional variation of zeolites (silicon to aluminium ratio) can be used to classify zeolites into low silica and high silica zeolites. Typical examples of low silica zeolites are A, X and Y. These zeolites cannot be synthesized over a wide range of silicon to aluminium ratio. On the contrary, high silica zeolites can be synthesized over a wide range of silica to alumina ratio, a classical example being ZSM-5, whose acidity can be tuned to desired level.

1.4 ZEOLITES AS CATALYSTS

Based on the applications, molecular sieves are suitably modified chemically or structurally or in both ways. Of the various ways, chemical treatment, hydrothermal treatment, chemical vapour deposition and selective coking are the well known ones. Molecular sieves are also modified by varying the composition. In zeolites the compositional variation can be achieved by varying the Si/Al ratio or the extent of exchange of cations. Another method that is of immense importance is variation by isomorphous substitution. The replacement of Si in a purely siliceous molecular sieve by statistically compatible element is termed as isomorphous substitution. Isomorphous substitution of various hetero elements like Al, B, Ga, Ti and Fe have been carried out on various molecular sieves and the resulting systems are promising catalysts for various selective reactions (Perego et al., 1986; Szostak, 1989; Corma, 1997; Arneds et al., 1997). Isomorphous substitution in general will be carried out either to generate acidic or redox properties with in the catalytic system.

Zeolites have been explored as industrial catalysts in petrochemical and fine chemical industries. In most of these cases, the catalytic activity is due to their acidic nature. This has been in general achieved by isomorphous substitution where tetrahedral silicon will be replaced by a heteroatom. In the case of zeolites this heteroatom will be in general aluminium (Holderich et al., 1991). With the substitution of one aluminium in silicon network, a unit negative charge will be generated. In general this negative charge will be compensated by sodium ions, which are present in the synthetic gel. However, ion-exchanging these sodium ions with ammonium ions followed by high temperature calcinations, one can generate acidic properties in the catalyst.

Zeolites are used in a host of acid catalyzed reactions such as alkylation and acylation. The active sites in zeolites are mainly Bronsted acid sites and to some extent the Lewis acid sites. Lewis acidity is formed as a result of trigonally co-ordinated aluminium ions in tetrahedral lattice. Among various zeolites, faujasite, mordenite and ZSM-5 type zeolites are widely used as catalysts. The faujasite type zeolite, namely zeolite- Y has been mainly used for the fluid catalytic cracking and hydrocracking reactions. Mordenite is used in isomerization of light alkenes for octane enhancement of gasoline. ZSM-5 is used widely for the production of fine chemicals. A large variety of organic reactions such as isomerization, rearrangement, alkylation and acylation have been studied and in all these cases, ZSM-5 has been exploited as a potential catalyst.

1.5 ALUMINOPHOSPHATES

Microporous aluminophosphates form another class of microporous solids, which has received considerable attention. These molecular sieves were first reported in 1982 by researchers of Union Carbide company (Wilson et al., 1982; Wilson, 1991). Neutral frameworks of these molecular sieves are composed of corner connected AlO_4 and PO_4 tetrahedra (Flanigen, 2001; Ashtekar et al., 1994). The structures of these materials are to some extent similar to those of zeolites. They possess high thermal stability as well as high sorption capacities. Aluminosilicates and aluminophosphates form two different classes of microporous solids and a representation of the microporous aluminophosphates is given in Fig. 1.2. Catalytic activity in these materials can be generated in a similar way as in zeolties. Flanigen et al. (1986) have incorporated various transition elements into the framework of these molecular sieves and the resulting systems have been shown to be of great importance in catalysis.

Today's environmental concerns demand the need for alternate catalytic processes for the production of fine chemicals in an environmentally friendly manner. For the production of fine chemicals, at present hazardous chemicals like sulphuric acid, phosphoric acid have been employed. The problem associated with these chemicals is handling in addition to the environmental pollution. By using transition metal ion incorporated molecular sieves, it has been made possible to overcome these problems to a certain extent.

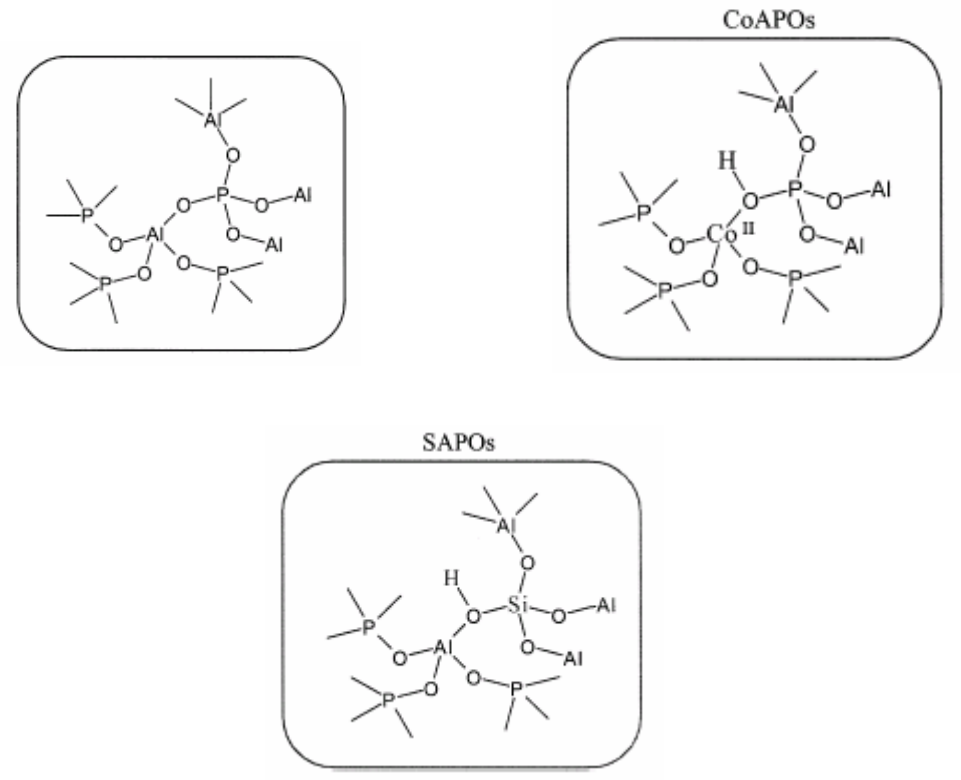

Fig. 1.2. Representation of aluminophosphates

Catalytic oxidation processes play an important role in the conversion of hydrocarbons to a variety of industrially useful fine chemicals. Among the various catalysts employed, solid catalysts such as zeolites have an edge over other systems due to their recyclable

nature, easy recovery and amenable to continuous processing compared to the homogeneous counterparts. Transition metal incorporated zeolite systems show better catalytic activity for the oxidation of various hydrocarbons (Kumar et al., 1995). In this regard Ti substituted zeolites with MFI structure (TS-l) show remarkable activity for various oxidation reactions under mild oxidation conditions, which are given in Fig.l.3. Likewise, transition metal ion incorporated aluminophosphates form another class of molecular sieves, which have received attention because of their potential applications in catalysis. Chromium substituted microporous aluminophosphate is shown in Fig. 1.4, which has been used for various selective reactions with 70 % TBHP as oxidizing agent (Sheldon, 1996). The multi- functional enhanced catalytic activity is thought of on the following lines (Chakraborty, 1998):

1. Confinement of the redox metal site in microenvironments of zeolite framework, which may mimic enzyme catalysis
2. Site isolation of the metal centers prevents the deactivation by di-/oligomerization
3. Incorporated metals are found to be stable and are not leaching out
4. Possibility of shape selective catalysis, because of well-defined channels
5. These systems will promote the oxidation reactions under mild oxidizing conditions.

1.6 ISOMORPHOUS SUBSTITUTION

Since these molecular sieves are neutral in synthesized form, there must be a suitable way to generate catalytic properties within these materials. This, in general, has been

achieved by isomorphous substitution. However, the following points have to be considered for an effective substitution (Szostak, 1989).

1. Substitution of A by B is governed by their radius ratio. Closer the difference between their radius values, greater is the extent of isomorphous substitution.

2. The ability of the ion to form tetrahedral oxide ion coordination decides the possibility of isomorphous substitution in molecular sieves.

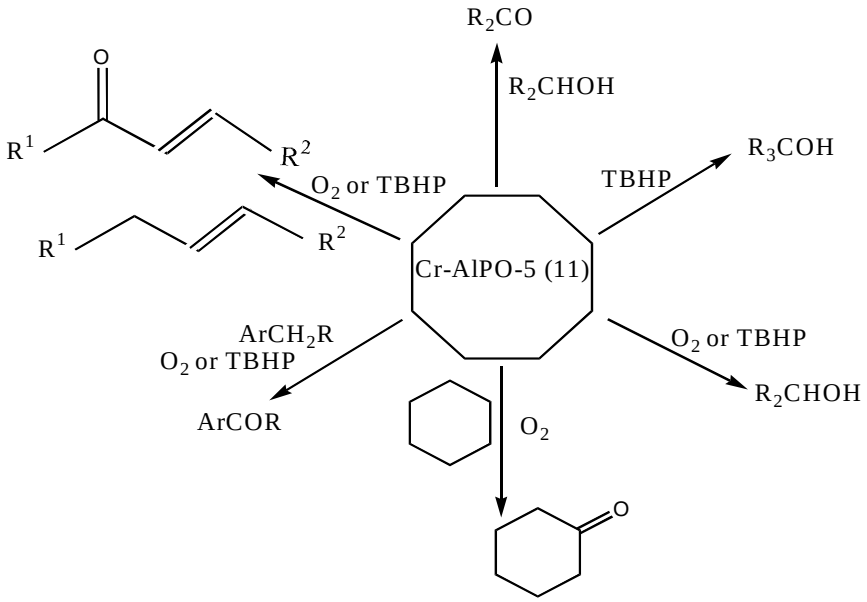

Fig. 1.4. Catalytic activity of Cr-$AlPO_4$ with 70 % TBHP

3. The ratios of electro negativities and ionization potentials of the ions A and B also limit isomorphous substitution.

However, it is important to note that ionic charge is not a deciding factor for the feasibility of isomorphous substitution. It only decides the overall framework charge of the molecular sieve. The ionic radii of some of the elements reported to have isomorphously substituted in the silicate matrix are given in Table 1.1

When titanium ion was isomorphously substituted in place of silica, the resulting catalyst, TS-1, exhibits remarkable activity for various selective reactions in mild conditions. In spite of the enhanced activity, TS-l suffers from certain drawbacks due to its pore opening, which is 5.5 Å. However, the success of TS-l stimulated the synthesis of other Ti-substituted molecular sieves. In this regard TS-2, catalyst having MEL topology was synthesized and its catalytic activity was examined. Incorporation of titanium into the uni-dimensional medium pore high silica zeolite, ZSM-48 was also

Table 1.1 Metal ions exhibiting tetrahedral coordination and their ionic radii (Szostak, 1989)

Metal ion	Radius (Å)
Al^{+3}	0.53
B^{+3}	0.25
Fe^{+2}	0.77
Fe^{+3}	0.63
Ga^{+3}	0.61
P^{+5}	0.31
Si^{+4}	0.40
Ti^{+4}	0.56
V^{+5}	0.49
Cr^{+3}	0.63

examined. In this sequence Ti-incorporated zeolite beta was also found to be active for oxidation of aromatic hydrocarbons. Still there existed a need for synthesis of better

catalysts, which can perform oxidation of higher aromatics. The success of Ti-substitution in various zeolites also stimulated the investigation on zeolites containing transition metal ions other than Ti.

1.7 NEED FOR MESOPOROUS ZEOLITES

Even though, zeolites, having pore dimensions of 5 to 7 Å, served the purpose for most of the industrial reactions by providing high surface area, the pore dimensions are not sufficient enough to accommodate broad spectrum of larger molecules. The performance of the zeolitic systems is limited by diffusional constraints associated with smaller pores (Maschmeyer, 1998). To a certain extent, it is possible to overcome this problem with aluminophosphates (AlPOs), microporous crystalline materials with pore dimensions up to 13 Å (Wilson et al., 1982; Davis et al., 1988; Ashtekar et al., 1994). However, these materials suffer from limited thermal stability as well as negligible catalytic activity due to framework neutrality. Moreover, there is a need for present- day catalytic studies dealing with processing of hydrocarbons with high molecular weights. These factors led to the discovery of mesoporous solids.

1.8 MESOPOROUS SOLIDS

Although the existing zeolites were found to be suitable for the catalytic transformation of a number of chemical reactions, their pore sizes limit their use in catalyzing reactions involving reactants of dimensions greater than that of their pores. This led to the need for molecular sieves having pore dimensions in mesoporous range. Materials with super large pores possessing catalytic properties are attractive candidates as catalysts for non-shape selective conversion of large molecules, especially for the cracking of heavier

petroleum feed stock. The large void volumes of such materials make them potential adsorbents with high adsorption capacity (Thomas, 1999; Rao, 1999; Janicke et al., 1998 & 1999; Goltner et al., 1999). The large pore can also act as host for various guest species so that the alteration of redox properties can also be achieved (Corma, 1997). A schematic representation of the evolution of zeolitic molecular sieve with time is given in Fig. 1.5.

With the first successful report on the mesoporous materials (M41 S) by Mobil researchers, with well defined pore sizes of 20- 500 Å, the pore-size constraint (l5 Å) of microporous zeolites was broken (Beck et al., 1992 & 1994). The high surface area (> 1000 m^2/g) and precise tuning of the pores are among the desirable properties of these materials (Aufdembrink et al., 1993; Hudson et al., 2000). Mainly, these materials ushered in a new synthetic approach where, instead of a single molecule as templating agents as in the case of zeolites, self-assembly of molecular aggregates or supra-molecular assemblies are employed as templating agent. The current state of mesoporous materials from the standpoint of compositional control will be discussed in the subsequent sections. The basic difference in the syntheses of microporous and mesoporous molecular sieves is shown pictorially in Fig. 1.6.

M41S series of mesoporous materials consists of uni-dimensional hexagonal MCM-41, three-dimensional cubic MCM-48 and lamellar MCM-50 (Beck et al, 1992), which are represented in Fig. 1.7. MCM-41 is the most investigated member of M41 S series, which has a honeycomb structure as a result of hexagonal packing of uni-dimensional cylindrical pores (Stockenhuber et al., 2001; Ahn et al., 1999; Christian et al., 2001). It

has high surface area (> 1000 m^2 /g) and large pore dimensions, which can be tuned in the range of 20-100 Å. MCM-48, the second member of this series

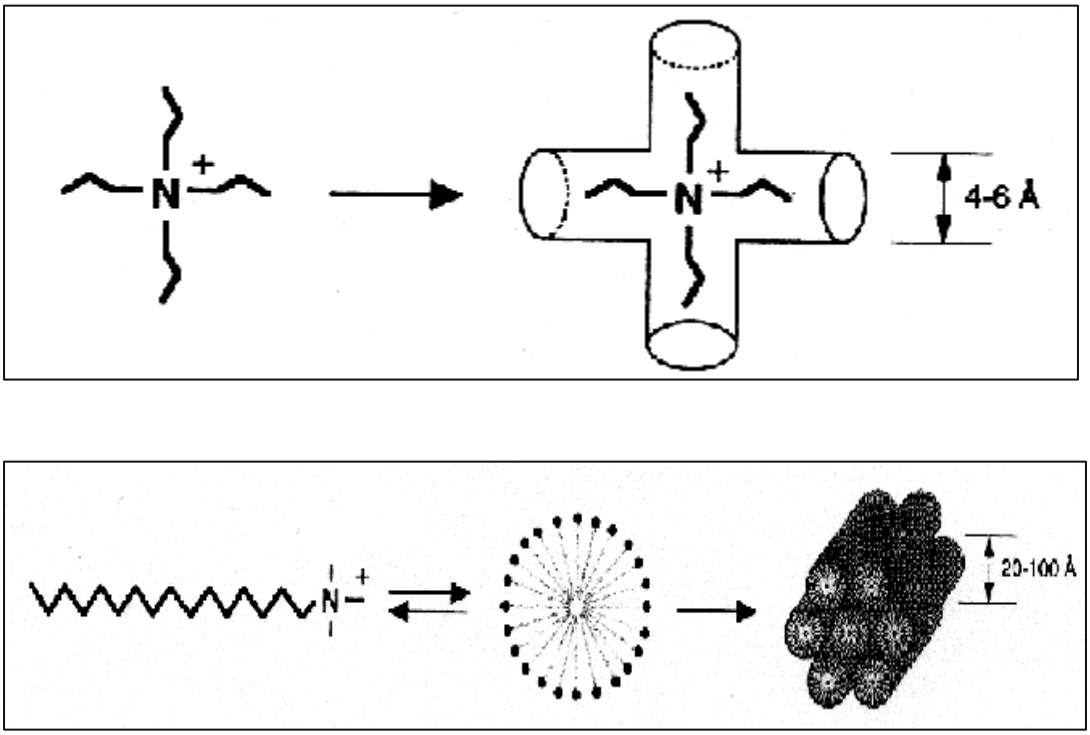

Fig. 1.6. Formation of microporous and mesoporous molecular sieves using small (top) and long (bottom) alkyl chain length quaternary directing agents

with a cubic structure is thought to be based on the gyroid form of an infinite periodic minimal surface model (^{230}Q) (Corma, 1997; 1998; Dellarocca et al., 2001; Morey et al., 1996 & 2000). The gyroid surface means that two molecules on each side of a surface will not meet. Three-dimensional inter-twined channels that do not intersect can represent the channel system of MCM-48 (Ryoo et al., 2001; Mathieu et al., 2001a & 2001b;

Schumacher et al., 1999; Anderson et al., 1999; Nishiyama et al., 1998). MCM-50 has a lamellar structure in the as synthesized form (Beck et al., 1992).

1.9 MECHANISM OF FORMATION OF MESOSTRUCTURES

There have been a number of models proposed to explain the formation of mesoporous materials and to provide rational basis for the various synthetic routes followed. All these models are proposed on the basis of surfactants or templates in solution guiding the formation of structure. Surfactants contain hydrophilic head groups and hydrophobic tail within the same molecule and will self-organize so as to minimize the contact with incompatible ends. Among the various synthetic routes, the main difference is the way in which the surfactants interact with inorganic species. In earlier stages, it was thought that the formation of these materials is as a result of electrostatic complementary between charged surfactant and inorganic species. At very low concentrations these molecules remain randomly arranged in solution. With increase in concentration, these amphiphiles reorganize themselves to form aggregates. At a particular critical concentration (CMC1), these aggregates form spherical micelles. The hydrophilic groups remain on the outer surface of the micelles with the hydrophobic tails directed inwards. As the surfactant concentration increases, these spherical micelles come closer to each other until a second critical micellar concentration (CMC2) is reached. At CMC-2, cylindrical rods of these micelles are formed. At still higher concentrations, these aggregates form liquid crystals. Auvray et al. (1989) demonstrated the formation of these liquid crystals pictorially with cetyltrimethylammonium bromide (CTAB) in water.

Later on, the mesostructured materials have been prepared by exploring various possible interactions other than electrostatic pathways. The formation of these materials can be

viewed alternatively as the interface chemistry between the surfactant and inorganic species. The mesoporous materials can be prepared by exploiting ionic, hydrogen bonding as well as covalent bonding interactions. Based on possible

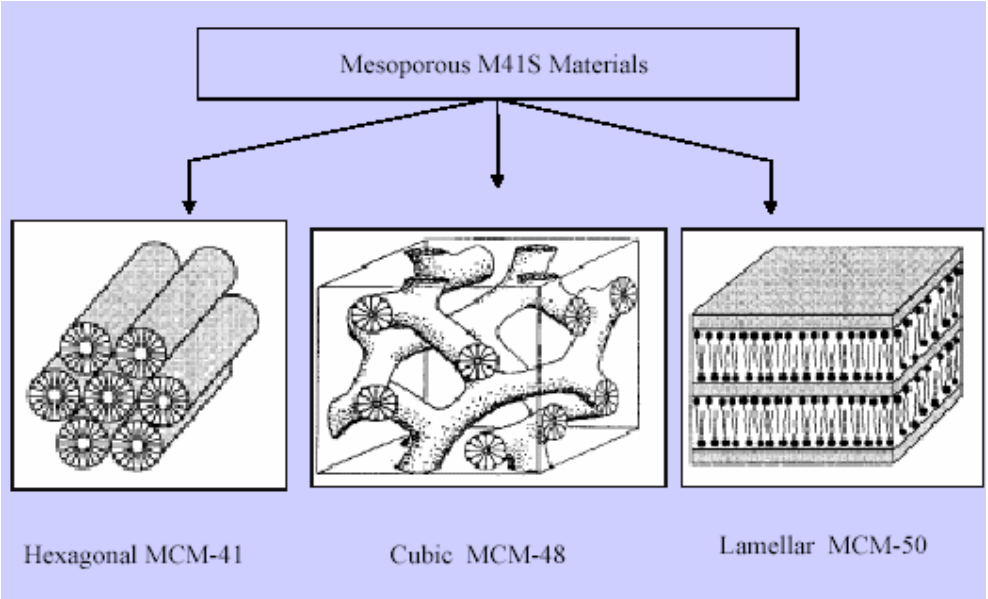

Fig. 1.7. M41S representation

interactions, various synthetic routes have been evolved and they are given in Table 1.2. In the case of direct pathway, surfactants are directly bonded to inorganic precursors through electrostatic interactions. So far, most of the materials have been prepared with cationic surfactants (quaternary ammonium cations) like cetyltrimethylammoniumbromide or chloride. However, a variety of surfactants can serve the purpose. In all these cases, control of pH is critical.

1.10 LIQUID CRYSTAL TEMPLATING (LCT) MECHANISM

The formation of M41 S type of materials can better be explained by Liquid Crystal Templating mechanism (Fig. 1.8), which was proposed by Mobil researchers (Beck et al., 1992), based on the similarity between liquid crystalline surfactant assemblies (i.e. lyotropic phases) and M41 S type materials. Two mechanistic pathways were postulated to understand the formation of meso- structures. In the first case, the aluminosilicate precursor species occupied the space between a pre- existing hexagonal lyotropic liquid crystalline (LC) phase and deposited on the micellar rods of the LC phase. (Initiated by LC phase), whereas in the case of second mechanism, the inorganic species mediated, in some manner, the ordering of the surfactants into the hexagonal arrangement (Co-operative templating mechanism). In both the cases the surfactant and inorganic species mutually react with each other that lead to the phase transition from lamellar to hexagonal structure. This layered intermediate has also been observed by Steel et al. (1994). They proposed a "puckering layer model" where the silicate species in aqueous solution form a layered structure and further ordering leads to puckering which results in hexagonal structure.

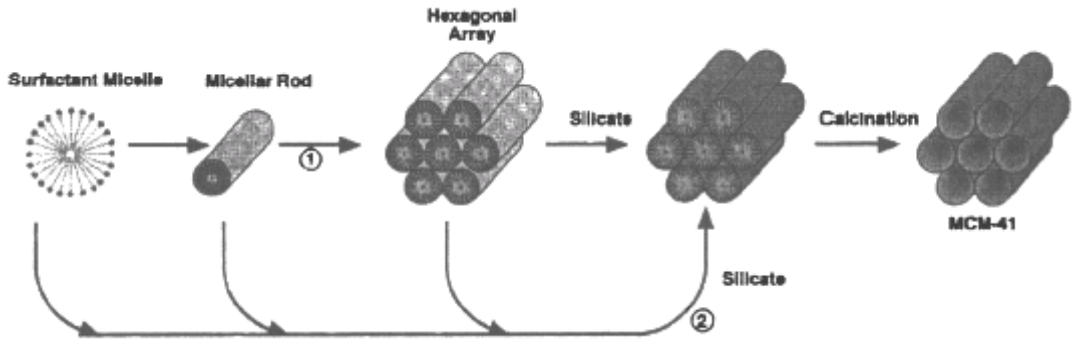

Fig. 1.8. LCT mechanism proposed by Beck et al. (1992)

1.11 SILICATE ROD ASSEMBLY

Davis and co-workers (Chen et al., 1993) concluded from the *in-situ* ^{14}N NMR studies, that the LC phase is not present in the synthesis medium of MCM-41. They proposed that the randomly ordered rod-like micells interact with the silicate species to yield tubular silica, which deposited around the external surface of the micellar rods. Then, the spontaneous ordering of the composite species resulted in the formation of hexagonal structure.

1.12 SILICATROPIC LIQUID CRYSTALS

Firouzi et al. (1995) found through ^{29}Si NMR studies, that at low temperatures and at high pH (~14) a true co-operative self -assembly of the silicates and the surfactants takes place. Further studies by these authors revealed that a micellar solution of CTAB is transformed into a hexagonal phase in the presence of silicate anions. This was consistent with the effect of the electrolyte on micellar phase transitions. The SLC phase behaved similar to the typical lyotropic systems, except that the surfactant concentrations were lower and the silicate counter ions were reactive. Heating the SLC phase caused the silicates to condense irreversibly onto MCM-41. However, it was observed that similar type of material can also be prepared with charge reversed situation, where the surfactant is negatively charged species (sulphonic acid or carboxylic acid derivatives) and the inorganic precursor can be cationic (acidic conditions). There materials have been prepared under acidic pH conditions. On careful observation, it was shown that this

approach is not a viable one because of certain limitations like cost of the surfactant and the stability of the materials prepared.

1.13 GENERALIZED LIQUID CRYSTAL TEMPLATING MECHANISM

A generalized mechanism based on the specific type of electrostatic interaction between a given inorganic precursor "I" and surfactant head group "S " was proposed by Huo et al. (1994). Based on the original LCT mechanism, which involves the anionic silicate species and the cationic quaternary ammonium surfactant, it could be categorized as the S^+I^- pathway. The other charge-interaction pathways are $S^- I^+$, $S^+ X^- I^+$, $S^-M^+I^-$ where X is a counter anion and M is a metal cation. In $S^+ X^- I^+$ approach, by operating well below the isoelectric point of silica (pH~2) under acidic conditions, where the silicate species were cationic, M41S materials can be prepared. In the same way, by maintaining higher pH conditions, it is possible to prepare mesoporous materials by $S^-M^+I^-$ pathway through metal ion mediation. In charge reversed situation, where the surfactants and inorganic species are negatively charged, the metal ion (where M can in general be either Na^+ or K^+) can act as mediator.

1.14 NEUTRAL TEMPLATING MECHANISM

In all the above-mentioned methods, calcination is the suitable way to remove the surfactant, however in some cases extraction with ethanol is also possible. Tanev et al. (1995) proposed an alternative route to synthesize mesoporous materials (Fig.1.9). These authors proposed a neutral templating mechanism based on hydrogen -bonding interactions between neutral primary amine (S^O), which acts as template, and neutral inorganic precursors (I^O) and hence the mechanistic pathway is S^oI^o. Hydrolysis of

tetraethylorthosilicate in an aqueous solution of primary amine yields the neutral $Si(OC_2H_5)_{4-x}$ $(OH)_x$ species, which then binds through H-bonding to the surfactant head group. This leads to the formation of rod like micelles. Further hydrolysis followed by condensation leads to the so-called Hexagonal Mesoporous Silica (HMS). The neutral templating route provides several advantages over materials prepared by electrostatic pathways, mainly the synthesis can be carried out at room temperature and the surfactant can be removed completely by extraction with ethanol. The thermal stabilities of the HMS materials are higher than that of M41S materials.

Even though this S^0I^0 process i.e. the neutral templating approach offers the practical advantage of facile template recovery by non-corrosive solvent extraction or evaporation methods, these surfactants have some limitations. Neutral amines are costly and toxic and not ideally suitable for the industrial applications. Later on it was observed that polyethylene oxide tri-block copolymer could be a promising surfactant. In a suitable solvent or combination of solvents these PEO/PPO/PEO tri-block polymeric surfactants will arrange into different lyotropic phases (Alexandridis et al., 1998). Figure 1.10 gives pictorial representation of the possible phases at various concentrations of ligands. Various materials have been prepared with these polymeric surfactants. The removal of surfactants can be achieved either by calcination or extraction. One of the practical advantages of this method is that with a minimum concentration of the surfactant, it could be possible to prepare the desired material with desired pore size. Moreover, to prepare a mesoporous solid with high pore size through direct interactions, there is a need to proceed with surfactants with long alkyl chains, which are costly in nature. However, with the use of polymeric surfactants it is possible to prepare the same at a lower

concentration. In addition to the above, since polymeric surfactants are soluble in organic solvents, it is possible to remove the same completely through extraction process.

1.15 LIGAND ASSISTED INTERACTIONS

By a different synthetic approach (Antonelli et al., 1995), it is possible to prepare the mesoporous materials through covalent interactions. Instead of relying on charge interaction, the surfactants were pretreated with the metal alkoxides in the absence of water to form ligand covalent bonded complexes. High quality materials are formed by the amine surfactants due to the strong affinity for nitrogen-metal bond formation between surfactant head group and the inorganic precursor (Fig. 1.11). In this ligand assisted templating approach, the control of the meso-structure was found possible by adjusting metal/surfactant ratio and it has been established that the M41 S family of mesoporous materials can be prepared through this approach.

1.16 REMOVAL OF TEMPLATE

Removal of surfactant plays an important role in the preparation of final mesoporous solid. In order to preserve the final meso-structure, in general, removal of the surfactant can be achieved by calcination process, where the as-synthesized material will be subjected to a controlled heat treatment. Calcination has to be done in a flow of inert gases at the initial stages followed by the flow of air. This is to maintain the crystallinity of the material. In the case of HMS materials prepared through hydrogen bonding interactions, the removal of the template can be achieved either by repeated extraction with ethanol or by calcination. The same procedure can be followed for MSU materials, since the polymeric surfactants used are biodegradable.

1.17 HEXAGONAL MCM-41

M41S series consists of three well-known members; among them the first one is MCM-41 with hexagonal lattice with one-dimensional channel system. Soon after the discovery of these solids, many modifications have been employed to these systems to generate either acidic properties by isomorphous substitution of trivalent atoms like $Al^{+3,}$ Fe^{+3} or redox properties by substitution of transition metal ions like Ti, V, Cr and others in place of silicon (Jing et al., 2001; 2002). As on today, more than a half of the elements in the periodic table has been incorporated into the framework of this material. Fig. 1.12 shows the possible modifications that have been carried out on this material.

1.18 MCM-41 IN CATALYSIS

MCM-41 materials have been used as acid catalysts by Corma group (Armengol et al., 1995 & 1997), which invoked the potential applications of these materials. Though it is generally observed that the acidity of these mesoporous solids are to an order less in acid strength, than zeolties, with these materials, it is possible to overcome the existing pore size constraints of microporous solids. The catalytic activity of H-AI-MCM-41 has been tested for Fridel-Craft's alkylation of 2,4-di-tert-butyl phenol with cinnamyl alcohol and the activities are compared with conventional acidic zeolites. This reaction has been well studied over acid catalysts, and there is a need to increase the conversion of the substrate to dihydrobenzopyran, which is one of the important products in the preparation of dyes. For the same reaction, being microporous in nature, catalytic activity of HY or HYM is limited compared to MCM-41 in which pores are in mesoporous range. With other catalysts like amorphous silica, alumina and sulfuric acid, though conversion is higher

than HY or HYM, the selectivity towards the product dihydrobenzopyran is low (Armengol et al., 1995).

Among the metal incorporated systems for the generation of acidic properties, most of the studies have been devoted to aluminium incorporation (Armengol et al., 1995 & 1997; Corma, 1997; Chakraborty et al., 1996; Umamaheswari et al., 2002). But recently, trivalent ferric ion has been incorporated in to MCM-41 and the resulting acid catalyst, H-Fe-MCM-41 has been shown to be a promising recyclable catalyst for the alkylation of phenol with tert. butanol (Badamali et al., 1998a ; 1998b). Alkylation of phenol in general gives thermodynamically favorable m-isomer than kinetically favorable o-and/or p-isomer. However, the exclusive formation of a particular product over the other is governed by the strength of the acid sites. This reaction has been performed over various acidic zeolites and it has been established that weak acid sites are responsible for the O-alkylation and moderate to strong acid sites for C-alkylation. For this particular reaction, even though Al-MCM-41 shows higher conversion, the selectivity to meta isomer is higher only with H-Fe-MCM-41 (Badamali et al., 1998a). However, the generation of acid and redox properties in general can be achieved by modification of the mesoporous solid. The possible modifications that have been employed on these solid materials are shown in Fig. 1.12

Modification of MCM-41

1) Generation of basic properties by ion exchange with lA group salt solutions

2) Alteration of acidic properties by incorporation of group +3 cations

3) Incorporation of transition elements to generate redox properties

4) Immobilization of metal complexes inside the cavities

5) Functionalization to generate chiral catalysts.

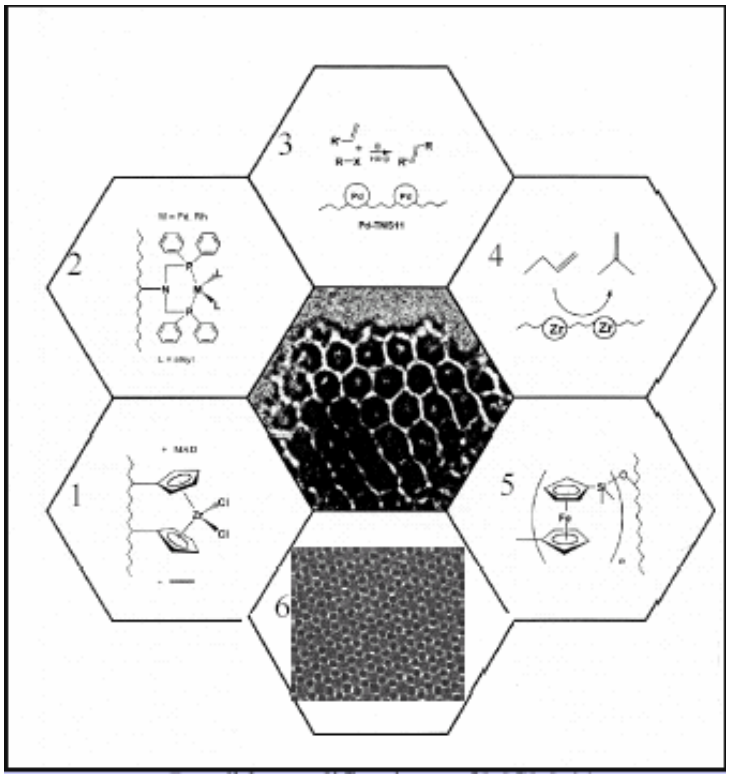

Fig. 1.12. Possible modifications of mesoporous materials

[Modifications have been carried out for anchoring of homogeneous polymerization catalyst zirconocene (1) heterogenization of homogeneous catalyst (2), support for various guest species (3) Framework incorporation to generate acid and redox catalysts (4), encapsulation of guest species within the pores (5) for the synthesis of carbon nanotubes (6)]

1.19 MCM-48

MCM-48 has been the second member of M41S family with three dimensional channel systems, which can be indexed to an *Ia3d* space group (Fig. 1.7). Alfredsson et al., 1996 and Anderson, 1997) built a computer model of a silicate MCM-48 and, by comparing experimental and modeled X-ray and electron diffraction patterns, they were able to confirm that the structure of MCM-48 is based on the gyroid form of an infinite periodic minimal surface model ^{230}Q. The gyroid surface partitions the space into two equal but nonintersecting compartments, which means that two molecules on each side of a surface will not meet. Three-dimensional intertwined channels that do not intersect may thus represent the channel system of MCM-48.

The MCM-48 silica was claimed to have the cubic space-group symmetry of *Ia*3*d* (No. 230) because of the similarity of its powder X-ray diffraction (XRD) pattern with that previously reported for lipids that belonged to the same space group as the periodic minimal surface of gyroid (G). All structural observations of the MCM- 48 silica were explained by assuming that the amorphous wall followed the G surface. The silica MCM-48 was later synthesized with crystal morphologies, and the crystallization process was studied by Ryoo et al. (2001). Recently, the structure of MCM-48 silica has been solved uniquely by electron crystallography (EC) (Carlsson et al., 1999). The main advantage of using the EC technique for mesoporous silica, compared to traditional X-ray single crystal diffraction, is that high-resolution electron microscope (HREM) images can be taken and that the phases of crystal structure factors (CSFs) are immediately made available from the Fourier transform of the image.

In spite of being advantageous because of its three-dimensional network of pores, still it has not well been studied. To some extent this might be due to the difficulty involved in

its synthesis. Till late 90s MCM-48 has been synthesized at higher concentrations of the surfactant preferably CTAB/Si >1. As the thermal stability of these materials is low, during removal of surfactant, the semicrystallinity of this material may collapse. However, three-dimensional network of pores can avoid pore blockages, if any, taking place with bulky substrates compared to one-dimensional channel system.

1.20 CHARACTERIZATION OF MESOPOROUS MATERIALS

The various characterization techniques, that have been employed in general, are given below. These techniques have been employed in order to understand the physico-chemical properties like thermal stability, pore size and active surface area. The foremost characterization technique required for the identification of mesophase is X -ray diffraction. However, the exact nature of the pore and identification of silicate in mesoporous network is still uncertain. The mesoporous materials are weakly crystalline or semi-crystalline in nature.

XRD ascertains the presence of mesophase

FT-IR indicates incorporation of heteroatom

N_2 adsorption-desorption determines the surface area and pore size distribution

UV -VIS DRS provides information of the presence of transition metal in different environments

Solid state NMR and ESR points out to the presence of different environment of the metal atom

Electron microscopy gives information on the morphology of the material (SEM) and pore size (TEM) and

XPS confirms the oxidation state

The arrangement of silica in the wall structure imparts semi-crystallanity to these materials. X-ray diffraction patterns containing three or more low angle peaks (below $2\theta = 10^{o}$) are obtained that can be indexed to a hexagonal hk0 lattice. Proposed structure has a hexagonal stacking of uniform diameter porous tubes whose size can be varied from about l nm to more than 10 nm. MCM-48, the cubic material, exhibits an X-ray diffraction pattern, consisting of several peaks in lower two theta. The structure of MCM-48 has been proposed to consist of two infinite three-dimensional, mutually inter twined networks of spherical cages separated by a continuous silicate network (Kruk et al., 2000). The structure can mimic an infinite periodic minimal surface of the gyroid form, ^{230}Q. Even though MCM-48 synthesis has been known since 1992, most of the research studies on this member have been concentrated during late 90s. It was observed by Corma et al. (1998); Carlsson et al. (1999); Koyano et al. (1997) that cubic MCM-48 shows higher catalytic activity compared to one-dimensional MCM-41. However, there is a need to synthesize MCM-48 at lower concentrations of surfactant in order to preserve the final structure.

1.21 MCM-50

The MCM-50 framework mimics the structure of a lamellar liquid crystal phase. The lack of any observable peaks at higher diffraction angels in the powder X-ray diffractogram of MCM-50 suggests that the silicate layers in this mesostructure are not as ordered as in the layered silicates such as kanemite or magadiite (Beck et al., 1992; Biz et al., 1998). This observation is consistent with the lack of pore size uniformity observed by argon adsorption. The MCM-50 lamellar structure lacks thermal stability and, unless post treated with TEOS, collapses upon surfactant removal. Catalytic

activity on this material is not reported since on calcination, the mesostructure collapses leading to a non-porous material.

1.22 Hydrothermal stability of mesoporous solids

It has been observed that mesoporous structures of MCM-4l and MCM-48 disintegrate in distilled water around 370 K, while the structure can be stable in 100% steam of 1 atmosphere pressure at higher temperatures around 820 K. Thus, the structure disintegration is thermodynamically more favorable in water than under the steaming conditions(Biz et al., 1998).

1.23 MESOPOROUS SOLIDS OTHER THAN SILICA

Soon after the discovery of M41S, the concept of synthesizing mesostructure with the aid of surfactant-based mechanism has been extended to synthesize other oxide materials in mesoporous form. A wide range of synthetic conditions has been explored in order to synthesize a variety of mesoporous oxide networks like sulfides and phosphates. Stucky and coworkers (Huo et al., 1994) reported a generalized procedure to synthesize transition metal oxides having mesostructures with cationic and anionic surfactants, using both acidic and basic conditions with low surfactant concentrations and temperatures. A variety of oxides with mesoporous networks have been reported using amphiphilic block copolymer surfactants.

One of the most interesting periodic mesoporous materials reported in recent times is a carbon molecular sieve. Ryoo et al. (2001) reported the successful synthesis of mesoporous carbon using MCM-41 and MCM-48 as templates. They used sucrose as carbon source in the presence of dilute sulphuric acid as catalyst and carbonization

temperature of around 1177 K. The template, mesoporous network can be removed either by immersing in sodium hydroxide or in hydrofluoric acid. Recent studies from the same group showed that mesoporous carbons can also be effectively used to disperse the active catalyst and the resulting composite can be used for various applications.

1.24 MESOPOROUS ALUMINOPHOSPHATES

Microporous aluminophosphates ($AlPO_4$) are another class of porous solids, which received considerable attention because of specific advantages like activation of molecular oxygen, which is in general difficult over zeolites. These are analogues to zeolites not only in their texture but also in synthesis. In general, the synthesis of $AlPO_4$s will be carried out in an autoclave using amine surfactants. Wilson et al. (1982) first reported the synthesis of microporous $AlPO_4$, which are neutral. There after, several modifications have been carried out in order to generate redox properties with in $AlPO_4$ network (Blackwell et al., 1988). In this series, silicon substituted aluminophosphate exhibits acidity comparable to highly acidic zeolites. Because of their high thermal stability and shape selective features, they are well exploited for production of fine chemicals. Flanigen et al. (1986) incorporated a series of transition elements in $AlPO_4$ network and the resulting systems are shown to be promising catalysts for various applications. Figure 1.4 highlights the essential applications of chromium substituted $AlPO_4$-5, which not only promotes oxidation of various aromatics with molecular oxygen but also a good recyclable catalyst. Thomas group of scientists carried out various selective reactions over Cr, Mn and Fe incorporated microporous $AlPO_4$ and they have shown that the resulting systems are good oxidation catalysts (Raja et al., 2000). It has been widely accepted that utilization of natural oxidants like air/ molecular oxygen will

always be advantageous not only due to handling problems but also on cost basis. However, the pore diameter of these systems cannot accommodate the bulky substrates, which are generally involved in fine chemicals industry. This particular aspect led to the discovery of mesoporous AlPOs where the pores will be in the range of 2-50 nm (Chakraborty et al., 1997; Zhao et al., 1997; Petrakis et al., 1995; 1997; Sayari, 1996; Luan et al., 1998a;1998b).

Soon after the discovery of mesoporous M41S series, the concept of preparing porous solids via surfactant based templating mechanism has been extended to synthesize mesoporous aluminophosphates. In this context, Chakraborty et al. (1997) reported the synthesis of silicon incorporated mesoporous aluminophosphate through hydrothermal synthesis. Mesoporous SAPO synthesized in this method is reported to have a BET surface area of 925 m^2/g with average pore size distributed around 28 Å. During the same period, Zhao et al. (1997) and Kapoor et al. (2000) have also reported the synthesis of mesoporous aluminophosphate, which was synthesized at room temperature. With the success of titanium incorporated molecular sieves as catalysts, titanium was also incorporated into the framework of aluminophosphate and successfully employed for epoxidation reactions. However, this particular field has not received much focus because of lack of proper synthetic means.

1.25 OTHER MESOPOROUS OXIDES

Even though it has been realized initially that non-silica based materials can also be prepared by the same mechanistic ideas, the first successful attempt to prepare mesoporous titania was made only in 1993 (Monnier et al., 1993). However, the removal

of surfactant caused collapse of the mesostructure. With modified synthetic approach, mesoporous titania was prepared in 1995 (Antonelli et al., 1995). However, the field of non-siliceous ordered mesoporous materials has received considerably less attention compared to that of mesostructured silica. Through a number of alternative surfactant-assisted synthetic approaches, essentially non-silicate mesoporous metal oxides were achieved using low molecular weight surfactants, e.g. titania (Antonelli et al., 1995; Jin-Yu et al., 2001; Muller et al., 2000), niobia (Stone et al., 1998), alumina (Bagshaw et al., 1996), tin oxide (Ulagappan et al., 1996b), ceria (Yang et al., 1998), and zirconia (Yang et al., 1998), vanadium oxide (Yang et al., 1998), aluminophosphates and vanadophosphates (Tiemann et al, 2001a). All the above materials are mesoporous in as-synthesized form but after removal of the surfactant, the mesoporous network collapsed. Attempts have been made to synthesize transition metal oxides in mesoporous form by optimizing the interaction between surfactant and inorganic precursor. Among the mesoporous transition metal oxides, synthesis of mesoporous titania is of particular interest.

1.26 OBJECTIVES AND SCOPE OF THE PRESENT THESIS

The advent of supra-molecular chemistry has given a new thrust to this field of porous solids. Even though various oxide materials have been prepared in mesoporous form, lack of proper crystallinity of the resulting solids made them not suitable for industrial applications. However, constructing solids with expected porous texture and architecture is one of the dreams of scientists. There are a number of possibilities and combinations for building up supra-molecular structures over which the porous solids can be constructed. It is therefore necessary to examine and probe scientifically the suitability

of these materials especially with respect to their surface properties for the possible technical applications envisaged. The motivation of the present study is therefore to synthesize mesoporous solids at lower concentrations of surfactant and to examine their catalytic activity for some typical organic transformations. Utilization of natural oxidants like molecular oxygen for oxidation of abundant hydrocarbons has been one of the topics on which emphasis has been laid.

The specific aims of the present study are

1. Syntheses of transition metal ions incorporated (Ti, V, Cr, Mn and Fe)-MCM- 48 materials under hydrothermal synthesis conditions using cetyltrimethylammonium bromide (CTAB) as surfactant at low concentrations.

2. Preparation of V, Cr and Fe incorporated mesoporous aluminophosphates under hydrothermal conditions using CTAB as the surfactant.

3. Physico-chemical characterization of the synthesized materials by low angle XRD, N_2 adsorption, FT-IR, Thermal analysis, UV-VIS DRS, ESR, XPS and electron microscopy.

4. Evaluation of catalytic activities of these materials for some typical organic transformations like alkylation (acid catalyzed) and oxidation reactions.

5. Exploitation of molecular oxygen/air as an oxidizing agent instead of the conventional oxidizing agents like peroxides for the oxidation of hydrocarbons.

6. In-situ synthesis and characterization of M41S materials on stainless steel grids.

7. Synthesis and characterization of thermally stable mesoporous titania.

CHAPTER 2

EXPERIMENTAL METHODOLOGY

2.1 PREPARATION OF THE CATALYSTS

2.1.1 Mesoporous aluminosilicates

The chemicals used for the synthesis of mesoporous aluminosilicates are tetraethylorthosilicate (Merk) and aluminium sulphate (AR, SRL) as the sources of silicon and aluminium, respectively. Cetyltrimethylammonium bromide (AR, CDH) was used as the surfactant. Tetramethylammonium hydroxide (25 % in water, SRL) and sodium hydroxide were used to maintain the pH of the medium.

Synthesis of MCM-48 was carried out in an indigenously designed stainless steel autoclave of 300 ml capacity under autogeneous conditions at 423 K. The autoclave was heated an oven, which maintained the temperature with an accuracy of ± 1 K. As-synthesized materials were calcined in a tubular furnace at a very slow heating rate. The temperature of the calcination was maintained with an accuracy of ± 2 K. 1 M ammonium nitrate was used to exchange the Na^+ ions with NH_4^+ ions in liquid phase. The details of the gel compositions are given in subsequent sections.

In a similar way, incorporations of other heteroatoms in the framework of MCM-48 were carried out. For this purpose, ferric nitrate nonahydrate (AR, CDH), tetrabutylorthotitanate (Lancaster), vanadium acetylacetonate (Fluka), chromium nitrate

nonahydrate (CDH) and manganese acetate (AR, CDH) were used as the sources of iron, titanium, vanadium, chromium and manganese, respectively. The synthetic procedure was same as that employed for purely siliceous material, except, addition of transition metal precursor was done along with silica source.

2.1.2 Mesoporous aluminophosphates

The chemicals used for the synthesis of mesoporous aluminophosphates (M-AlPOs) were aluminium hydroxide (Merk), phosphoric acid (AR, SRL) as aluminum and phosphorous sources respectively. Tetramethylammonium hydroxide (25 % in water, SRL) was used to maintain the pH of the synthetic gel. Cetyltrimethylammonium bromide (CDH) was employed as template. Ferric nitrate nonahydrate (AR, CDH), vanadium acetylacetonate (Fluka), chromium nitrate nonahydrate (CDH) were used as iron, vanadium and chromium sources, respectively.

Stainless steel autoclave was used for the synthesis of mesoporous AlPOs under conditions similar to that reported earlier in 2.1.1. Details of the synthetic gel compositions are given in the respective sections.

H-Al-MCM-41 was synthesized according to the reported procedure (Chakraborty, 1998) and zeolites were obtained from Sud Chemie .

2.1.3 Coatings of M41S on stainless steel grids

The support used for the preparation of the structured mesoporous materials was stainless steel AISI 316 type supplied by Haver and Boecker (Oelde Westfalen, Germany). Chromium containing (16.5-18.5%), Ni (11-14%), Mo (2-2.5%), and Fe (65-70%). The

wire diameter and the mesh size were 250 and 800 μm, respectively. The support packing was 50 mm in length and 34 mm in width and was formed by the superposition of 7 plates. Each plate (9cm^2) was separated from the others by steel rings of 4 mm length. Detailed descriptions of the synthetic conditions employed are given in chapter 5.

2.1.4 Mesoporous titania

For the preparation of mesoporous titania, cetyltrimethylammonium bromide (CDH) and tetrabutylorthotitanate (Lancaster) were used as surfactant and the titanium precursor respectively. Tetramethylammonium hydroxide (25 % in water, SRL) was used to maintain the pH of the synthetic medium. Mesoporous titania was prepared under autogeneous pressure in a stainless steel autoclave as in the previous methods.

2.2 CHARACTERIZATION OF THE CATALYSTS

2.2.1 X-ray diffraction studies

The XRD patterns of M-MCM-48 [M= Si, Ti, V, Cr, Mn and Fe], mesoporous M-AlPOs [M= V, Cr and Fe] and mesoporous titania were recorded on a D500 Siemens powder diffractometer (θ / 2θ) using monochromatised Cu-Kα radiation (λ=1.5406 Å) in the 2θ range of 0.5-10° with the steps of 0.04° and a step time of 8 s. The d spacing values were calculated by using the Bragg's equation $n\lambda = 2d \sin\theta$ where n represents the order of reflection, λ, the wavelength of the incident X-ray beam and d, the spacing between reflecting crystal planes.

2.2.2 Surface area and pore size distribution

Nitrogen adsorption isotherms of calcined M-MCM-48 samples at 77 K were obtained using Sorptomatic 1990 Carlo Erba instrument. All the samples were out gassed at 400 K for 12 h. High pure nitrogen was used as adsorbate at liquid nitrogen temperature. The surface area of the samples were calculated by applying the BET equation

$$p/v(p_0-p) = 1/v_m\, C + (C-1)p/\, v_m C.p_0$$

where v is the volume of nitrogen gas adsorbed at an equilibrium pressure p , p_0 is the saturated vapour pressure of nitrogen gas in equilibrium with liquid nitrogen (77 K), v_m is the monolayer volume and C is a constant depending on the heat of liquefaction (Q_1) and heat of adsorption (Q_a)of N_2 gas. From the adsorption isotherm, v_m was obtained and from that specific surface area (SSA) was calculated. Pore size distribution was computed from the desorption branch of isotherm using BJH analysis by adopting Kelvin's equation.

$$\ln p/p_0 = -\, 2\sigma\, v \cos\theta/\, r_k\, R$$

Where R is the gas constant, θ is the wetting angle, σ is the surface tension and r_k is Kelvin's radius and v is the volume adsorbed.

2.2.3 Thermogravimetric studies

Thermal analyses of the synthesized samples were carried out on Perkin Elmer TGA (Delta series TGA 7) with a steady heating rate of 20 K/ min. Thermal analyses were performed to understand the nature of interaction of the surfactant with the inorganic precursor.

2.2.4 Infrared studies

Infrared studies in the range 4000-400 cm^{-1} for MCM-48 samples were recorded on Shimadzu photometer. The samples were mixed well with KBr in 1: 100 ratio and then pelletized.

2.2.5 Electron microscopic studies

Scanning electron microscopy (SEM) and high-resolution transmission electron microscopy (HRTEM) were employed to study the morphology of mesoporous silica. HRTEM measurements were carried out on a Philips CM300UT FEG with 300 kV field emission gun. SEM images were recorded using JEOL JSM-6300F electron microscope operating at a voltage of 5 kV

2.2.6 UV-VIS measurements

UV-VIS spectra of Ti, V, Cr, Mn and Fe – MCM-48 materials were recorded on Cary 5E UV-VIS-NIR spectrophotometer. The sample was diluted with nujol oil and ground well in a mortar. The resulting paste was then soaked on a Whatmann -41 filter paper and was introduced in to the spectrometer. Prior to that, background correction was done with nujol-soaked filter paper.

2.2.7 ESR measurements

ESR spectra of V, Cr, Mn and Fe- substituted materials were recorded with Varian E–112 spectrometer at liquid nitrogen temperature (77 K). About 50 mg of the sample was

taken in a quartz tube. Variable temperature ESR measurements were performed on iron substituted mesoporous samples.

2.2.8 X-ray photoelectron spectroscopy

X-ray photoelectron spectroscopic measurements (XPS) of V and Cr- substituted mesoporous aluminophosphates were performed on PHI-550 ESCA-System (Perkin-Elmer GmbH).

2.2.9 Temperature programmed reduction and desorption studies

Temperature- programmed- reduction (TPR) studies were done using 100 mg of the catalyst loaded on a quartz reactor. The samples were first treated with argon for 1 h at room temperature, followed by H_2/Ar. Desorption was carried out at a heating rate of 10^oC / min. Temperature programmed desorption of ammonia serves as a dependable technique for the quantitative determination of the acid strength distribution. In TPD studies, pelletized catalyst was activated at 700°C inside the reactor under nitrogen flow for half an hour. After cooling to room temperature, ammonia was injected in the absence of the carrier gas flow and the system was allowed to attain equilibrium. A current of nitrogen was used to flush out the excess and physi-sorbed ammonia. The temperature was then raised in a stepwise manner at a linear heating rate of about 20°C/min. The ammonia desorbed from 100°C to 600°C at intervals of 100°C was then trapped in dilute sulphuric acid solution and estimated volumetrically by back titration with NaOH.

2.2. 10 ICP analysis

The amount of vanadium present in mesoporous solids was determined by ICP-MS technique using UltraMass (Varian, Australia) instrument. In a similar way, ICP-AES was used to estimate Cr content in mesoporous samples.

2.3. CATALYTIC STUDIES

Vapour phase alkylation of naphthalene was performed in a fixed bed flow reactor (Fig.2.1) working at atmospheric pressure. The reactants were fed into the reactor by a motar-driven syringe infusion system. The feed rate was maintained accurately by proper calibration from time to time.

The reactor was made up of a pyrex tube of about 35 cm length and 2 cm in diameter. The inlet tube was spiraled around three fourth of the length of reactor before its inlet through the top of the reactor. This enabled the vaporization of the reactants and preheating of the vapour to the set reaction temperature before entering the catalyst zone. The powdered catalysts were held between two quartz wool plugs with a thermocouple well touching the catalyst bed as shown in Fig. (2.2). The reactor was kept in an indigenously fabricated furnace, made of ceramic tube wound with kanthal wire as heating element, which was electrically heated. Its temperature being controlled by a temperature programmer with an accuracy of $\pm$ 1 K. Reactants were fed into the reactor when the difference in temperature between the furnace and the catalyst bed was not more than 2K.

For vapour phase reaction, about 0.5 g of the catalyst was used for each run. Products collected for the first 20 min were discarded to ensure the attainment of the steady state.

The products coming out of the reactor in vapour phase was cooled by means of a double walled liebig condenser and liquid products were collected in a cold trap maintained at the temperature of freezing mixture (ice+ NaCl). The catalysts were regenerated after each run by passing air at 723 K for 6h. The experimental details of the liquid phase reactions carried out over different catalytic systems are given in subsequent sections.

2.4 PRODUCT ANALYSIS

The reaction products were identified by GC-MS (Hewlett-Packard, HPG 1800A GCD system, HP-5) and analyzed by gas chromatography (Shimadzu GC-14A, 30m HP-5. FID).

CHAPTER 3

SYNTHESIS, CHARACTERIZATION AND CATALYTIC ACTIVITY OF TRANSITION METAL INCORPORATED MCM-48

3.1 INTRODUCTION

In the early nineties, Mobil researchers reported the successful synthesis of mesoporous materials whose pore dimensions are in the range 2 to 50 nm. The M41S family consists of uni- dimensional hexagonal MCM-41, cubic MCM-48 and lamellar MCM-50 as known members (Beck et al., 1992). These materials were initially prepared through a structure-directing agents, which have been proven necessary for the preparation of mesoporous materials (Hudson et al., 2000). The so-called mesoporous materials possess a periodic framework of regular mesopores, whose dimensions depend mainly on the surfactant chain length. These mesoporous materials possess interesting physical properties that make them potential candidates as catalysts or catalytic supports. They usually possess high surface area around 1000 m^2/g with high pore volume around 0.7-1.2 cc/g. In addition to these features, they also exhibit thermal stability up to 1073 K. Even though M41S series consists of three members, attention has been paid extensively to the syntheses and catalytic exploitation of MCM-41 materials (Armengol et al., 1997; Alfredsson et al., 1994; Attard et al., 1995; Walker et al., 1997). In this series, there has been a considerable number of papers and reviews dealing with the above-mentioned aspects (Corma, 1997; Christian et al., 1998; Ying et al., 1999, Biz et al., 1998). This is mainly due to the fact that synthesis of MCM-41 requires less severe reaction conditions compared to that of MCM-48 (Corma, 1997; Corma et al., 1994a; 1994b). Since their

discovery, various synthetic strategies have been evolved and at present it is possible to prepare MCM-41 materials under hydrothermal conditions, room temperature or/and refluxing conditions. Recent reports on MCM-48, a cubic member of M41S family suggests that cubic structure would be advantageous for catalytic reactions or even as catalytic supports (Keiko et al., 1996; Mathieu et al., 2000; 2001a; Koyano et al., 1996). Very recently, it has been proved that mesoporous carbons prepared by using MCM-48 as template has superior characteristics when compared to the one prepared by using MCM-41 as template (Ryoo et al., 2001). On careful observation of the MCM-48 structure (Fig. 3.1), it can be seen that three-dimensional interwoven structure would resist pore blockages (Corma 1998; Kim et al., 1998; Gallis et al., 1997; 1998). In spite of specific advantages, very little attention has been paid to explore the MCM-48 materials. As mentioned earlier, to some extent this is due to the difficulty in its synthesis, which require conditions that are different from MCM-41 synthesis. Till late 90s this material was synthesized at high concentrations of the surfactant where the surfactant arrange in liquid crystalline cubic phase (Beck et al., 1992). But in this case, complete removal of the template can be achieved only through calcination. So it would always be desirable to synthesize MCM-48 at low concentrations of the surfactant (Schumacher et al., 1999; Anderson et al., 1999; Nishiyama et al., 1998). Keeping this aspect in mind, attempts have been made to synthesize MCM-48 at lower concentrations of the surfactant. Catalytic functionalities have also been generated by substituting Al and various transition elements like Ti, V, Cr and Mn in place of silicon. Alkylation of naphthalene with alcohols has been carried out as a probe reaction to examine the acid catalytic

activity of (Al, Fe)-MCM-48 where as, partial oxidation of phenol has been carried out to examine the redox behavior of (Ti, V, Cr and Mn)-MCM-48.

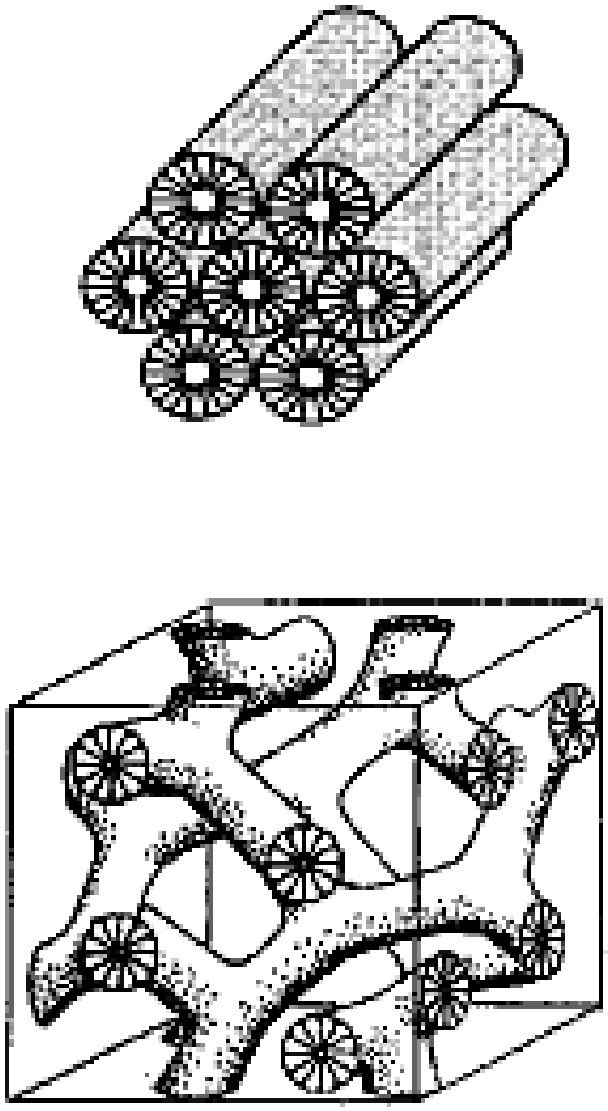

Fig. 3.1. Representation of MCM-41(top) and MCM-48 (bottom)

3.2 EXPERIMENTAL

3.2.1 Synthesis of Si,Al and Fe substituted MCM-48

MCM-48 materials were prepared under hydrothermal reaction conditions in 300 ml or 750 ml stainless steel autoclave. Cetyltrimethylammonium bromide (CTAB, CDH

chemicals) was employed as structure-directing agent and tetraethylorthosilicate (TEOS, MERK) as silica source. Aluminium sulphate was used as aluminium source whereas, tetrabutylorthotitanate (Lancaster), vanadium acetonylacetate (Fluka), chromium nitrate nanohydrate (CDH), manganese acetate (SRL) and ferric nitrate (CDH) as the titanium, vanadium, chromium, manganese and iron sources respectively. pH of the synthetic medium was maintained with aqueous NaOH, however, tetramethylammonium hydroxide was used in the case of titanium-substituted material. Ethanol was used as co-solvent whose function is discussed in detail in section 3.3.1.

MCM-48 molecular sieves were prepared *via* S^+/I^- templating route. Schematic representation of the procedure adopted in the present study is given in Scheme 3.1. MCM-48 materials have been prepared under hydrothermal synthesis conditions using cetyltrimethylammonium bromide as structure-directing template and tetraethylorthosilicate as the silica source. In a typical synthesis, TEOS (12.7ml) was mixed with an aqueous solution of CTAB (2.5g) and to this NaOH (.57g) in H_2O (100g) and ethanol (3.5 ml) were added. Here, ethanol acts as co-solvent (Gallis et al., 1998). The homogeneous gel thus obtained was found to have the composition 2 SiO_2: 0.24 CTAB: 0.5 NaOH: 1-3 EtOH: 195 H_2O. After ageing at room temperature for 3 hours, this homogeneous gel is transferred to a static autoclave and hydrothermally treated under autogeneous pressure at 423 K for 10-15 h. The autoclave was then removed from oven and cooled to room temperature. After that the solid was recovered by filtration, washed with plenty of water and oven dried. The powder was then calcined in air at 823 K for 12 h to remove the template. During the calcination, initially, nitrogen atmosphere was

maintained in order to preserve the structure. MCM-41 was synthesized according to literature reported by Chakraborty et al., 1996.

3.2.2 Characterization

The X-ray diffraction (XRD) patterns were recorded on D500 Siemens powder diffractometer (θ / 2θ) using monochromatized Cu-Kα radiation (λ=1.5406 Å) in the 2θ range of 0.5-10° in the steps of 0.04° and a step time of 8 s.

Surface area measurements were done by the adsorption-desorption of N_2 at 77 K using Sorptomatic 1990 (Carlo Erba) instrument. Samples before the measurements were out gassed for 12 h to remove the physi-sorbed gases. The specific surface area values (SSA) of the samples were calculated employing the BET equation, while BJH method was applied for the calculation of pore volume and pore-size distribution (PSD).

FT-IR and UV-VIS spectra were recorded on Perkin-Elmer spectrophotometer. The spectra were recorded in nujol mode. ESR-spectra were recorded on Varian-115 spectrometer at room temperature and in the case of vanadium samples, the same was recorded at liquid nitrogen temperature.

Scanning electron microscopy (SEM) and high-resolution transmission electron microscopy (HRTEM) were employed to study the morphology of mesoporous silica. HRTEM measurements were carried out on Philips CM300UT FEG with 300 kV field emission gun. SEM images were recorded using JEOL JSM-6300F electron microscope operating at a voltage of 5 kV. Thermal analyses of the samples were made with thermal analyzer (Perkin Elmer model TGA 7) at a heating rate of 20 ^{o}C/min

3.2.3 Catalytic activity

The catalytic activities of Al-MCM-48 and Fe-MCM-48 were tested for the alkylation of naphthalene with n-butanol and n-propanol as alkylating agents. These reactions were performed in the temperature range 598-673 K. Oxidation of phenol was carried out as probe reaction to examine the catalytic activity of transition metal incorporated MCM-48. This reaction was performed in liquid phase in a three-necked round bottom flask. Identification of the products was done with gas chromatograph coupled with mass spectroscopy (GC-MS) and quantitative analysis of the products was done through Shimadzu gas chromatograph fitted with a capillary column.

3.3 RESULTS AND DISCUSSION

3.3.1 Acid catalysts

Scheme 3.1 represents the schematic representation of the synthesis of Si-MCM-48, Al-MCM-48 and Fe-MCM-48. During the course of present study, MCM-48 materials were synthesized at lower concentrations of the surfactant unlike the one reported by Mobil researchers where higher concentrations of the surfactant are mandatory. It was observed that addition of ethanol plays an important role as it directs the final structure. The role of ethanol is probably to stimulate transformation of MCM-41 to MCM-48 by allowing the proper condensation of silanol groups. To emphasize this point, the same procedure was adopted with out adding ethanol, which resulted in MCM-41 type of material only. Fig. 3.2a represents the XRD pattern of the material synthesized in the presence of ethanol and Fig. 3.2b represents the one synthesized in the absence of

ethanol. Ethanol thus facilitates the condensation process and directs the cubic interwoven structure.

3.3.2 Synthesis of H-(Al/Fe)-MCM-48

The calcined Na-MCM-48 samples thus obtained were stirred with 1M-ammonium acetate solution at 333 K for 24 h. This resulted in the exchange of Na^+ ions by ammonium ions. This exchange will be facilitated by increasing the temperature. The process was repeated thrice to ensure the complete exchange. The solid was then recovered by filtration and washed several times with distilled water to remove the ions present on the extra framework. The powder was then dried in an oven and calcined in air at 773 K for 6h to drive off the ammonia gas. Thus, H-MCM-48 samples were obtained. For comparison, the purely siliceous sample was also subjected to the ammonium acetate treatment in the same manner.

3.3.3 Powder X-ray diffraction study of H-MCM-48

The low angle X-ray diffraction patterns of the MCM-48 samples (Si, Al, Fe)-MCM-48 are given in Fig. 3.3 and 3.4. The diffraction pattern consists of peaks corresponding to (211), (220), (321) and (400) reflections, which can be assigned to a cubic MCM-48 lattice similar to the one reported by Beck et al. (1992). This XRD pattern is characteristic of the material with semicrystalline nature. The lattice parameter ‘a’ was calculated using the formula proposed by Beck et al.(1992)

$$a=d_{211}.\sqrt{h^2+k^2+l^2}$$

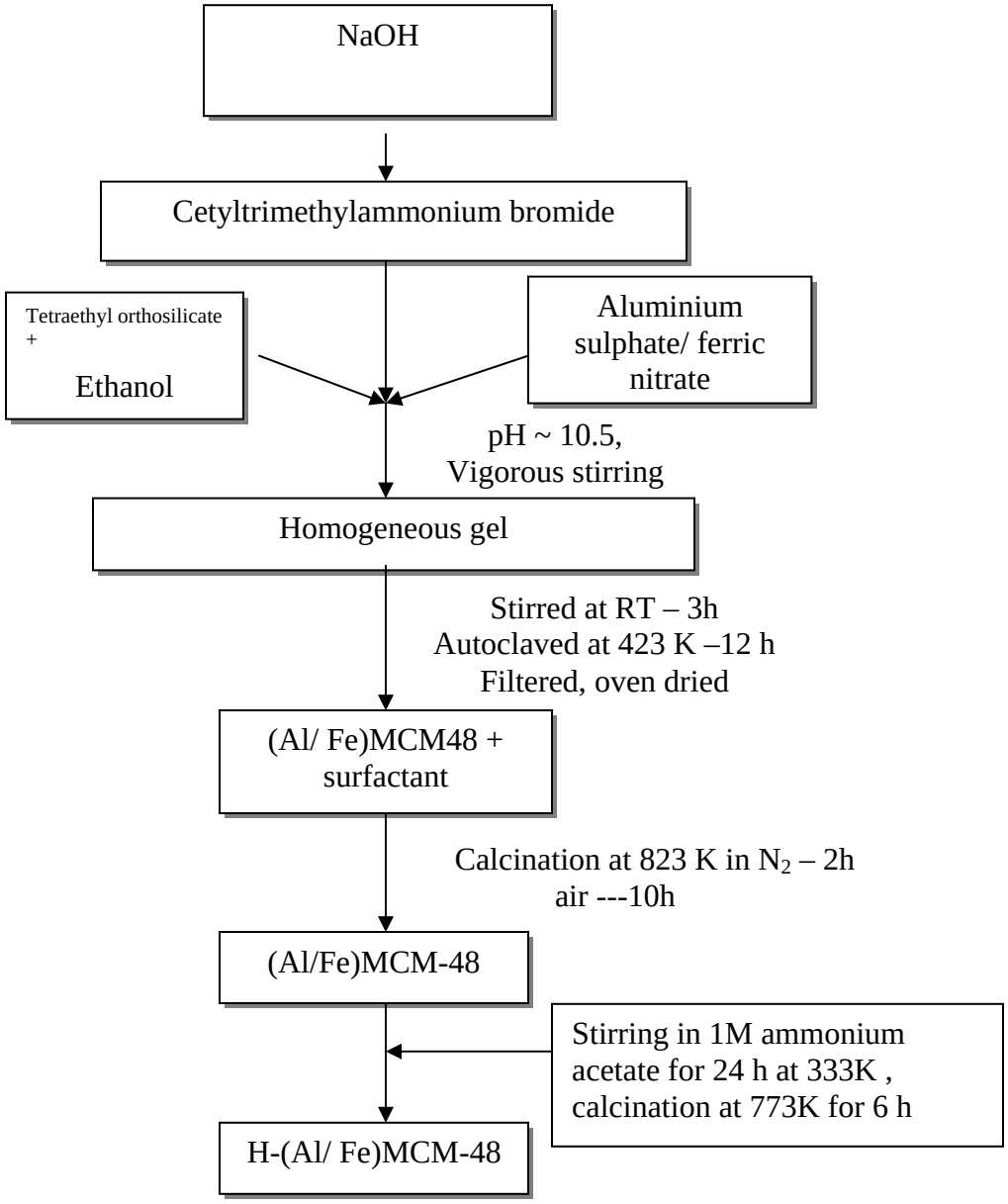

Scheme 3.1. Schematic representation of the synthesis of H-(Al/Fe)-MCM-48

The presence of a few peaks in the XRD pattern suggests the lack of long-range crystallographic order in these materials (Beck et al., 1992). These materials are thus different from zeolites, which are highly crystalline microporous materials. It is well known in the case of MCM-41 materials that with the incorporation of heteroatoms into the framework, the crystalline order of the parent material decreases. Higher loadings of heteroatom lead to the collapse of the structure. This is due to the fact that purely

siliceous material is found to posses pore wall with highly flexible O-Si-O linkages. Thus, substitution of heteroatom like Al results in less flexible O-Al-O linkages, which might give rise to defect structure with less crystallographic order. The XRD data along with cell parameter values are given in Table 3.1 from which it is clear that with the incorporation of heteroatom in the framework, the cell parameter value increases slightly. Even though this cannot be taken into account for the incorporation of subsequent atoms in the framework, it provides first hand information regarding the presence of heteroatom.

Table 3.1. XRD data of Si, Al and Fe-MCM-48 catalysts

Catalyst	d_{211} (uncalc.) Å	d_{211} (calc.) Å	a= d $(h^2+k^2+l^2)$ Å
Si-MCM-48	33.7	32.9	80.5
Al-MCM-48	33.69	32.75	80.22
Fe-MCM-48	34.75	33.1	81.07

It is well known that transition metal ions like Fe, V, and Ti etc., at higher loadings will result in the formation of extra framework oxides. Keeping this aspect in mind, the incorporation of the Al and Fe was restricted only to Al/M= 150 and 100.

Calcination of the as-synthesized MCM-48 (Fig.3. 4) did not result in collapse of the structure, in addition, the sample maintains the same XRD pattern with almost same intensity indicating that the sample is maintaining the same morphology even after calcination. However, a slight decrease in d_{211} spacing was observed indicating contraction of the structure during calcination. This type of contraction was also

observed by Beck et al. (1992), Janicke et al. (1998), Cheng et al., (1997) and Chen et al. (1993). However, in all these cases, the extent of contraction varies depending on the synthetic procedure. This contraction may be due to the recondensation of the inorganic matrix with the removal of the surfactant molecules from as-synthesized material.

Figure 3. 5. represents the XRD pattern of the NH_4-MCM-48 material. XRD pattern of NH_4-MCM-48 is similar to that of Na-MCM-48. This is due to the fact that mere cationic exchange of Na^+ and NH_4^+ did not affect the structure to a noticeable extent. However, calcination of NH_4-MCM-48 samples brought about a significant deterioration in the structure as revealed by XRD.

3.3.4 N_2 adsorption-desorption isotherms

N_2 adsorption-desorption isotherms provide information on the textural properties of the prepared catalyst in addition to the specific surface area and pore size distribution (Thomas, 1999; Rao, 1999; Storck et al., 1988). N_2 adsorption-desorption isotherms of calcined Si-MCM-48, Al-MCM-48 and Fe-MCM-48 are shown in Fig. 3.6. A typical type IV isotherm with a hysteresis loop was observed, which is characteristic of mesoporous solids (Beck et al., 1992; Corma et al., 1998; Chen et al., 1993; Branton et al., 1993). This hysteresis loop is due to the capillary condensation, in the mesopores. Adsorption at lower relative pressures (p/p_0) is due to the formation of monolayer of nitrogen molecules on the walls of mesoporous MCM-48. This followed by a sharp inflection, which is due to the capillary condensation within the mesopores (Hyde, 1996). From the sharpness of the step corresponding to the filling of the mesopores, once can expect a uniform pore size distribution. The relative pressure corresponding to the

inflection point is related to the diameter of the mesopores. The BET surface area values are tabulated in Table 3.2. In all these cases, the nature of the isotherm at lower relative pressures is same. Though the point of inflection corresponding to the capillary condensation within the mesopores differs, still it is not very significant. The catalysts studied show another inflection at higher relative pressure around $p/p_0 = 0.9$, which is due to macropore filling or to the filling of inter particle pores. This macro pores and inter particle pores resulted during the process of calciantion.

Table 3.2. N_2 adsorption data of Si, Al and Fe-MCM-48 catalysts

Catalyst	BET surface area (m^2/g)	Pore size (Å)	Pore volume (cc/g)
Si-MCM-48	1,020	28	1.01
Al-MCM-48	975	28.5	0.95
Fe-MCM-48	840	28	0.91

3.3.5 Thermogravimetric analysis (TGA)

The thermograms of the Si, Al and Fe incorporated MCM-48 materials are shown in Fig. 3.7. Thermogram of as-synthesized catalyst revealed different nature of interactions of the surfactant molecules with the framework species. In the case of siliceous MCM-48, a 45 % weight loss is observed in a three-step decomposition process. In the first step, the observed weight loss around 373 K is mainly due to the water, which is adsorbed on the catalyst surface. The second and main weight loss observed in the temperature range 423-623 K is due to the removal of the template, which is occluded in the mesopores. The final weight loss above 623 K is due to the removal of the water due to the

condensation of silanol groups (Antochshuk et al., 1998; Montes et al., 1998; Firouzi et al., 1997).

In the case of Al and Fe-substituted materials also, a similar trend was observed. Significant difference in the behavior of thermogram was not observed, as the amount of heteroatom is less in all the cases. This observation is in accordance with the literature (Janicke et al., 1998).

3.3.6 Infrared Spectroscopy

The lattice vibrations of the zeolite framework are observed in the range 400-1300 cm^{1}. IR spectra of pure Al-MCM-48 and Fe-MCM-48 materials in the region 4000-400 cm^{1} are given in Fig. 3.8. The vibration band at 1089 cm^{-1} is for the pure siliceous compound. In general, the band at 960-980 cm^{-1} can be taken as indication for the presence of heteroatom within the framework. In the case of both Al-MCM-48 and Fe-MCM-48, a band at 960 cm^{-1} was observed which confirms the presence of heteroatom in the tetrahedral framework. The assignment of the various frequencies observed is given in Table. 3.3.

Table 3.3. Assignment of various IR frequencies

Frequency in (cm^{-1})	Assignment
3739	ν_s (isolated Si-OH)
1635	ν_s (OH)
1230	ν_δ (H_2O)
1089	ν_{as} (Si-O)
960	ν_{as}(Si-O-Ti)
790	ν_δ (Si-O)
460	ν_{as}(Si-OH)

3.3.7 Temperature programmed desorption (TPD)

Temperature programmed desorption of ammonia serves as a dependable technique for the quantitative determination of the acid strength distribution. For TPD studies, palletized catalyst was activated at 700°C inside the reactor under nitrogen flow for half an hour. After cooling to room temperature, ammonia was injected in the absence of the carrier gas flow and the system was allowed to attain equilibrium. The excess and physi-sorbed ammonia was flushed out by a current of nitrogen. The temperature was then raised in a stepwise manner at a linear heating rate of about 20°C/min. The ammonia desorbed from 50°C to 600°C at intervals of 50°C was trapped in dilute sulphuric acid solution and estimated volumetrically by back titration with NaOH.

TPD profiles of the acid catalysts are shown in Fig. 3.9. The desorption of ammonia is monitored and depending upon the interaction of ammonia with acidic site, a

definite pattern is observed. Evolution of ammonia depends on the amount of heat energy required to break this interaction. TPD pattern of Al-MCM-48 shows the presence of three different types of acid sites. The sites present in the low temperature region are due to the attachment of ammonia to weakly acidic sites. These sites represent physi-sorbed hydroxyl groups. With increase of temperature, evolution of ammonia from moderately strong acid sites can be seen. Literature deals these sites as Bronsted acid sites (Kosslick et al., 1999). Similarly, at higher temperature, desorption of ammonia is due to the removal of chemisorbed ammonia from Lewis acid sites. Similar behavior is also observed in the case of H-Fe-MCM-48.

3.3.8 Transmission electron microscopic study (TEM)

In the case of porous solids, transmission electron microscopic study provides information regarding the surface morphology and pore structure. Detailed structural characterization has been done for MCM-41, MCM-48, SBA-1 and SBA-15 using TEM. In all these cases, the presence of the pore network has been clearly visualized.

TEM image of MCM-48 (Fig. 3.10) confirms the mesoporous nature of the catalyst synthesized and also supports the value as obtained from N_2 adsorption data of 28 A^o for the average pore size. In addition, transmission electron micrograph provides information regarding the arrangement of the pores. From Fig. 3.10, it is clear that the material formed in the present study possesses regular channels arranged in three dimensions.

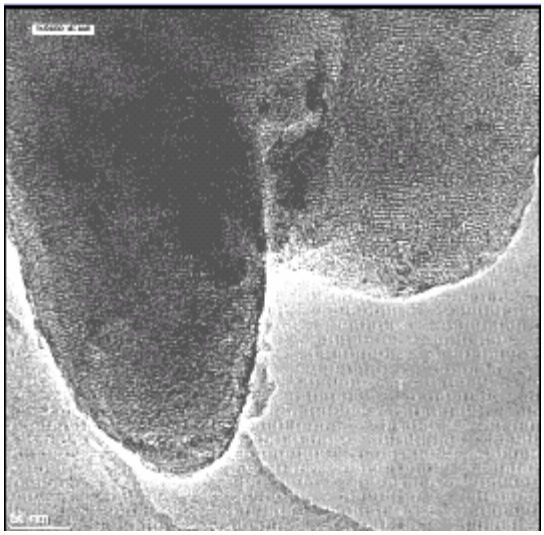

Fig. 3.10. TEM image of Si-MCM-48

3.3.9 UV-VIS (nujol)

If bulk oxides were present in less quantities, it would be difficult to use conventional techniques like XRD to identify the presence of these species in the material. However, UV-VIS can provide information regarding the presence of the heteroatom with in the framework even in such low concentrations. It also provides information regarding the environment of the heteroatom present in the framework. Especially, in the case of transition metal substituted molecular sieves, heteroatom can present either inside the framework or inside the cavity as bulk oxide. If the substituted species is present on the external surface, it can be easily identified through UV-VIS, by observing the weakly forbidden d-d transitions.

In this series, specific attention has been paid to incorporate iron in the molecular sieves like zeolites, $AlPO_4$ and mesoporous materials (Goldfrab et al., 1994; Park et al., 1992, Das et al., 1992, Badamali et al., 1998a; 1998b; Dapurkar et al., 2001; Selvam et al.,

2001; Mohapatra et al., 2002a). They have observed two prominent bands at 290 and 230 nm, which they have assigned to the charge transfer transitions arising from oxygen to metal ion. Several studies confirm the absence of extra framework bulk oxide species through UV-VIS by the absence of a band around 350 nm, which is due to the forbidden d-d transitions. Similar observations were also made in the literature for microporous ferrite and other iron substituted aluminosilicates (Goldfrab et al., 1994).

UV-VIS spectra of as-synthesized and calcined mesoporous Fe-MCM-48, which are recorded in nujol mode, are given in Fig 3.11. As-synthesized MCM-48 shows a band around 240 nm, which is also observed in clacined sample. Based on the earlier reports, this band is assigned to the ligand to metal charge transfer transition, indicating the presence of isolated FeO_4^- type species. Interestingly, in both uncalcined and clacined samples, the bands corresponding to d-d transitions are absent indicating the absence of extra framework bulk Fe_2O_3 species. On calcination, the band observed around 240 nm was retained indicating the presence of iron in the framework of calcined sample.

3.3.10 Electron Spin Resonance (ESR)

Since ferric iron is paramagnetic in both the low-spin and high –spin electronic configurations, ESR spectroscopy should be a method for characterizing the iron sites in zeolites and related materials like aluminophosphates (Goldfrab et al., 1994; Park et al., 1992, Das et al., 1992, Badamali et al., 1998a; Dapurkar et al., 2001; Selvam et al 2001; Mohapatra et al., 2002). The interpretation of the ESR spectra is difficult due to complications associated with the homogeneous broadening, which arises from the zero field splitting and over lapping signals (Wang et al., 2002b; Szegedi et al., 2001; Zhang et

al., 2001; Xu et al., 2001; Goldfrab et al., 1994). However, Badamali et al. (1998a) observed three different signals at g= 4.3, 2.0 and 2.02 which were assigned to the presence of iron in distorted tetrahedral, framework tetrahedral and octahedral environments respectively. The X-band ESR spectrum usually consists of three major signals at g= 4.3, 2.2-2.4 and 2.0. These signals have been assigned to the framework iron, iron in interstitial oxide or hydroxide phases and iron in cation exchange sites respectively (Fig 3.12). This assignment is also in accordance with the earlier observations (Stockenhuber et al., 2000; Zhao et al., 2001). The appearance of the signal at g= 4.3 has often been taken as evidence for the framework substitution in zeolites and AlPO's

3.4 CATALYTIC ACTIVITY

Catalytic alkylation of aromatics with a variety of alkylating agents has been the subject of extensive research because of the shape selective features of the reaction (Suji et al., 1994). Even though zeolites can perform a variety of shape selective reactions, their pore size limits their applications. Alkylation of polynuclear aromatics with lower olefins, alcohols and alkyl halides in general are carried out in the presence of mineral acid catalysts or Lewis acids, which yield non-selective product mixtures which are not environmentally acceptable (Olah, 1964).

Alkylation of naphthalene by zeolites, especially methylation has been studied extensively (Suji et al., 1994; Katayama et al., 1991; Frenkel et al., 1986; Komatsu et al., 1994). Frenkel et al. (1986) observed a higher conversion for vapour phase methylation of naphthalene over large pore zeolites *viz* H-M and H-Y in comparison to medium pore

H-ZSM-5. Diisopropylation of biphenyl and naphthalene in liquid phase have been studied by Katayama et al. (1991), Moraeau et al. (1992a & 1992b) and Suji et al. (1994). These studies have revealed that isopropylation takes place at 4, 4' positions of biphenyl, where as it is at 6,6' for naphthalene. Disubstituted naphthalenes are industrially important as they are the starting materials for the formation of polymers. Alkylation of naphthalene over acidic MCM-41 with alcohols was studied by Chakraborty et al. (1996). Alkylation of naphthalene with alcohols has been also studied by Kamalakar et al. (2000; 2002) over various acidic zeolites and they have observed MCM-41 exhibits lesser conversion when compared to zeoliets. Over zeolites, in general, alkylation was performed below 523 K either in liquid or gas phase, as at higher temperatures cracking and oligomerization reactions predominate giving undesirable products.

In the present study, gas phase alkylation of naphthalene was performed over Al and Fe-MCM-48 with n-propanol and n-butanol. This reaction is chosen to test the acid catalytic activity of these catalysts. The activities obtained are compared with that obtained on H-ZSM-5, H-Y, H-MCM-41. The temperature range chosen for the present study is 598-678 K. This temperature range would be ideal to test the stability of the synthesized catalysts, as it is known that these systems are not stable at higher temperatures. With this background the present study is aimed at studying the alkylation of naphthalene with n-propanol and n-butanol as alkylating agents.

3.4.1 Propylation of naphthalene

Data on the catalytic activity of propylation of naphthalene at various flow rates in the temperature range 598-673 K are given in Tables 3.4 and 3.5. At a given feed rate, it

was observed that the conversion of naphthalene decreases with increase in temperature. This decrease is predominant over H-Y zeolite when compared to mesoporous solids.

Propylation of naphthalene proceeds simultaneously by several mechanisms. The selectivity is determined by all these routes and as well as by the molecular sieving effects, when the catalysts employed are porous in nature. In the case of propylation of naphthalene both α and β positions are likely to be alkylated (Olah, 1964). Kinetic factors favour alkylation at α positions where as thermodynamic factors favor at β position. Even though, at initial stages alkylation takes place on α site, due to the peri interactions, the α product will be destabilized and there by results in more stable β alkylated naphthalene. Under the reaction conditions employed in the present study, over Al-MCM-48 and Fe-MCM-48 mainly monosubstituted products resulted. However, a little amount of 2,6 disubstituted products are also observed.

When the reactant molecules diffuse through the pores of the molecular sieves, there is a preferential adsorption of n-propanol over naphthalene on the acid sites of the catalysts thereby resulting in the formation of primary carbocation. As primary carbocation is relatively unstable, it isomerizes on strong acid sties to give a stable secondary carbocation. The formation of β-isopropyl naphthalene is as a result of the attack of stable secondary carbocation at β position of the ring, where as the formation of β-n-propyl naphthalene is due to the attack of the primary carbocation on the ring β position. This alkylation of naphthalene by these carbocations will follow Friedel-Craft's mechanism, which is given in Scheme 3.2. Among the catalysts employed, H-Al-MCM-48 shows higher activity when compared to H-Fe-MCM-48 and H-Al-MCM-41. This is

due to the fact that H-Al-MCM-48 will impose less diffusional constraints for the diffusion of the products. Since MCM-48 has three dimensional channel system, it will allow the products to diffuse easily through its channels.

At higher temperatures, conversion of naphthalene is less because the oligomerisation reaction is preferred on stronger acid sties of H-Y zeolites compared to other mesoporous solids. Thus, the conversion with respect to naphthalene is less over these zeolite catalysts. However, the observed activity is due to the presence of stronger acid sites on the surface of H-Y zeolite. At lower temperatures, it was reported that MCM-41 exhibits comparable activity to that of H-Y zeolite (Armengol et al., 1997)

Another interesting feature is the formation of n-propyl naphthalene on mesoporous catalysts. This observation can be explained based on the less acidity of mesoporous solids, which facilitates the stabilization of n-propyl carbocation. Since the isomerization of n-propyl to secondary propyl carbocation demands the need for stronger acid sties, complete conversion of the same might not be possible on the surface of mesoporous solid.

When the flow rate of the reactants is increased, the conversion of naphthalene is found to increase on all the catalysts studied. This is due to the fact that when the flow rate is less, the reactants will be in contact with the acid sites for a longer time, resulting in oligomerization reaction.

Table. 3.4. Propylation of naphthalene over acid catalysts

Catalyst	Temp. (K)	Conv. (%)	Product selectivity (%)		
			β-isopropyl naphthalene	β-n-propyl naphthalene	di-substituted naphthalene
H-Y	598	28.6	78.0	--	22.0
H-MCM-41	598	33.2	82.0	13.0	5.0
H-Al-MCM-48	598	34.1	84.1	9.5	6.4
H-Fe-MCM-48	598	32.8	71.9	22.1	--
HY	623	17.3	88.0	-	12.0
H-MCM-41	623	30.5	83.5	13.0	3.5
H-Al-MCM-48	623	30.5	85.0	10.0	5.0
H-Fe-MCM-48	623	29.4	72.5	27.5	--
HY	648	12.5	>99	--	--
H-MCM-41	648	30.5	83.5	13.0	3.5
H-Al-MCM-48	648	34.5	87.0	6.6	6.4
H-Fe-MCM-48	648	28.5	84.7	15.1	traces
HY	673	7.4	>99	--	--
H-MCM-41	673	18.7	96.0	--	4.0
H-Al-MCM-48	673	19.4	92.0	--	8.0
H-Fe-MCM-48	673	14.6	>99	traces	--

Reaction conditions: Weight of the catalyst=500 mg, Flow rate =10ml/h

Naphthalene: Alcohol= 1:100

Table. 3.5. Propylation of naphthalene over acid catalysts

Catalyst	Temp. (K)	Conv. (%)	Product selectivity (%)		
			β-isopropyl naphthalene	β-n-propyl naphthalene	di-substituted naphthalene
H-Y	598	34.6	80.0	--	--
H-MCM-41	598	35.8	84.5	15.1	traces
H-Al-MCM-48	598	37.5	83.5	12.8	3.7
H-Fe-MCM-48	598	34.0	87.1	12.9	--
H-Y	623	20.2	90.0		10.0
H-MCM-41	623	31.3	88.5	11.4	traces
H-Al-MCM-48	623	32.7	87.0	10.5	2.5
H-Fe-MCM-48	623	29.9	90.1	9.9	--
H-Y	648	15.0	95.0	--	4.7
H-MCM-41	648	27.4	90.0	9.8	traces
H-Al-MCM-48	648	27.4	87.5	11.5	1.0
H-Fe-MCM-48	648	25.6	91.1	8.9	--
H-Y	648	9.2	98.0	--	traces
H-MCM-41	673	24.0	89.1	10.2	traces
H-Al-MCM-48	673	24.7	90.2	9.5	traces
H-Fe-MCM-48	673	22.9	87.1	12.9	--

Reaction conditions: Weight of the catalyst=500 mg, Flow rate =12.5 ml/h

Naphthalene: Alcohol= 1:100

Mechanism

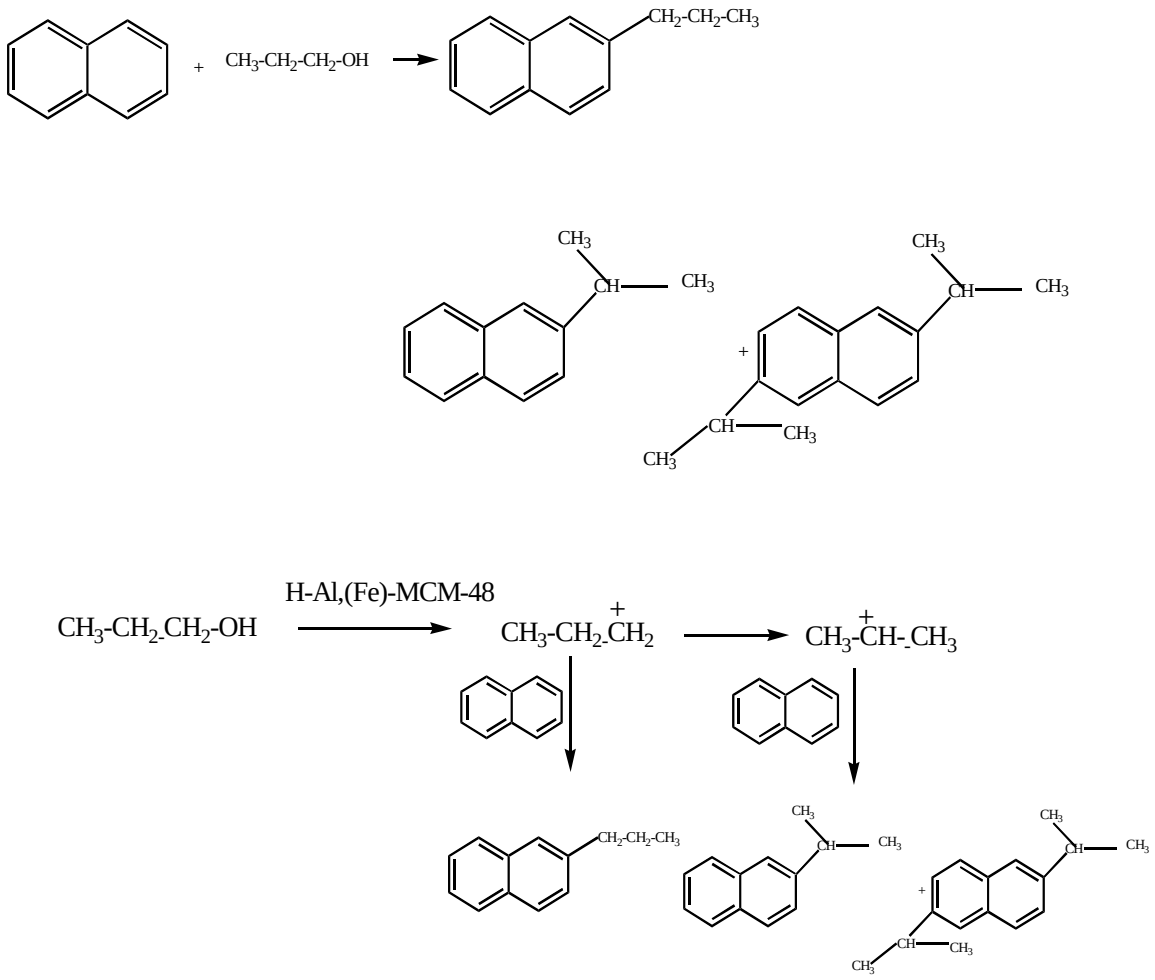

Scheme 3.2. Mechanism of propylation of naphthalene

3.4.2 Butylation of naphthalene

The results on the butylation of naphthalene in the temperature range 598- 673 K are given in Tables 3.6 and 3.7. It is observed that the results follow a similar a trend as that of propylation, except for the fact that over the catalysts studied, exclusive formation of

secondary butylated product is observed. This reaction is expected to follow the path shown in Scheme 3.3

The conversion observed for butylation of naphthalene reaction is lower when compared to propylation. H-ZSM-5 is not active for this reaction. This might be due to the fact that the pore diameter of H-ZSM-5 is around 0.54 nm, which might impose diffusional limitations. It is also interesting to note that n-butyl derivative of naphthalene is not observed over H-Al-MCM-48 and H-Fe-MCM-48. This is because n-butyl carbocation is unstable and it readily isomerizes to stable secondary carbocation, however this isomerization step depends on the strength of the acid sties. Among the mesoporous catalysts, H-Al-MCM-48 is more active when compared to its iron substituted cubic analogue.

Table. 3.6. Butylation of naphthalene over acid catalysts

Catalyst	Temp. (K)	Conv. (%)	Product selectivity (%)	
			β-isobutyl naphthalene	di-substituted naphthalene
H-Y	598	0.0	--	--
H-MCM-41	598	5.4	>99	traces
H-Al-MCM-48	598	5.4	95	5.0
H-Fe-MCM-48	598	4.9	>99	--
H-MCM-41	623	5.5	>99	--
H-Al-MCM-48	623	5.7	91.2	8.8
H-Fe-MCM-48	623	5.2	>99	--
H-MCM-41	648	5.5	>99	--
H-Al-MCM-48	648	6.4	92.0	8.0
H-Fe-MCM-48	648	5.1	>99	-
H-MCM-41	673	5.0	>99	-
H-Al-MCM-48	673	5.8	92.8	7.2
H-Fe-MCM-48	673	4.3	>99	---

Reaction conditions: Weight of the catalyst=500 mg, Flow rate =10ml/h

Naphthalene: Alcohol= 1:100

Table. 3.7. Butylation of naphthalene over acid catalysts

Catalyst	Temp. (K)	Conv. (%)	Product selectivity (%)	
			β-isobutyl naphthalene	di-substituted naphthalene
H-MCM-41	598	5.0	> 99	-
H-Al-MCM-48	598	5.4	95	5.0
H-Fe-MCM-48	598	4.5	>99	--
H-MCM-41	623	5.6	> 99	--
H-Al-MCM-48	623	6.0	97	3.0
H-Fe-MCM-48	623	5.2	> 99	--
H-MCM-41	648	5.0	> 99	--
H-Al-MCM-48	648	5.0	99	traces
H-Fe-MCM-48	648	4.8	> 99	--
H-MCM-41	673	4.8	> 99	--
H-Al-MCM-48	673	5.0	> 99	--
H-Fe-MCM-48	673	4.5	> 99	--

Reaction conditions: Weight of the catalyst=500 mg, Flow rate =12.5 ml/h

Naphthalene: Alcohol= 1:100

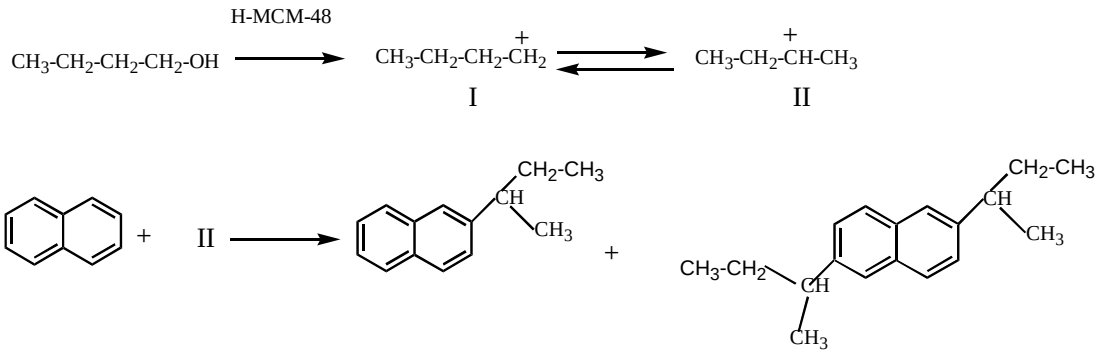

Scheme 3.3. Mechanism of butylation of naphthalene

3.5 SYNTHESIS OF REDOX M-MCM-48 CATALYSTS (M= Ti, V, Cr and Mn)

Depending on the conditions employed i.e. surfactant to inorganic precursor ratio, hexagonal MCM-41, cubic MCM-48 or lamellar MCM-50 can be synthesized. There have been a considerable number of publications and reviews dealing with the syntheses and catalytic activities of these materials (Uphade et al., 2002; Dellarocca et al., 2001; Pena et al., 2001, Oye et al., 2000; Tanev et al., 1994; Zhang et al., 1996a; 1996b). One can generate catalytic functionalities in these materials either by framework modification or pore modification. The framework modification can be achieved by isomorphous substitution, which can be achieved either by adding the required quantity of the heteroatom precursor during the synthetic gel formation, or after the synthesis, framework can be modified by grafting of various species followed by calcination (Tatsumi, 2000).

So far, hexagonal MCM-41 has been shown to be a potential catalyst for various selective reactions and it has been well exploited. Corma et al. (1994b) first synthesized Ti-MCM-41, which showed promising catalytic activity for various reactions. Later several publications dealt with the syntheses and catalytic activity of titanium substituted MCM-41 materials (Kayano et al., 1996&1997; Tatsumi et al., 1998; Blasco et al., 1995). In similar way, other transition elements like V (Chatterjee et al., 2001; Mathieu et al., 2000 & 2001a; Dejoz et al., 2001; Lee et al., 2000) and Cr have also been incorporated into the framework of MCM-41 (Sakthivel et al., 2001a; 2001b; 2002a & 2002b; Wang et al.,

2002a; Srinivas et al., 2002; Mahalingam et al., 1999). When compared to MCM-41, the other active member, MCM-48 has received less attention. This might be due to the fact that synthesis of MCM-48 demands conditions different from MCM-41 synthesis (Beck et al., 1992). But on careful observation, it would be clear that cubic MCM-48 is a better choice as catalyst or catalytic support, which would impose less diffusional limitations to the bulky substrates. With this back ground M-MCM-48 [M= Ti, V, Cr and Mn] materials have been prepared at lower concentrations of the surfactant and catalytic activity of the synthesized materials are tested for the hydroxylation of phenol under mild conditions.

3.6 SYNTHESIS OF M-MCM-48 [M= Ti, V, Cr and Mn] AND CHARACTERIZATION

Syntheses of MCM-48 materials have been carried out in the same manner given for the synthesis of Al and Fe-MCM-48. M-MCM-48 materials [M = Si, Ti, V, Cr and Mn] were synthesized under hydrothermal conditions at 423 K in a static stainless-steel autoclave. In a typical synthesis of M-MCM-48, to a 25% aqueous solution of cetyltrimethylammoniumbromide (CTAB) (S.D. Fine Chem.) tetraethylorthosilicate (TEOS, 98%, Merck-Schuchardt) was added along with the required amount of transition metal precursor. The pH of the gel was adjusted to 10.0-10.5. The typical molar gel composition was SiO2: M_xO_y: CTAB: Na_2O: EtOH: H_2O = 2.0: 0.015: 0.24: 0.5: 5.0: 195. The gel was stirred for 3h at room temperature and autoclaved at 423 K for 10 h. The solid product was filtered, washed several times with deionized water, oven dried and calcined for 1h in N_2 atmosphere followed by air at 823 K for 10 h. Pure silica materials were also prepared by the same procedure. Various characterization techniques

have been used to ensure the formation of cubic phase and as well as to understand the physico-chemical characteristics of the materials synthesized.

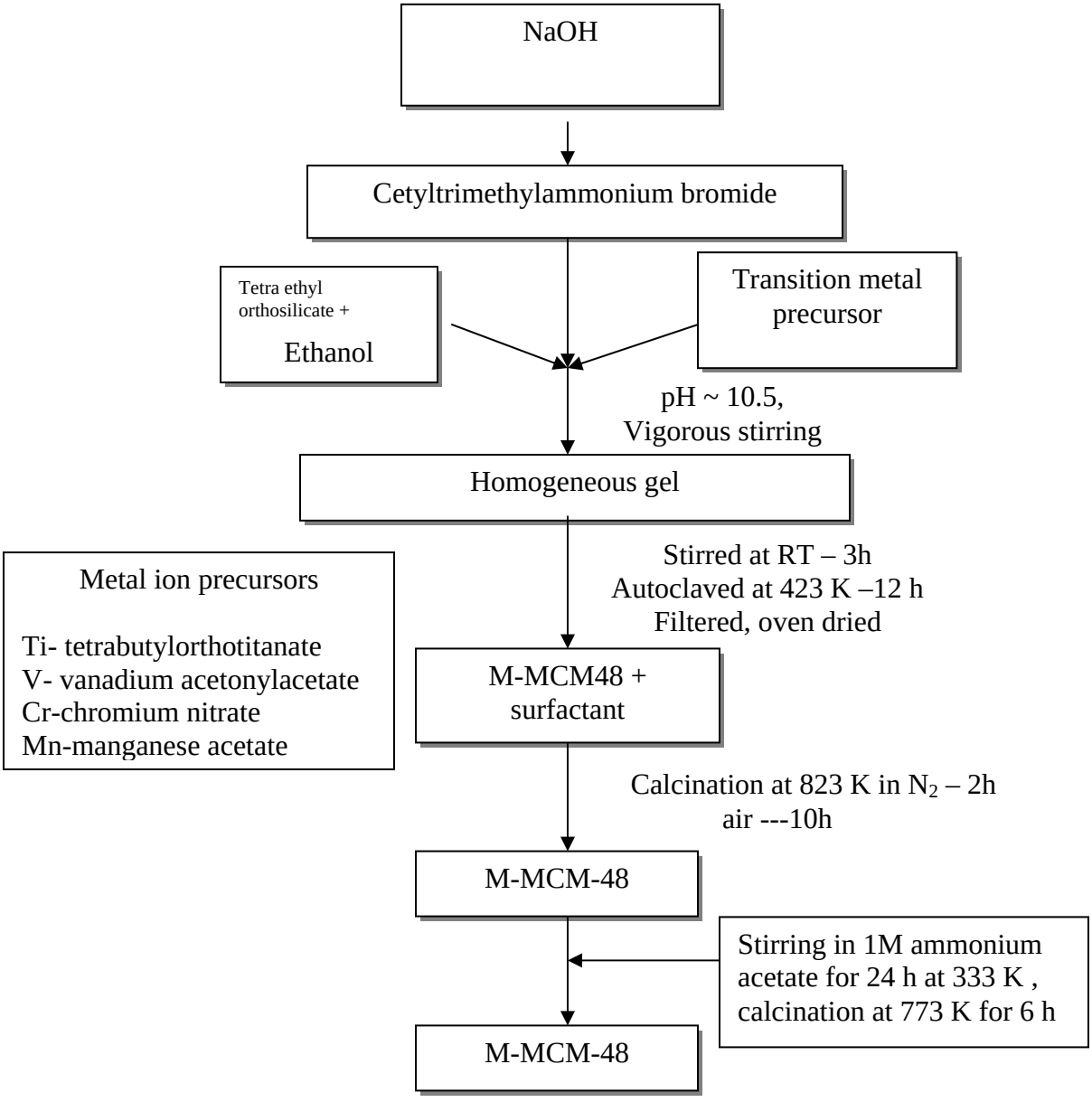

Scheme 3.4. Synthetic procedure for the preparation of Ti,V, Cr and Mn-MCM-48

3.6.1 Catalytic activity

Phenol hydroxylation was carried out in liquid phase in a three-necked round bottom flask equipped with reflux condenser. The reaction was performed at 333 K in different solvents such as water, acetone and acetonitrile. The temperature of the reaction was maintained by a thermostated oil bath. After each experiment the catalyst was filtered and dried. The dried catalysts were then calcined in air at 673 K for 6 h and reused. It was observed that the performance of the catalyst was not significantly affected even after two runs. After each experiment, XRD was recorded to examine the morphological changes. The catalyst maintained the same morphology after the completion of the reaction. The reaction products were identified by GC-MS (Hewlett-Packard, HPG 1800A GCD system, HP-5) and analysed by gas chromatography (Shimadzu GC-14A, 30m HP-5. FID).

3.7 RESULTS AND DISCUSSION

3.7.1 XRD

Low angle XRD patterns of the transition metal substituted mesoporous materials are given in Figures 3.13 and 3.14. It can be seen that highly ordered MCM-48 materials have been formed during the course of present study. Data on the XRD patterns of the Ti, V, Cr and Mn-MCM-48 materials are given in Table 3.8. The observed patterns can be indexed to a cubic lattice. As-synthesized Ti, V, Cr and Mn -MCM-48 show a maximum intense peak corresponding to 211 reflection whose d value decreased slightly upon calcination. This is due to the contraction of the unit cell during the calcination process, which is also reported in the literature (Beck et al., 1992; Corma et al., 1998).

From Table 3.8, it is clear that with incorporation of heteroatom in the framework of silica, a slight increase in the d_{211} spacing is observed, indicating the presence of the heteroatom within the framework. Upon calcinations also similar trends were observed indicating the presence of the various heteroatoms in the framework of silica. The cell parameter was calculated using the following equation

$$a= d_{211} .\sqrt{h^2+k^2+l^2}$$

Table 3.8. XRD data of [Si,Ti, V, Cr and Mn]- M-MCM-48

Catalyst	d_{211} (uncalc.) Å	d_{211} (calc) Å	a= $d\sqrt{(h^2+k^2+l^2)}$ Å
Si-MCM-48	33.7	32.90	80.50
Ti-MCM-48	34.5	32.90	80.50
V-MCM-48	35.3	33.45	81.95
Cr-MCM-48	35.9	33.65	82.42
Mn-MCM-48	36.4	34.10	83.52

One of the interesting features observed in the case of heteroatom incorporated MCM-48 is that with incorporation of heteroatom, the reflections at higher 2θ are not well resolved. This might be due to the fact that with incorporation of heteroatoms in the framework, the crystallinity of the MCM-48 decreases, thereby resulting in an increase in disorder of the MCM-48 network. This is also observed by various groups who dealt with the incorporation of the various transition metal ions into the framework of mesoporous materials. It is well documented in the literature that with this type of incorporation, the framework order of mesoporous solids decreases because of their semicrystallinity.

From Table 3.8, it can be seen that all the catalysts synthesized are of cubic in nature. Removal of the surfactant caused a slight decrease in d-spacing value of the maximum intense peak.

3.7.2 N_2 adsorption

Table 3.9 represents the data on the nitrogen adsorption-desorption isotherms of Si, Ti, V, Cr and Mn containing cubic MCM-48 materials. For comparison, data of the Si-MCM-48 are also given. In all the cases the isotherms are almost of the same type, clear type IV behavior, consistent with the earlier made observations (Beck et al., 1992; Corma et al., 1998; Morey et al., 1996; 2000). Figure 3.14 represents the adsorption –desorption isotherms of Si, Ti, V, Cr and Mn-MCM-48 catalysts. In each case, an initial increase in the uptake of nitrogen was observed which is due to uni-molecular adsorption on the catalyst surface. Adsorption at these relative pressures is due to monolayer adsorption of nitrogen on the walls of the mesopores. This monolayer adsorption is followed by a sharp increase in the uptake of nitrogen along with an inflection in the relative pressure of p/p_0 0.2-0.4. This inflection indicates the capillary condensation of the adsorbed nitrogen in mesopores, which signifies the multilayer adsorption behavior (Beck et al., 1992; Corma et al., 1998; Morey et al., 1996). Another inflection was also observed at p/p_0 close to 1. This inflection is due to the adsorption of nitrogen in macropores. In all the cases, a hysteresis loop was observed which is due to the capillary condensation. This type of hysteresis loop is characteristic of mesoporous materials with a slightly broad pore size distribution. In all the cases, pore size is distributed around ~ 28 Å. The BET surface area of the synthesized purely siliceous material is as high as 1020 m^2/g where as for Cr-MCM-48 it is minimum around 640 m^2/g. This decrease in the BET surface area with incorporation of heteroatom supports the observation made earlier by XRD studies. This decrease is due to the disorder in the pore texture with the incorporation of heteroatom in mesopore. This assignment is also in agreement with the literature reports.

Table. 3.9. Data on N_2 adsorption on M-MCM-48

Catalyst	BET surface (m^2/g)	Pore size(Å)	Pore volume (cc/g)
Si-MCM-48	1,020	28	1.01
Ti-MCM-48	953	28	0.85
V-MCM-48	745	29	0.77
Cr-MCM-48	640	29	0.70
Mn-MCM-48	850	28	0.87

The N_2 adsorption isotherms represented in Fig. 3.14 clearly indicate the formation of mesoporous materials.

3.7.3 Thermal analyses

The thermograms of Si, Ti, V, Cr and Mn-MCM-48 are given in Fig. 3.15. It can be seen in all the cases, a three-stage weight loss with a total weight loss of around 40 %. The three-stage weight loss can be explained as follows: The first weight loss in the temperature < 373 K is due to the physi-sorbed water, which is present in mesopores. The second and main weight loss in the temperature range 373-573 K is due to the removal of surfactant which has occluded into the mesopores and the final weight loss above 573 K is due to the removal of water formed due to the condensation of silanol groups (Beck et al., 1992; Antochshuk et al., 1998; Montes et al., 1998; Firouzi et al., 1997). All the mesoporous solids synthesized follow almost the same pattern indicating similar type of interaction between the surfactant and the inorganic precursor.

3.7.4 Infrared spectroscopy

Infrared spectroscopy provides information regarding the presence of heteroatoms with in the framework. The presence of a band around 960-980 cm^{-1} was often taken into the consideration for the presence of heteroatom. The assignments of various observed bands were already given in previous section. IR-spectra of Ti, V, Cr and Mn-MCM-48 are shown in Fig. 3.16 from which the band corresponding to Si-O-M [where M= Ti, V, Cr and Mn] can be clearly seen. This supports the presence of successive transition metals with in the framework of MCM-48.

3.7.5 UV-VIS (nujol)

UV-VIS spectroscopy provides information on the presence of transition metal ion either in the framework or on the external surface. If it is present as extra framework bulk oxide species, the forbidden d-d transitions will be observed, where as if it is located in the framework, a ligand to metal charge transfer band in general will be observed.

UV-VIS data of Ti, V, Cr and Fe-MCM-48 materials are summarized in Table 3.10. Fig. 3.17 represents the UV-VIS spectrum of as-synthesized and calcined Ti-MCM-48 recorded in nujol mode. As-synthesized material shows a band in the range 210-230 nm, which is also retained in the calcined material. This band is also observed by various groups on earlier studies for the incorporation of titanium in zeolitic as well as mesoporous frameworks. Tanev et al. (1994) first reported the synthesis of Ti-MCM-41 and successfully employed for the oxidation of 2,6 di-tert. butyl phenol and benzene with 30% H_2O_2. Corma's group (Blasco et al., 1995) also reported the synthesis of titanium containing MCM-41 where they have assigned this band to ligand oxygen to metal

charge transfer band. Thereafter, several groups claimed the synthesis of Ti-MCM-41 and in all the cases; this band was reported (Ahn et al., 1999, Rana, 1999; Stockenhuber et al., 2001). This band can be easily differentiated from the bulk TiO_2 whose UV-VIS spectrum after calcination around 550 ^oC is dominated by the band around 330 nm. This 330 nm band is characteristic of anatase phase (Tatsumi et al., 1998; Blasco et al., 1995).

With the success of titanium containing mesoporous solids for liquid phase oxidation reactions under mild conditions, attempts have been made to incorporate other transition elements into the framework of mesoporous solids. In this series, vanadium has been incorporated into the framework of mesoporous solid by Sayari group (Reddy et al., 1996). This catalyst was active for the liquid phase oxidation reactions. But later studies proved that most of the activity shown by this catalyst is due to the homogeneous catalysis which is taking place. Various groups also observed leaching of vanadium from the framework. However, by minimizing the loading of vanadium, truly heterogeneous nature of the mesoporous catalysts was reported by Zhang et al. (1996a), Lee et al. (2000), Srinivas et al. (2002), Sakthivel et al. (2001a & 2002b), Ye et al. (2002) and Davidson et al. (1992). In these cases, UV-VIS DRS provided the information on the presence of vanadium either in the framework or in the external surface (Wark et al., 1998; Hassan et al., 2000).

UV-VIS DRS spectra of V-containing mesoporous samples showed two prominent bands one around 340 nm, which is due to charge transfer band of V^{+4} to oxygen (Reddy et al., 1996) and another band around 250 nm due to the charge transfer band of oxygen to V^{+},[5] confirming the presence of vanadium in the framework. Similar observations were also

made by various other groups (Sivasankar, 1998; Pena et al., 2001; Sayari, 1996; Sakthivel et al., 2001a)

UV-VIS spectra of V-MCM-48 samples synthesized are shown in Fig. 3.18, which also shows two bands, one around 350 nm and another around 250 nm, confirming the presence of vanadium in the framework. However, these bands are clearly different from the extra framework V_2O_5 species, which will be observed around 650 nm.

Likewise, chromium substituted mesoporous materials have been synthesized by various groups. They used UV-VIS to confirm the presence of chromium in the framework. Ulagappan et al. (1996a) observed two bands in UV-VIS DRS of Cr-MCM-41. The first one, around 440 nm, due to d-d transition and another one around 370 nm on calcination, due to charge transfer transition between Cr (VI) to ligand oxygen, confirming the presence of chromium in tetrahedral network. Similar observations were made by Das et al., 1997 and Sakthivel et al., 2002b. From these observations it is clear that Cr(III) in as-synthesized sample mostly occupies extra framework sites. This is due to the fact that LFSE of Cr (III) in tetrahedral network is only 66.9 kJ/mol, which is lower than that of Cr (III) in octahedral environment whose value is 224.5 kJ/mol (West, 1988). Due to this energy difference, Cr (III) in tetrahedral network would be difficult to achieve.

UV-VIS (nujol) spectra of as-synthesized and calcined Cr-MCM-48 are shown in Fig. 3.19. As-synthesized sample shows prominent bands around 440 nm and 610 nm corresponding to the d-d transitions of octahedral hexavalent chromium. On calcination, chromium gets oxidized to higher oxidation states. This is confirmed by a charge

transfer band around 370 nm, which is due to the charge transfer transition between ligand oxygen to hexavalent chromium. This confirms the presence of chromium in the framework of calcined material. However, this oxidation of trivalent chromium to higher oxidation state varies from system to system and there are no clear explanations for the conditions to be employed for the complete oxidation to hexavalent state (Sakthivel et al., 2002a; 2002b, Ulagappan et al., 1996a; Mahalingam et al.,1999).

3.7.6 ESR spectroscopy

Electron spin resonance spectroscopy provides information regarding the presence of the heteroatom in different environments, which can be used in combination with other techniques to confirm the presence of paramagnetic ion in various environments. In general, ESR spectra will be recorded with DPPH, a highly symmetrical and stable radical whose g value will be observed around 2.0023. Any value close to this signifies, the presence of respective species in highly symmetrical environment. Even though extensive studies have been carried out on vanadium incorporated molecular sieves, successful incorporation of vanadium into the framework of molecular sieves is still controversial. Available studies reveal that only at liquid nitrogen temperature the anisotropic behavior of the sample can be seen clearly, which is characteristic of vanadium incorporated systems (Sen et al., 1996, Carrington et al.,1988). There are several reports on the vanadium containing molecular sieves using ESR spectroscopy for the detection of V (IV) in VASPO and VAPO-5, 11, 31, 37, 40 and 41 VPI-5 bonded strongly to oxygen ions in the matrix (Rigutto et al., 1993a; 1993 b; Jhung et al., 1990; Song et al., 1993).

Since V^{+4} has a spin of I = 7/2, it would exhibit eight line spectrum and the hyperfine coupling values depend on the nature of the host lattice. A detailed description was given by Carrington et al (1988). Sen et al. (1996) prepared the V-MFI in two different methods i.e. in acidic and basic conditions. ESR spectra of the acid synthesized materials showed an eight-line hyperfine spectrum with a broad background. The ESR parameters observed for this material are $g_{\parallel}$ = 1.935, $g_{\perp}$ = 1.982, $A_{\parallel}$ = 188.5 and $A_{\perp}$ = 82 G indicating that the vanadium is present in distorted octahedral coordination. These signals have been assigned to the VO^{2+} ions present in distorted Oh environment. On calcination, the signal intensity decreased along with narrowing of the signals. This is due to the fact that during the process of calcination, part of the total vanadium gets oxidized to V^{+5}, which is a d^0, ESR inactive state.

Data on the ESR spectra of V, Cr and Mn-MCM-48 materials are given in Table 3.11. The ESR spectra of as-synthesized and calcined V-AlPO samples recorded at liquid nitrogen temperature are shown in Fig. 3.20. An axially symmetrical signal of tetravalent vanadium was observed, which originated from the d^1 electron interaction with nuclear spin (I_n = 7/2) of ^{51}V. As-synthesized sample exhibits ESR signals with a broad background. The EPR parameters ($g_{\parallel}$ = 1.948, $g_{\perp}$ = 1.99, $A_{\parallel}$ = 191 G, $A_{\perp}$ = 70 G) indicate that V^{+4} is present in a distorted O_h environment (Sen et al , 1996, Carrington et al., 1988). Upon calcination, the signal intensity decreased and sharpness of the signal increased. This is due to partial conversion of V^{+4} to V^{+5} during calcination process. This also supports the observed band in UV-VIS in the region 285-340 nm. UV-VIS in combination with ESR studies confirms the presence of vanadium in calcined material.

Various literature reported systems utilized ESR to ensure the presence of chromium in the lattice of both silicates and aluminophosphates (Sakthivel et al., 2001b; 2002a; 2002b; Wang et al., 2002; Srinivas et al., 2002; Mahalingam et al., 1999). Even though, as-synthesized materials show a signal that corresponds to Cr(III) around g=1.98, the observations made are different over calcined materials. This is due to the fact that in some cases complete oxidation of Cr (III) to ESR inactive Cr(VI) takes place (Ulagappan et al., 1996a) and in some cases, incomplete oxidation of Cr(III) leads to a mixture to Cr(V) and Cr(VI) (Sakthivel et al., 2001b; 2002a; 2002b). In literature, for chromium substituted systems, the presence of a broad band around g= 1.98 was assigned to the presence of Cr (III) in extra framework species (Ulagappan et al., 1996a). The UV-VIS band around 440 nm further supports this observation. The presence of Cr(V) can be easily differentiated as it gives a signal around g= 1.97.

As- synthesized material shows a broad singlet with g value of 1.98, indicating Cr^{+3} ions in octahedral co-ordination (Fig. 3.21). The ESR spectrum of calcined mesoporous Cr-AlPO shows a g value at 1.97, characteristic of pentavalent chromium in tetrahedral or distorted tetrahedral co-ordination. In a similar way, in Cr-MCM-48 as-synthesized material, the presence of a broad signal around g~1.98 suggests the presence of trivalent chromium in octahedral coordination. On calcination, the signal intensity partially decreased, resulting in a narrow signal centered at g ~1.97 which is characteristic of pentavalent chromium in tetrahedral co-ordination. Similar observations were also made by Das et al.,1997 and Sakthivel et al., 2002b.

Kevan's group studied extensively on manganese substituted mesoporous solids like MCM-41 and MCM-48 and they have observed in the case of as-synthesized materials a

six line hyperfine spectrum with g= 2.007 and A= 97 G at 77 K (Xu et al., 1998; 1999). On calcination, Mn^{+2} species are oxidized to Mn^{+3} whose ESR spectrum would be difficult to record because of zero field splitting (Zhang et al., 2002; Xu et al., 1998; 1999; Zhao et al., 1995). There is some ambiguity on the location of Mn^{+3} species, which will be produced after calcination. It was also reported that after calcination, the species are present inside the cavities of mesoporous materials and not on the walls. However, partial oxidation of divalent manganese to trivalent was reported by Zhang et al. (2002) and Xu et al. (1998), where as complete oxidation was reported by Zhao et al., 1995. During the course of the present study, after calcination, ESR spectrum was not observed indicating the complete oxidation of Mn^{+2} to Mn^{+3}. In as-synthesized material, very less quantity of the material (Si/Mn ratio in the homogeneous gel was fixed to 100) might have been oxidized to higher oxidation state (Mn^{+3}), which is ESR in active.

3.8 CATALYTIC ACTIVITY OF M-MCM-48

Phenol hydroxylation(Ti,V,Cr ,Mn and Si)-MCM-48

Reaction conditions

Temperature = 333 K, Duration = 4 h,

Mole ratio of the reactants = phenol: H_2O_2: Solvent = 1: 1: 10

Table. 3.12. Hydroxylation of phenol in H_2O

Catalyst	Conv. of phenol (%)	Product selectivity (%)		
		Catechol	Hydroquinone	Para benzoquinone
Ti-MCM-48	12.65	51.4	43.3	5.3
V-MCM-48	10.50	50.5	41.7	7.8
Cr-MCM-48	10.60	50.7	40.7	8.6
Mn-MCM-48	10.65	51.5	40.4	8.1
Si-MCM-48	traces	--	--	--

Table 3.13. Hydroxylation of phenol in CH_3CN

Catalyst	Conv. of phenol (%)	Product selectivity (%)		
		Catechol	Hydroquinone	Para benzoquinone
Ti-MCM-48	10.25	52.6	31.3	16.1
V-MCM-48	4.46	50.7	22.7	26.6
Cr-MCM-48	4.96	59.1	20.0	20.9
Mn-MCM-48	7.86	51.5	18.7	29.8
Si-MCM-48	traces	--	--	--

Table 3.14. Hydroxylation of phenol in CH_3COCH_3

Catalyst	Conv. of phenol (%)	Product selectivity (%)		
		Catechol	Hydroquinone	Para benzoquinone
Ti-MCM-48	10.70	58.9	24.6	16.5
V-MCM-48	3.57	50.1	17.9	32.0
Cr-MCM-48	7.53	51.8	20.5	27.7
Mn-MCM-48	8.12	61.1	23.5	15.4
Si-MCM-48	0.00	--	--	--

Catalytic activity

Catalytic oxidation of aromatics has been widely used in the manufacture of fine chemicals. Phenol hydroxylation has been studied over various catalysts, which include both homogeneous and heterogeneous catalysts. Though these metal ions in homogeneous phase are active for diphenols production, the reaction rate and selectivity to diphenols are not appreciable (Sheldon, 1996 & Sheldon et al., 1998). Other than simple metal ions, metal complexes, have also been used. Though these metal complexes exhibit better catalytic activity and selectivity than metal ions, these complexes are not desirable for industrial applications due to shortcomings of handling and recovery of these homogeneous catalysts.

Homogeneous catalysts have also been immobilized in the cavities of well-defined microporous zeolites and used as catalysts for phenol hydroxylation. However, the results are disappointing due to the narrow pores of the host species. Zeolites containing

transition metal ions in their framework exhibit unique redox properties in oxidizing organic substrates with peroxides as oxidizing agents. The success of TS-1, a microporous titanosilicate, as selective oxidation catalyst with 30% H_2O_2 under milder conditions, has led to the synthesize molecular sieves containing transition metal ions other than titanium. However, applications of the microporous catalysts are limited due to their narrow pore sizes. In the present study, the catalytic activity of M-MCM-48 [M = Ti, V, Cr, Mn and Si] for phenol hydroxylation with 30 % H_2O_2 will be discussed.

Phenol hydroxylation has been carried out at 333 K in water, acetone and acetonitrile as solvents and the results are given in Tables 3.12, 3.13 and 3.14. It has been observed that all the catalysts are active for phenol hydroxylation and in all the cases, a mixture of catechol, hydroquinone and benzoquinone are formed. The formation of catechol and hydroquinone could be more likely due to electrophilic substitution of ($^{\cdot}$OH) on the benzene ring of phenol at *ortho* and *para* positions. Further oxidation of hydroquinone leads to benzoquinone. When the reaction is performed in the absence of solvent, conversion of phenol is low [< 2%] which indicates the requirement of the solvent. Among the solvents, water is a better solvent compared to acetone and acetonitrile for phenol hydroxylation. The reason may be that phenol and H_2O_2 can reach the active sites more easily in water medium than in the organic solvents. It has been observed that Ti-MCM-48 shows higher conversion compared to the other members. This could be due to optimized hydrophobic/hydrophilic environment of the pore walls of Ti-MCM-48. It has been observed that next to Ti, Mn substituted systems show better conversion, which may be due to high dispersion of Mn species in Mn-MCM-48, which is necessary for oxidation of phenol. Under the reaction conditions employed in the present study, Si-

MCM-48 shows very less activity. This might be due to the lack of active species, which can promote the hydroxylation of phenol.

3.9 CONCLUSIONS

Transition metal substituted derivatives of the cubic mesoporous MCM-48 have been prepared at lower concentrations of the template with good crystallinity. Among the acid catalysts, H-Al-MCM-48 shows higher activity for naphthalene alkylation with alcohols over H-Fe-MCM-48 and H-Al-MCM-41. All the four M-MCM-48 [M= Ti, V, Cr and Mn] catalysts are active for the hydroxylation of phenol giving rise to a mixture of catechol and hydroquinone/ para benzoquinone. Ti substituted systems show higher catalytic activity compared to the rest of the systems.

CHAPTER 4

SYNTHESIS, CHARACTERIZATION AND CATALYTIC ACTIVITY OF TRANSITION METAL INCORPORATED MESOPOROUS ALUMINOPHOSPHATES

4.1 INTRODUCTION

The structure directed syntheses of AlPOs started in 1982 with the introduction of the microporous aluminosphosphates, which are crystalline (Wilson et al., 1982). In general, the preparation of these materials is similar to zeolites in the sense of involvement of structure-directing templates. However, the synthesis of mesostructured aluminophospahtes, which will be discussed in this chapter, uses the so-called supra-molecular amphiphiles as the structure directing templates (Zhao et al., 1997, Chakraborty et al., 1997). Contrary to the microporous materials, materials prepared by supra-molecular aggregates, though periodically ordered, are amorphous with respect to their short-range atomic arrangements (Holland et al., 1997; Stein et al., 1997). Due to this reason, these materials are termed as semi crystalline solids.

One of the principle goals in the synthesis of mesostructured materials has been the utilization of these systems as potential heterogeneous catalysts. To meet this requirement various mesoporous systems were synthesized and characterized. In this series, next to silica based systems, aluminophosphates are important. Keeping the potential applications of microporous aluminophosphates in mind, various attempts have

been made to synthesize these aluminophosphates in mesoporous form, which are discussed in subsequent sections.

Feng and co-workers were the first to report the mesoporous aluminophosphates (Feng et al., 1997), who employed a procedure in which cetyltrimethylammonium bromide solution was mixed with aluminium isopropoxide and to this phosphoric acid was added in the presence of dilute hydrofluoric acid. The pH was maintained at 8.3 with tetramethylammonium hydroxide. The material thus synthesized has got Al/P ratio slightly greater than one and consists of a three-dimensional inorganic network in which the surfactant is arranged in hexagonally packed rod like arrays, comparable to that of MCM-41. However, the product turned out to be unstable after the removal of the surfactant. Zhao and co-workers (Zhao et al., 1997) synthesized mesoporous aluminophosphate by mixing appropriate amounts of cetyltrimethylammonium chloride, phosphoric acid and aluminium hydroxide under aqueous conditions by maintaining the pH at 8.5. They obtained a mesoporous solid with Al/P ratio slightly greater than one, thermal stability up to 1073 K and a BET surface area ~ 700 m^2/g. They also succeeded in incorporating silicon into the framework of mesoporous aluminophosphate under the same reaction conditions.

Chakraborty et al. (1997) reported the aqueous synthesis of hexagonal silicoaluminophosphate materials with surface area of ca. 900 m^2/g after calcination at 973 K. They used CTAC, H_3PO_4 and Al (O^i Pr)$_3$ under aqueous conditions at pH 2.5. Powder XRD data revealed that the degree of structural order in these materials is remarkably high. BET surface area values of these materials are as high as 900 m^2/g with pore size distributed around 30 Ă.

Particular attention has been paid to the synthesis of transition metal incorporated mesoporous alminophosphates due to their significance in redox catalysis (Luan et al., 1998a; 1998b; 1998c). Among the successful attempts, incorporation of Mn (Mn/Al up to 0.2) leads to a better thermal stability, where as V (V/Al up to 0.1) causes a decrease in structural order and stability. Kimura's group (Kimura et al., 1997; 1998a & 1998b) synthesized mesostructured aluminophosphates with hexagonal structure, utilizing the same raw precursors as used by Zhao et al. (1997). Calcination at 973 K resulted in a porous material with a BET surface area of ~ 450m^2/ g. Further studies proved that the final material has a maximum contribution from micropores than mesopores.

Another interesting attempt has been made by Holland et al. (1997; 1999), where in polyoxometalate clusters ($AlO_4Al_{12}(OH)_{24}(H_2O)_{12}^{7+}$, $GaO_4Al_{12}(OH)_{24}H_2O_{12}^{7+}$ have been used as the Al and Ga sources respectively. These positively charged clusters are precipitated as layer salts in the presence of an anionic surfactant at pH 3.0. The surfactant can be removed by calcination or by anion exchange and the reported surface area is 630 m^2/g. However, the poor thermal stability (only up to 623 K) limits the practical applications of this material. Among other significant contributions to this area, Khimyak et al.(2000a; 2000b; 2001, 2002) used CTAB under aqueous conditions to prepare tubular porous materials from H_3PO_4 and Al ($O^iPr)_3$. The material thus prepared has a high surface area of 990 m^2/g along with a broad distribution of pores in both micro- and mesoporous regions. Interestingly, the final materials had Al/P ratio less than one (in the range 0.6-1). Similar results were also reported by Kapoor et al. (2000), who prepared titanium containing mesoporous aluminophosphate, which showed promising

activity for epoxidation of various olefins with 30 % H_2O_2. The Al/P ratio in this material is greater than one i.e. 1.25.

Syntheses of mesostructured aluminophsophates have been reported in the recent past by various groups (Tiemann et al., 2000; 2001b;2002; Nieto et al., 2001; Rajesh et al., 2001; Klinowski, 2002). A few transition elements have been incorporated into the framework of mesoporous aluminophosphates. TiAlPO has been employed as a catalyst for the oxidation of aromatics under mild conditions (Zhao et al., 2001; Kapoor et al., 2000). Khimyak et al. (2001) have reported the synthesis of magnesium whereas Yuan et al. (2001) reported the incorporation of silicon and cobalt. Trivalent iron has been substituted by Mohapatra et al. (2002a), who successfully employed the same for the liquid phase oxidation of cyclohexane. The same group has also reported the cobalt substitution (Mohapatra et al.,2002b), which has been utilized for transfer hydrogenation reactions in liquid phase. The literature spans a wide range of different synthesis mechanisms, including the utilization of various surfactants (Chester et al., 2001; Bae et al., 2000; Kron et al., 1999; Perez et al., 1998; Galanos et al., 1998). However, in most of the cases, main emphasis has been given for the synthesis and characterization, but not for the catalytic activity of the resulting systems (Tiemann et al., 2000; 2002; Masson et al., 2001; Thomas et al., 2001; Cabrera et al., 2000; D' Arbonneau et al.,1999). Kuroda's group synthesized mesoporous aluminophosphates using a variety of surfactants (Kimura et al., 1998a; 1998b; 1999a; 1999b). The purpose of the present investigation is to rationalize the synthesis conditions for the preparation of V, Cr and Fe substituted mesoporous aluminophosphates and subsequent catalytic activity of the resulting materials particularly for oxidation reactions.

4.2 EXPERIMENTAL

4.2.1 Synthesis of mesoporous AlPO & V-AlPO

The mesoporous aluminophosphates were synthesized under hydrothermal conditions in a stainless steel autoclave. Mesoporous aluminophosphates and vanadium incorporated AlPOs were prepared using CTAB (S.D. Fine Chem.) as surfactant and vanadium acetonylacetate (Fluka) as the vanadium precursor. The schematic representation of the synthetic procedure is given in Scheme 4.1. In a typical synthesis, to 4.2 g of aqueous solution of phosphoric acid, 3.53g of aluminium hydroxide was added under vigorous stirring. Stirring was continued for 30 minutes and this mixture was added to an aqueous solution of vanadium precursor. Finally, after stirring for one more hour, surfactant solution (12 g of CTAB in 100ml water) was added and stirring was continued further. In optimized synthetic procedure, the resulting gel was aged at room temperature for 3-12 h, which was found to have the following gel composition. $0.95Al_2O_3$: $1P_2O_5$: $0.05V_2O_5$: 0.4-0.5 CTAB: 300 H_2O. After ageing at room temperature, the resulting gel was transferred into a stainless steel autoclave and hydrothermally treated in an oven at 423 K for 24 h. The autoclave was removed from oven, cooled to room temperature. The solid was collected after filtration, washed with plenty of water and oven dried. It was observed that calcination was the preferred route to remove the surfactant from as-synthesized material. It was also observed that the precursors of aluminium and the base source play an important role in the successful formation of the desired aluminophosphates. To ensure this point, influence of various parameters was also studied. Various sources of aluminium have been tried and aluminium hydroxide was chosen as the source. The pH of the gel was maintained at 9.5 with tetra methyl

ammonium hydroxide, as the use of other sources like NaOH and NH_4OH resulted in amorphous materials. This might be due to the fact that, the small cations like Na^+ and NH_4^+ compete with the negatively charged inorganic precursor and thereby decreasing the sufficient interaction of the later with the cationic surfactant, CTAB. The solid was filtered, washed several times with de-ionized water and calcined at 773 K for six hours to remove the organic template. The calcination was performed in nitrogen atmosphere

for first two hours followed by air in order to preserve the semicrystalline nature of these materials. Pure aluminophosphate was also prepared under the same conditions.

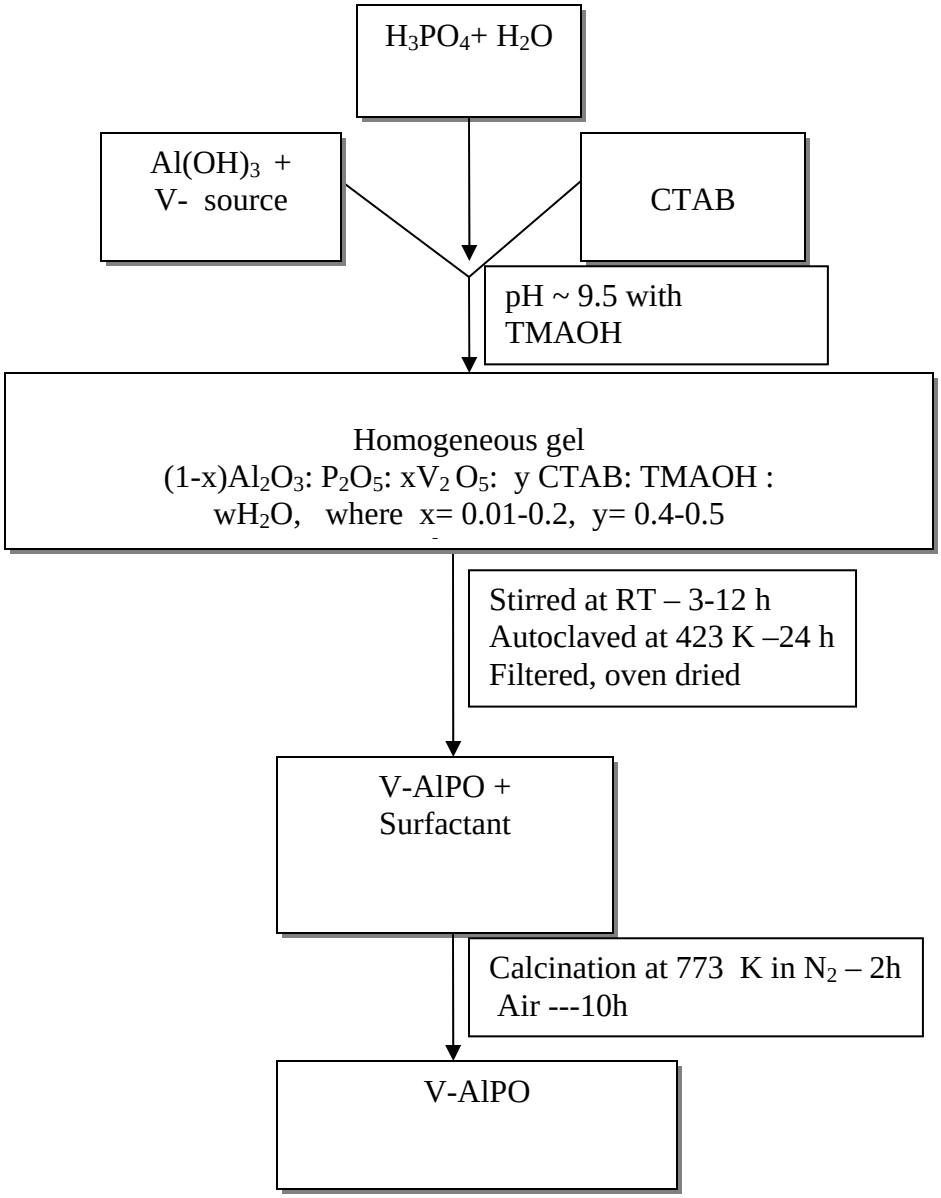

Scheme 4.1. Representation of the preparation of mesoporous aluminophosphates

4.2.2 Characterization and catalytic activity

Various techniques have been used for the characterisation of the materials synthesised. For all the mesoporous aluminophosphate materials, in order to confirm the formation of the mesophase, the low angle X-ray diffraction patterns of the samples were recorded on a Siemens D 500 ($\theta/2\theta$) using monochoromatised Cu Kα radiation (λ = 1.5406 Å) with a scan speed of 1^o/ min over the range $2<2\theta<10^o$. ICP-AES was done with Labtam Plasma Lab 8440. Thermal analyses of the samples were made with thermal analyser (Perkin Elmer model TGA 7) at a heating rate of 20 ^{o}C/min. Diffuse reflectance UV-VIS DRS spectra were recorded on Cary 5E UV-VIS-NIR spectrophotometer. ESR spectra were recorded with Varian E–112 spectrometer at liquid nitrogen temperature (77 K). N_2 adsorption–desorption measurements at 77 K were made using CE instruments, Sorptomatic 1990. The samples were out gassed at 473 K for 12 h. X-ray photoelectron spectroscopic measurements (XPS) were performed on PHI-550 ESCA-System (Perkin-Elmer GmbH).

Oxidation of toluene was carried out at 333K in a three necked round bottomed flask under reflux conditions using 70 % TBHP as oxidant. Acetone, acetonitrile and methanol were used as solvents. The temperature was maintained by a thermostated oil bath. After each experiment, XRD was recorded to examine the morphological changes. The reaction products were identified by GC-MS (Hewlett-Packard, HPG 1800A GCD system, HP-5) and analysed by gas chromatograph (Shimadzu GC-14A, 30m HP-5. FID).

4.3 RESULTS AND DISCUSSION

4.3.1 XRD

In general, low angle X-ray diffraction data will provide the information regarding the formation of the mesophase. The XRD patterns of mesoporous AlPO and V-AlPO materials are given in Fig. 4.1 and 4.2. As-synthesized mesoporous AlPO shows a maximum intense peak with d-spacing value 33.2 Å, which corresponds to the 100 reflection. Upon calcination in air, d_{100} spacing decreased to 32.1 Å. This decrease is due to the contraction of the unit cell during the calcination. This type of decrease in d spacing is known for mesoporous materials (Beck et al., 1992; Corma et al., 1994a; Feng et al., 1997). Being semi crystalline in nature, these mesoporous solids tend to undergo this sort of contraction during the calcination process. The observed XRD patterns have been indexed to uni-dimensional hexagonal lattice characteristic of MCM-41 type structure. The presence of a few peaks in the XRD pattern suggests lack of strict crystallographic order in these materials. These materials thus differ from the existing microporous zeolites as the later are highly crystalline in nature having well defined sharp peaks in their XRD patterns. In a similar manner, mesoporous as-synthesised V-AlPO material also shows a maximum intense peak corresponding to (100) reflection with d-spacing value of 34.5 Å followed by a broad peak corresponding to (110) and (200) reflections that can also be indexed to a hexagonal lattice. After calcination, the intensity of d_{100} of mesoporous V-AlPO slightly decreased to 33.0 Å, which is in agreement with the previously made observations that during the process of calcination structural contraction will take place. However, the sample retained its hexagonal structure after calcination.

An organic base, tetramethylammonium hydroxide (25% TMAOH), was used to maintain the pH of the gel. The pH of the gel was maintained at 9.5, since at lower pH amorphous

materials resulted. It was observed that mild basic conditions are required to produce the hexagonal aluminophosphates. During the procedure employed in the present study, mesoporous AlPO resulted only at a pH > 9.0 whereas in the acid pH conditions, amorphous materials resulted. Under the reaction conditions, more likely, a modified S^+--I^- ion-pair process will be operative. The inorganic precursors are non-ideal aluminophosphate species of low degree of polymerisation with some hydroxyl groups. When tetramethylammonium hydroxide is added, it reacts with the hydroxyl groups of these aluminophosphates to produce a weak ion-pair of the type I^-.TMA^+, since TMA^+ has got larger ionic radius it facilitates such a formation. These ion-pair species diffuse to the surfactant assembly interface and interact strongly with the cationic surfactant head groups. The interaction of the aluminophosphate species with TMA^+ is strong (Luan et al., 1997b). During the process of ageing, condensation process and polymerisation of adjacent aluminophosphate species takes place to form an ordered hexagonal mesostructure. The function of organic ammonium cation from TMAOH is probably to modify the strength of the electrostatic interactions between the aluminophosphate species and the cationic surfactant micelle assembly to form the S^+ I^- / TMA^+ ion pair. However, with NaOH or NH_4OH only amorphous materials were formed. If either NaOH or NH_4OH is used, the smaller cation Na^+or NH_4^+ competes with the aluminophosphate species and thus restricts the interaction with the positively charged cationic surfactant (Zhao et al., 1997). Figures 4.3 & 4.4 represent the XRD patterns of as-synthesized materials prepared using NaOH and NH_4OH as bases, which clearly highlight the need to proceed with a mild base like TMAOH. As stated earlier, aluminium hydroxide may form a less polymerised aluminophosphate with many

hydroxyl groups and favour the assembly of the mesostructure compared to other aluminium sources. The same observation was also made by Zhao et al. (1997), who used aluminium hydroxide to produce the mesoporous solid. No collapse of the structure was observed after calcination. This suggests that no residual carbon could be formed under the calcination conditions.

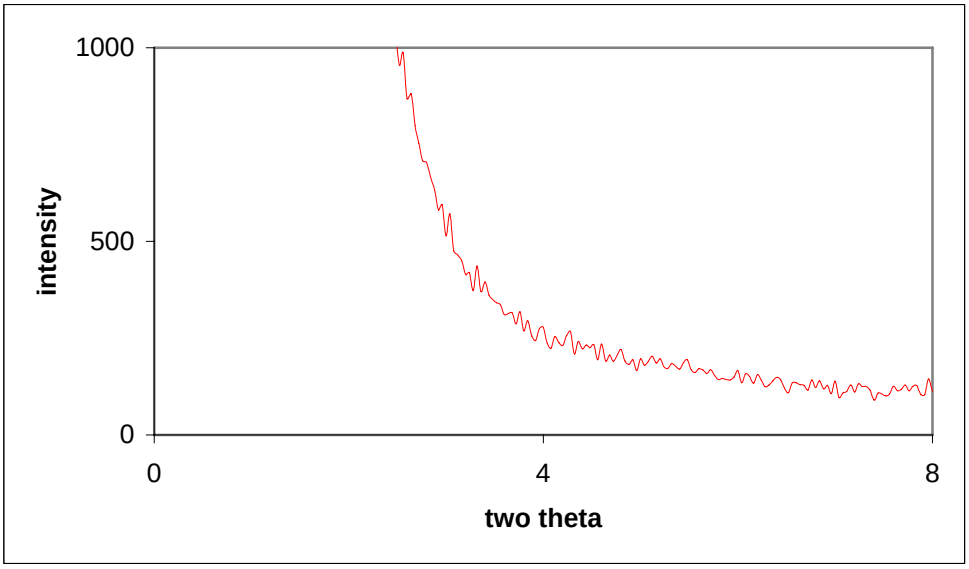

Fig. 4.3. XRD pattern of mesoporous AlPO prepared with NaOH

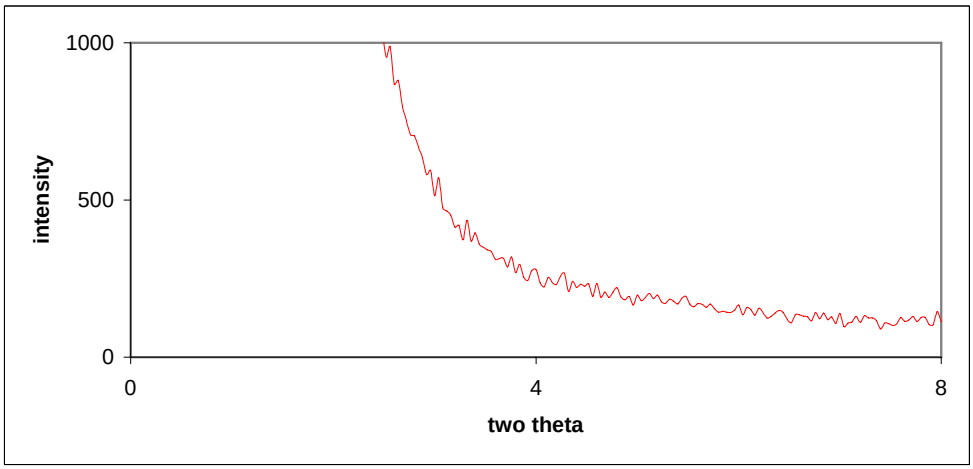

Fig. 4.4. XRD pattern of mesoporous AlPO prepared with NH_4OH

4.3.2 N_2 adsorption

Nitrogen adsorption- desorption data provide information regarding the porous nature and the surface area of the materials prepared. Figure 4.5 represents the nitrogen adsorption-desorption isotherms of mesoporous aluminophosphate and vanadium substituted analogue recorded at liquid nitrogen temperature (77 K). These two isotherms are simple and do not differ much from each other. The low-pressure region ($P/P_0 < 0.25$) refers to the monolayer formation region followed by sharp inflection that corresponds to capillary condensation. The high-pressure regions are marked by sharp inflections suggesting capillary condensation occurring in the macropores or intercrystalline regions formed during the calcination process. The values of BET surface area along with pore size distributions are given in Table 4.1 in comparison with the same heteroatom substituted aluminosilicate analogue (whose synthesis is given in detail in chapter 3). It can be seen that the surface area values of mesoporous aluminophosphates are less compared to silicate analogues indicating the less degree of thermal stability.

Table 4.1. Physico-chemical data of vanadium substituted mesoporous solids

Catalyst	d [uncalc] Å	d [calc] Å	a= Å	BET surface area (m^2/g)	Pore size (Å)	Pore volume (cc/g)
AlPO	33.2	32.1	37.47[1]	695	28	0.65
V-AlPO	34.5	33.0	38.10[1]	650	28	0.65
MCM-48	33.7	32.9	80.50[2]	1,020	29	0.99
V-MCM-48	35.30	33.45	81.95[2]	745	28	0.77

1----$a= 2d_{100}/\sqrt{}$

2----$a= d_{211}.\sqrt{(h^2+k^2+l^2)}$

The BET surface area values computed form the isotherms is around 695 m^2/g with a pore size distributed around 28 Å clearly indicating the mesoporous nature of the prepared aluminophosphate. In the case of V-AlPO material, N_2 adsorption isotherms show typical hysteresis loop characteristic of mesoporous materials. The existence of a small hysteresis indicates disorder in shape. BET surface area of V-AlPO is 650 m^2/g; with an average pore size of 28 Å. In both the cases, the isotherms are intermediate between type I and type IV isotherms, which is to some extent contradictory to that of siliceous materials where a strict type IV isotherm is observed. Similar observations were also made by Kapoor et al., 2000; Zhao et al., 1997 ; 2001b; Luan et al., 1998b, who assigned this type of trend based on the irregular pore structure of these materials. This confirms that textural order of mesoporous aluminophosphates is to a slight degree less than that of mesoporous aluminosilicate materials (Tiemann et al., 2001b).

4.3.3 Thermal analysis

The problem associated with earlier reports on mesoporous aluminophosphate preparation was the removal of the surfactant. Though, technically it is possible to prepare these materials with a variety of surfactants like cationic (CTAB), anionic (acid derivatives) and neutral species (tri-block polymers and primary amines), the one prepared with cationic surfactant appears to be a better one. This is due to the fact that proper condensation of the inorganic species gives a solid material with high framework thickness, which directly reflects in thermal stability of the prepared material. In the case of the surfactants other than CTAB, to an extent, it is possible to remove the surfactant either by extraction with proper solvent or by

the calcination at ambient temperatures. But with CTAB, complete removal of the same could be achieved only by the calcination process. Keeping this point in mind, an attempt was made, where care was taken to preserve the final structure by adopting controlled calcination. At initial stages the calcination was performed in nitrogen atmosphere followed by heating in air at 823K. The thermogram for AlPO samples (Fig. 4.6) in the temperature range 323-1073 K, shows mainly three weight loss regions and total weight loss corresponds to 40 %. This weight loss includes a first region at 353-393 K corresponding to the loss of physi-sorbed water. The second and main weight loss in the region 493-533 K corresponding to the removal of the template and the final one above 533 K corresponds to the loss of water due to condensation of the hydroxyl groups (Antochshuk et al., 1998; Montes et al., 1998; Firouzi et al., 1997). It is observed that AlPO samples are stable up to 1073 K unlike the earlier reported value of 973 K. A similar weight loss behaviour was observed for V-AlPO material. Figure 4.7 represents the thermogram of the V-AlPO material in the temperature region 323-1073 K. In the case of V-AlPO also three-weight loss regions are observed which corresponds to the loss of physi-sorbed water, surfactant and the removal of water due to the condensation of the hydroxyl groups respectively.

4.3.4 UV-VIS nujol

Ultraviolet visible spectroscopy provides information regarding the presence of the heteroatom. With this technique, it is possible to ascertain the location even though it cannot be taken as the confirmatory evidence. But UV-VIS data in combination with other data obtained with techniques like ESR and XPS can indicate the

presence of the transition metal either in framework or extra framework positions. There has been a large interest in synthesizing vanadium analogous of molecular sieves both in aluminosilicates and aluminophosphates because of their potential redox behaviour, which can be tuned as per the demand. Though vanadium incorporation in aluminosilicates and aluminophosphates is known for decades (Sen et al., 1996; Haanepen et al., 1997; Weckhuysen et al.,1996; Blasco et al., 1995; Escalante et al., 1997; Centi et al., 1992, Moudrakovski et al., 1994) , still it is a matter of controversy due to the tendency of incorporated vanadium to leach into the solution under experimental conditions. In most of the cases, the observed catalytic activity of V- substituted molecular sieves is mainly reported due to the homogeneous catalysis and not due to true heterogeneous nature. Reddy et al. (1996) synthesized vanadium substituted mesoporous material through neutral templating mechanism and based on the results they have concluded that more than 80 % of the framework substituted vanadium leached out into the solution and contributed to the homogeneous catalysis. Various researchers (Sheldon et al., 1998; Hartmann et al., 1999) concluded that true isomorphous substitution in molecular sieves is still a questionable matter. However, they have also stated that this could be controlled to some extent through incorporating a small amount there by generating isolated sites, which will promote the desired reaction in heterogeneous manner. In mesoporous solids also the same problem was reported by various researchers (Pena et al., 2001; Reddy et al., 1996, Selvem et al., 2001; Wark et al., 1998; Hassan et al., 2000; Sung et al., 1990). In spite of these controversies some reports claimed the true isomorphous substitution of vanadium

in the framework sites. For these considerations, UV-VIS provided valid information.

The presence of distinct bands in UV-VIS spectrum confirms the presence of the heteroatom and its environment. In the present study, the UV-VIS spectra of the as-synthesised and calcined AlPO samples are given in the Fig. 4.8. As-synthesized V-AlPO shows a band in the region 250-285 nm characteristic of V^{4+} charge transfer band of VO_2^+ species. The same observation was also made by various groups for microporous VAPOs (Sen et al., 1996; Centi et al., 1992; Moudrakovski et al., 1994; Cavani et al., 1988). However, the presence of an additional band between 285-340 nm confirms the presence of V^{5+} in T_d environment. This confirms the fact that during the process of synthesis, part of the vanadium, which was present in tetravalent state, gets oxidized to pentavalent state. This is in agreement with earlier observations (Pena et al 2001, Sen et al 1996; Rigutto et al., 1993a; 1993b; Song et al., 1993; Jhung et al., 1990). Reddy et al. (1996) also observed similar spectral features for V-HMS samples and they also considered these bands, which arise due to the presence of vanadium in the network. It can be seen from the Fig. 4.8c that the observed bands are different from the bulk V_2O_5 suggesting the incorporation of the heteroatom with in the framework of the mesoporous AlPO. Sen et al. (1996) also observed these two bands in the UV-VIS spectrum of the V-in MFI molecular sieve. Based on these observations, the first band can be assigned to the charge transfer transition arising from ligand to metal and the second one around 330 nm is due to the presence of vanadium in tetrahedral coordination.

4.3.5 ESR spectroscopy

Electron spin resonance spectroscopy provides information regarding the presence of the heteroatom in different environments. Though extensive literature is available on vanadium incorporated zeolite systems, only a few reports devoted to ESR studies (Rigutto et al., 1993a; Luan et al., 1998a 1998 b; Jhung et al., 1990; Song et al., 1993; Davidson et al., 1992; Sung et al., 1990; Hassan et al., 2000). Available studies reveal that only at liquid nitrogen temperature the anisotropic behaviour of the sample can be seen, which is characteristic of vanadium incorporated systems (Sen et al., 1996, Carrington et al., 1988). Since V^{+4} has a spin of I = 7/2, it exhibits eight line spectrum. The hyperfine coupling values depend on the nature of the host lattice. A detailed description was given by Carrington et al (1988). Sen et al. (1996) prepared the V-MFI in two different methods i.e. in acidic and basic conditions. ESR spectra of the synthesised materials in acid medium showed an eight-line hyperfine spectrum with a broad background. The ESR parameters are found to be $g_{\parallel} = 1.935$, $g_{\perp} = 1.982$, $A_{\parallel} = 188.5$ and $A_{\perp} = 82$ G which indicate that the vanadium is present in distorted octahedral coordination. They have assigned these signals to the VO^{2+} ions present in distorted Oh environment. On calcination the signal intensity decreased along with narrowing of the signals. This is due to the fact that during the process of calcination, part of the total vanadium gets oxidised to V^{+5}, which is a d^0 state. Various groups have also made similar observations (Sakthivel et al., 2001a; Haanepen et al., 1997; Reddy et al., 1996; Pena et al., 2001; Luan et al., 1998a).

The ESR spectra of as-synthesised and calcined AlPO samples recorded at liquid nitrogen temperature are given in Fig. 4.9. It exhibits an axially symmetrical signal

of tetravalent vanadium, which originated from the d^1 electron interaction with nuclear spin (I_n = 7/2) of ^{51}V. As-synthesised sample exhibits ESR signals with a broad background. The EPR parameters ($g_{||}$ = 1.948, $g_{\perp}$ = 1.99, $A_{||}$ = 191 G, $A_{\perp}$ = 70 G) indicate that V^{+4} is present in a distorted O_h environment (Sen et al , 1996, Carrington et al., 1988; Luan et al., 1998a). Upon calcination, the signal intensity decreased and sharpness of the signal increased. This is due to partial conversion of V^{+4} to V^{+5} during calcination process. This also supports the observed band in the region 285-340 nm in UV-VIS spectrum.

4.3.6 XPS

X-ray photoelectron spectroscopy provides the information regarding the oxidation state as well as the surface composition of the catalytic systems. Extensive studies have been carried out on vanadium incorporated zeolites (Wark et al., 1998) and aluminophosphate (Hassan et al., 2000; Sung et al., 1990, Luan et al., 1998a) systems and in all these cases, XPS was proved to be a versatile tool not only in identifying the surface composition but also in finding out the oxidation state of the various species.

The XPS spectrum of calcined V-AlPO in V_{2p} region (515-518 eV), shown in Fig.4.10 indicates two peaks: one corresponding to V^{+4} at 516 eV and other corresponding to V^{+5} at 517.4 eV. This confirms that during calcination partial oxidation of vanadium takes place. XPS in combination with UV-VIS DRS and ESR data confirm the presence of both +4 and +5 oxidation states of vanadium.

4.3.7 Oxidation of toluene over V-AlPO

Having synthesized and characterized the V- incorporated aluminophosphate, the catalytic activity was tested for the partial oxidation of toluene with both 30 % H_2O_2 and 70 % TBHP as oxidizing agents. The observed catalytic activity was compared with that of vanadium substituted silicate analogue MCM-48 whose synthesis and characterization were discussed in the chapter 3. The oxidation of toluene with 70 % TBHP as oxidising agent was carried out with V-AlPO and V-MCM-48 at 333 K in a variety of solvents and the results are summarised in Tables 4.2 and 4.3, respectively. The oxidation of toluene produced benzaldehyde, benzoic acid and benzyl alcohol with high selectivity towards aldehyde. Interestingly, under the reaction conditions employed for the oxidation of toluene with TBHP, it was observed that both V-AlPO as well as V-MCM-48 have not produced any detectable amount of cresols indicating that these catalysts are promising side chain oxidation catalysts. When the reaction was performed in the absence of solvent, conversion and selectivity were low. This may be due to the fact that the products that were formed on the active sites might not have diffused out. It was observed that acetone was a better solvent for oxidation of toluene with TBHP compared to other solvents like acetonitrile and methanol. This could be due to the solubility of the initially formed polymer products in acetone (Saji et al., 1998). In order to examine the catalytic activity due to leached metal ions, in a separate experiment, the reaction mixture was filtered after 2 h in hot condition and the experiment was continued with the filtrate. Increase in conversion was not observed, indicating homogeneous catalysis is not taking place under the reaction conditions. The results obtained are compared with results on various heterogeneous catalytic systems reported in

literature like V-AlPO-31 (Flenigen et al., 1986), Cr-S-1 (Singh et al., 1996), VS-1 (Rao et al., 1992) and VAPO-5 (Rigutto et al., 1993a) and are summarized in Table 4.4. From the table, even though it appears that VAPO-31 has higher conversion (44%), the selectivity to side chain oxidation product is less compared to mesoporous materials. The oxidation of toluene over mesoporous catalysts produced benzaldehyde/acid and benzyl alcohol with high selectivity towards aldehyde/acid (up to 97%). Interestingly, under the reaction conditions employed no cresol was detected over V-AlPO or V-MCM-48 indicating that these catalysts are promising side chain oxidation catalysts. Among the mesoporous catalysts, V-AlPO showed a slightly higher conversion and selectivity over aluminosilicate analogue. This could be due to the higher dispersion of active species in mesoporous aluminophosphate network. The stability of vanadium containing mesoporous aluminophosphate materials for liquid phase oxidation reactions with TBHP suggests that the aluminophosphate framework (Al^{+3}, r = 0.053 nm) can accommodate vanadium ($V^{+4/+5}$, r = 0.059/0.046 nm) centres in a better way than the silicate framework (Si^{4+}, r = 0.040 nm) of MCM-48.

Table 4.2. Catalytic activity of V-AlPO for toluene oxidation with 70% TBHP (Catalyst = 100 mg, Substrate: TBHP: Solvent = 1: 2: 5 (mole ratio), T= 333 K, t= 6h)

Solvent	Conversion (%)	Product selectivity (%)			
		Benzal-dehyde	Benzoic acid	Benzyl alcohol	Others
None	8.5	78.5	16.5	2.0	3.0
Acetone	27.4	76.5	20.4	3.1	---
Acetonitrile	21.5	73.3	22.8	3.9	--
Methanol	14.3	39.0	26.1	6.3	28.6[a]
Acetone(1st recycled)	22.5	76.1	19.5	4.4	--

Table 4.3. Catalytic activity of V-MCM-48 for toluene oxidation with 70% TBHP (Catalyst = 100 mg, Substrate: TBHP: Solvent = 1: 2: 5 (mole ratio), T = 333 K, t= 6h)

Solvent	Conversion (%)	Product selectivity (%)			
		Benzal dehyde	Benzoic acid	Benzyl alcohol	Others
None	5.5	71.4	20.0	5.1	3.5
Acetone	23.2	74.4	21.1	4.5	--
Acetonitrile	19.4	70.9	23.9	2.5	3.0
Methanol	11.2	34.4	24.0	10.5	31.1[a]
Acetone (1st recycled)	20.1	75.0	21.3	3.7	--

Table 4.4. Comparative activity of V-AlPO with some literature reported systems

Catalyst	Temp (K)	Conv. Of Toluene (%)	Product selectivity (%)			
			(o / p) cresols	Benzaldehyde / Benzoic acid	Benzyl alcohol	Others
VAPO-31	303	44.0	---	65.0	6.0	29.0
V-AlPO[a]	333	21.5	---	96.1	3.9	--
V-MCM-48[a]	333	19.4	---	94.5	2.5	3.0
Cr-S-1	353	18.4	0.7	28.5	25.7	45.1[#]
VAPO-5	343	13.0	---	89.0	5.0	6.0
VS-1	353	8.3	8.0	58.0	24.8	---
Cr/S-1	353	3.3	5.6	57.4	37.0	---
Blank	353	2.1	---	>99	---	---

Reaction conditions: weight of the catalyst = 100 mg,

Solvent ---acetonitrile, reaction duration (t) = 24 h

[a] reaction duration ---6 h; # -- dibenzyl

For comparison, the same reaction has been performed with 30 % H_2O_2 with acetonitrile as solvent and the results are given in Table 4.5. V-AlPO is found to be more active and selective towards benzaldehyde over other V-substituted molecular sieves. Considerable quantity of cresols has been observed in all the cases. The catalytic activity of V-AlPO was compared with that of V-MCM-41 and V-MCM-48. It was observed that V-MCM-

48 shows a slightly higher conversion when compared to V- MCM-41. The data on the comparative activity of various catalytic systems like V-Al-Beta (Sen et al., 1995), V-MCM-41 (Chatterjee et al., 1999), vanadium peroxo complex (Mimoun et al., 1983) and heteropolyacids (Athilakshmi et al., 1996) for the oxidation of toluene with 30% H_2O_2 in acetonitrile are given in Table 4.6. Homogeneous catalysts show higher activity for toluene oxidation, their selectivity being higher for ring oxidation giving cresols as major products. However, heterogeneous catalysts show higher selectivity to side chain oxidation giving aldehyde/acid and alcohol. Under the reaction conditions employed, among the heterogeneous catalysts, V-AlPO exhibits higher conversion (28.4%) with higher selectivity (~78%) to side chain oxidation products. This could be due to the interwoven network of cubic MCM-48 where the diffusional constraints are less compared to the one-dimensional hexagonal MCM-41 network. The higher activity of V-substituted mesoporous materials suggests high dispersion of vanadium in mesoporous framework, which is a prerequisite for the oxidation reactions.

Table 4.5. Comparative activity of various catalysts for toluene oxidation with 30 % H_2O_2 (Catalyst = 100mg, Toluene: 30 % H_2O_2 : Acetonitrile = 3:1:10, T= 353 K, t= 24h)

Catalyst	Conversion (%)	Product selectivity (%)					
		Benzal dehyde	Benzoic acid	Benzyl alcohol	O-Cresol	P-Cresol	Others
V-AlPO	28.4	64.4	8.8	4.0	12.0	9.8	1.0
V-MCM-48	22.7	67.2	6.0	1.5	15.5	10.5	4.0
V-MCM-41	20.8	62.0	--	2.0	20.0	14.0	2.0
V-Al-Beta	14.0	56.0	--	4.0	21.0	17.0	2.0
VS-1	11.7	52.2	--	7.7	19.7	17.1	3.7
V-AlPO(1st recycled)	24.6	65.0	5.6	4.0	11.8	10.1	3.5

Table 4.6. Comparative activity of V-AlPO with some literature reported systems

Catalyst	Temp (K)	Conv. Of Toluene (%)	Product selectivity (%)			
			(o / p) cresols	Benzaldehyde / acid	Benzyl alcohol	Others
V-AlPO[a]	333	28.4	21.8	73.2	4.0	1.0
V-MCM-48[a]	333	22.7	25.5	68.5	1.5	4.0
V-MCM-41[a]	333	20.8	34.0	62.0	2.0	2.0
V-Al-Beta[a]	333	14.0	38.0	56.0	4.0	2.0
VS-2[a]	333	11.7	36.8	52.2	7.7	3.7
Vanado peroxo complex	303	52.0	96.2	3.8	--	---
$H_4PVMo_{11}O_{40}$	303	21.6	89.2	10.1	< 1	--
$H_5PV_2Mo_{10}O_{40}$	303	25.6	91.5	7.7	<1	--
$H_6PV_3Mo_9O_{40}$	303	48.3	91.6	8.4	--	--
$H_5PV_2Mo_{10}O_{40}$	331	35.4	91.4	8.6	--	--

Weight of the catalyst = 100 mg; solvent –acetonitrile,
duration of the reaction (t) = 3 h
[a]duration of the reaction (t) = 18 h

4.4 CONCLUSIONS

The incorporation of vanadium in the framework of aluminium phosphate materials has been achieved through structure directing template route. Vanadium (V^{4+}/V^{5+}) substituted AlPO's have been shown to be promising oxidising catalysts with 70 % TBHP and 30 % H_2O_2 as oxidising agents. V-AlPO showed higher activity as compared to that of other similar porous materials like V-MCM48 and V-MCM 41.

4.5 MESOPOROUS Cr-AlPO

4.5.1 Introduction

Transition metal incorporated molecular sieves have been the subjects of extensive research over the decades due to their potential use as catalysts and sorption capacities. Among heterogeneous catalysts, zeolites and related materials received considerable attention because of their promising potential applications. Heteroatom incorporated aluminosilicates and aluminophosphates are important class of heterogeneous catalysts. Metal substituted molecular sieves also appear to be more stable towards leaching of the metal compared to conventional supported catalysts. This is probably due to more difficult accessibility of the M-O bonds, which attach the metal to the surface. Situating the catalytic site on the internal surface of a molecular sieve also provides the possibility for shape selective catalysis. Further, the size and hydrophobic/hydrophilic character of the redox cavity can be fine-tuned to give tailor made catalysts that replicate enzymes. Hence, such materials can be regarded as mineral enzymes or so called zeozymes.

The first example of a redox molecular sieve is TS-1, developed by Enichem workers (Notari, 1991), where titanium is isomorphously substituted in place of silica. Later, various heteroatoms have been incorporated into lattices of both silicates and phosphates. In this connection, heteroatom substituted aluminophosphates have received greater attention due to their potency as catalytic material. Starting with titanium, more than half of the elements in the periodic table have been incorporated into both silicate and phosphate lattices (Sheldon et al., 1998; Hartmann et al., 1999). Inspite of the fact that aluminophosphates are recyclable promising class of microporous solids, they have received lesser attention. The reports on these molecular sieves have started appearing

only in 1982 (Wilson et al., 1982) unlike the aluminosilicates, which were reported as early as in sixties. Among the known reported heteroatom incorporated aluminophosphates, V, Cr , Mn, Fe and Co – incorporated systems are of particular interest because of various reasons. On the surface of these catalysts, the oxidation-reaction in general, can proceed either in oxometal pathway or in peroxometal pathway (Hartmann et al., 2000). Chromium is an example of a redox metal that typically involves an oxometal species as the intermediate. Moreover, stoichiometric hexavalant chromium oxidants are widely used in organic synthesis. Inspite of the serious environmental problems associated with chromium-containing waste, still effort has been focused on the use of catalytic amounts of chromium in conjunction with oxygen donors such as *tert*.butylhydroperoxide (TBHP). However, the separation problems made the heterogeneous catalysis to be preferred over the conventional homogeneous catalysis.

Selective oxidation of alkylbenzenes is one of the interesting and challenging reactions in organic chemistry, due to the importance of the products for various industrial applications. Both homogeneous and heterogeneous catalysts have been used for these reactions. But, for the large-scale production of fine chemicals, replacement of conventional homogeneous systems by heterogeneous systems will be advantageous, in the sense of catalyst recovery and reduction of undesirable side reactions.

In literature, Cr-AlPO-5 and Cr-AlPO-11 are shown to be recyclable redox catalysts with oxidants like TBHP or molecular oxygen (Sheldon, 1996; Sheldon et al, 1998; Hartmann et al., 1999). One of the striking features of Cr-substituted systems is that these systems promote oxidation in presence of molecular oxygen. Microporous Cr-AlPO material was shown to be an active and recyclable catalyst for the oxidation of saturated and

unsaturated hydrocarbons with either TBHP or O_2 (Raja et al., 2000). Even though several groups have claimed the incorporation of chromium in the aluminophosphate network, the extent of the chromium present in tetrahedral network was questioned only later. This is due to the fact that isomorphous substitution requires tetrahedral coordination of Cr (III), which is rare in inorganic complexes because the crystal field stabilization energy of octahedral Cr (III) (224.5 kJ/mol), is greater than that of tetrahedral Cr (III) (66.9 kJ/mol) (West, 1988). Therefore, tetrahedral coordination of Cr (III) in aluminophosphates is difficult to achieve. In literature, though there are several claims regarding the synthesis of Cr-AlPO's only limited effort was made to characterize these materials in a convincing manner.

In spite of this ambiguity, Cr- substituted microporous catalysts are potential and unique oxidation catalysts. However, the activity of microporous catalyst is limited due to its narrow pore size and stability of the active metal ion in the microenvironment. In fact, the potential of chromium containing porous solid catalysts in liquid phase is limited because of the leaching of the active metal from the framework (Sakthivel et al., 2001b). Moreover, it is always desirable to choose molecular oxygen as oxidant due to its availability in nature. Use of molecular oxygen as oxidant can increase the applications of chromium containing catalysts. Since the reaction is taking place in gas-phase, the leaching of chromium from the framework can be avoided. Thus the present study is devoted to the synthesis and characterization of the Cr-Substituted mesoporous aluminophosphate material. The catalytic activity of Cr-AlPO will be discussed for the partial oxidation of toluene using molecular oxygen. In the second part of the work,

liquid phase oxidation of ethylbenzene and benzyl alcohol over mesoporous Cr-AlPO material with 70 %TBHP as oxidant will be discussed.

4.6 EXPERIMENTAL

4.6.1 Synthesis of mesoporous Cr-AlPO

The mesoporous chromium incorporated aluminophosphates were synthesized under hydrothermal conditions in a stainless steel autoclave by adopting the same procedure used for the synthesis of mesoporous aluminophosphates. CTAB (S.D. Fine Chem.) was used as surfactant and chromium nitrate nonahydrate as the chromium precursor. In a typical synthesis, to an aqueous solution of phosphoric acid, aluminium hydroxide was added under vigorous stirring. This was continued for 30 minutes and this mixture was added to an aqueous solution of chromium nitrate . Finally after stirring for one more hour, surfactant solution was added and stirring was continued further. In optimized synthetic procedure, the resulting gel was aged at room temperature for 3-12 h and the resulting gel was found to have the following gel composition. $0.95Al_2O_3$: 1.00 P_2O_5: $0.05Cr_2O_3$: 0.40-0.50 CTAB: 300 H_2O. After ageing, the resulting gel was transferred into a stainless steel autoclave and hydrothermally treated in an oven at 423 K for 24 h. The autoclave was removed from oven, cooled to room temperature, solid was collected after filtration, washed with plenty of water and oven dried. The influence of various parameters was also studied. As reported in the previous case, various sources of aluminium have been tried and finally aluminium hydroxide was chosen as the source. The pH of the gel was maintained at 9.5 with tetra methyl ammonium hydroxide, as the use of other sources like NaOH and NH_4OH have led only to amorphous materials. The solid was filtered, washed several times with de-ionized water.

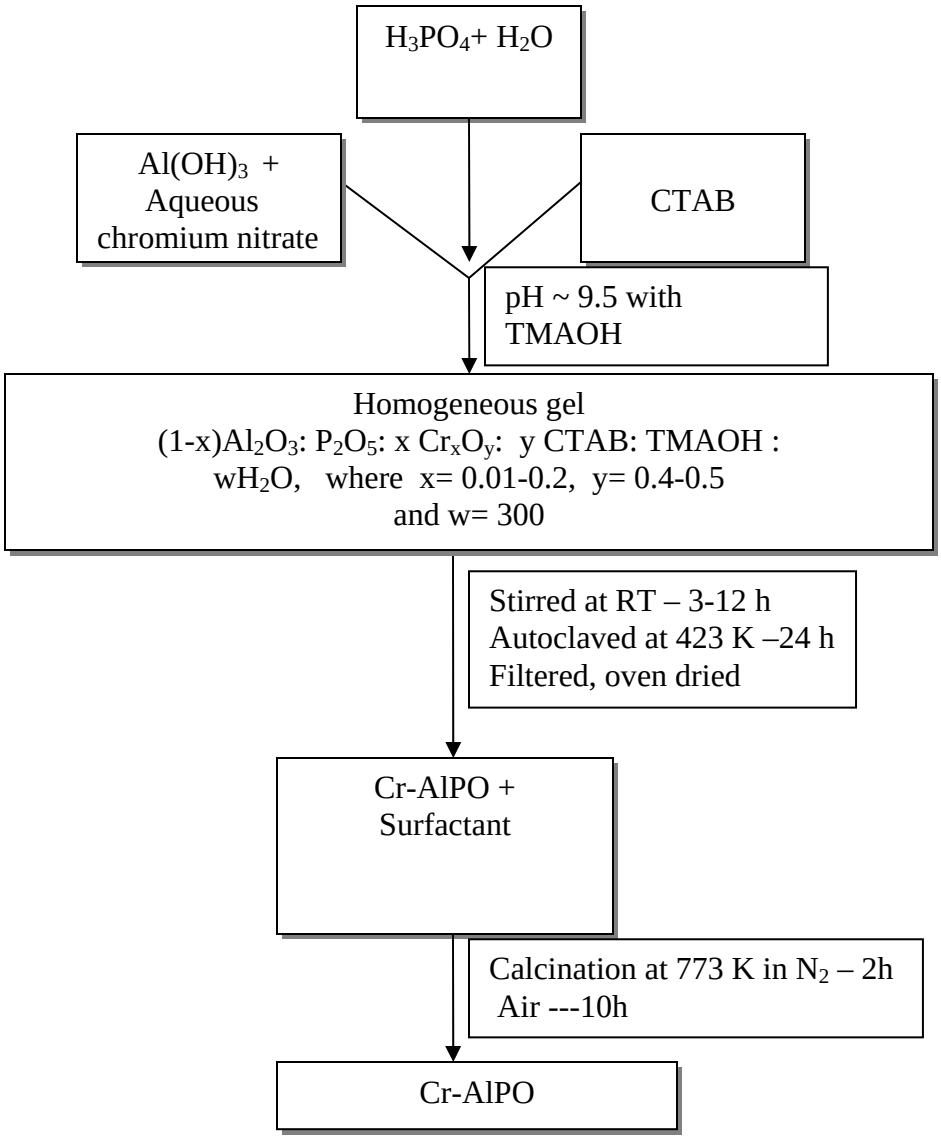

Scheme 4.2. Systematic procedure for the synthesis of mesoporous Cr-AlPO

Calcination was performed in nitrogen atmosphere for first two hours followed by air in order to preserve the semicrystalline nature of these materials. Pure aluminophosphate was also prepared under the same conditions. Scheme 4.2 represents the systematic representation of the synthetic procedure adopted for the preparation of the mesoporous aluminophosphates.

4.6.2 Experimental set up and characterization of the products

The experimental set-up consisted of three parts: the gas supply system, the reactor and the analytical system. The gases O_2 (99.995%) and Ar (99.998%) (Carbagas, Lausanne, Switzerland) were used without further purification. The feed was regulated through mass flow controllers. Flow A contained oxygen, argon and toluene vapour. Flow B was used for the pre-treatment of the catalyst with oxygen diluted in Ar. Gases A and B were mixed at a pressure of 101 kPa. The loading of the catalyst and the gas flow were maintained constant throughout the study at 0.2 g and 1 ml/s. The catalyst was diluted with quartz powder in a 1:1 ratio. All lines and valves were heated up to 423 K in order to avoid the condensation of the products. The catalyst was pretreated in O_2 (40-vol% O_2, rest Ar) at 573 K before the reaction. The temperature was decreased and the flow was switched to the mixture of 2 vol% toluene and 40-vol % O_2 in Ar.

Catalytic activity of mesoporous Cr-AlPO for liquid phase oxidation of ethyl benzene and benzyl alcohol with 70% TBHP was carried out in a three-necked 100 ml round bottom flask equipped with a water condenser. The reactions were performed at 333 K in acetone and acetonitrile as solvents. The temperature of the reaction was maintained by a thermostated oil bath. After each experiment the catalyst was filtered and dried. The dried catalysts were then calcined in air at 673 K for 6 h and reused. It was observed that the performance of the catalyst was almost same even after the second run of the experiment. After each experiment, XRD was recorded to examine the morphological changes. The catalyst maintained the same morphology after the completion of the reaction. The reaction products were identified by GC-MS (Hewlett-Packard, HPG

1800A GCD system, HP-5) and analyzed by gas chromatography (Shimadzu GC-14A, 30m HP-5. FID).

The low-angle X-ray diffraction pattern of the sample was recorded on a Siemens D 500 ($\theta/2\theta$) using monochoromatised Cu Kα radiation (λ = 1.5406 Å) with a scan speed of 1^o/ min over the range $2<2\theta<10^o$. High-resolution transmission electron microscopic images were observed with a Philips EM430ST operated at 300 kV. Thermal analyses of the samples were made with a thermal analyzer (Perkin Elmer model TGA 7) at a heating rate of 20 ^{o}C/min. Diffusive reflectance UV-VIS spectroscopy was carried out on a Cary 5E UV-VIS-NIR spectrophotometer. ESR spectra were recorded with a Varian E–112 spectrometer at room temperature. N_2 adsorption–desorption measurements at 77 K were made using CE instruments, Sorptomatic 1990. The sample was out-gassed at473 K for 12 h. Temperature- programmed- reduction (TPR) studies were carried out using 100 mg of the catalyst loaded in a quartz reactor. The samples were first treated with argon for 1 h at room temperature, followed by H_2/Ar. Desorption was carried out at a heating rate of 10^oC / min. Temperature programmed desorption of ammonia serves as a dependable technique for the quantitative determination of the acid strength distribution. For TPD studies, palletized catalyst was activated at 700°C inside the reactor under nitrogen flow for half an hour. After cooling to room temperature, ammonia was injected in the absence of the carrier gas flow and the system was allowed to attain equilibrium. A current of nitrogen flushed out the excess and physi-sorbed ammonia. The temperature was then raised in a stepwise manner at a linear heating rate of about 20°C/min. The ammonia desorbed from 100°C to 600°C at intervals of 100°C was trapped in dilute sulphuric acid solution and estimated volumetrically by back titration with NaOH. A

Blazers QMG-421 mass-spectrometer and a Perkin-Elmer Autosystem XL gas chromatograph were used for the gas phase analysis. ICP-AES has been used to obtain elemental composition. Toluene and other organic products were separated in an SPB-5 capillary column and analyzed by FID. Ar/O_2, CO, CO_2 and H_2O were analyzed using a Carboxen-1010 capillary column and analyzed by TCD.

4.7 RESULTS AND DISCUSSION

4.7.1 XRD

XRD patterns obtained for the chromium substituted mesoporous aluminophosphates are shown in Fig.4.11. As-synthesized materials show a maximum intense peak at d spacing of 35.0 Å. In addition to this peak, clearly visible peaks were observed at higher 2θ value in the range 3-5^o. These reflections can be indexed to a uni-dimensional hexagonal lattice. The maximum intense peak is due to the (100) reflection and the broad peak in the 2θ range 4-5^o corresponds to the (110) and (200) reflections. In addition, the presence of a few peaks in low angle XRD pattern confirms the less long-range crystallographic order. Upon calcination, this spacing decreased to 33.4 Å, indicating the contraction of the structure during the process of calcination. Moreover, calcination caused a decrease in the d-spacing value of the maximum intense peak, confirming shrinkage of the structure during the calcination process. For the successful preparation of the mesostructure, maintaining optimum pH is the prerequisite as the synthesis at higher pH resulted only in amorphous materials. In the synthesis procedure adopted in the present study, pH of the synthesis gel was adjusted to 9.5 with tetramethylammonium hydroxide. For this purpose, various basic sources were tried and it was observed that alkylammonium cations are efficient ones for the same. To ensure this point, NaOH and

NH_4OH were used as basic sources. When NaOH or NH_4OH was used as base instead of tetramethylammonium hydroxide, only amorphous material was obtained. This was in accordance with the observation made earlier in the case of V-AlPO. It was also observed that aluminium hydroxide is a better aluminium source, since it might provide a less polymerized aluminophosphate network that is favourable for the assembly of the mesostructure.

4.7.2 Chemical analysis and N_2 adsorption studies

Substitution of chromium in mesoporous aluminosilicate and aluminophosphate network has been verified by ICP analysis, which resulted in 0.87 mass% in mesoporous Cr-$AlPO_4$ and 0.93 mass% in Cr-MCM-48 respectively. Chemical composition of the material is Al: P: Cr = 0.92 :0 .98: 0.087 for mesoporous Cr-AlPO. Mesoporous Cr-AlPO material shows an isotherm with a small hysteresis loop characteristic of mesoporous materials (Fig. 4.12). Physico-chemical properties of the catalysts studied are given in Table 4.7. The type of isotherm is intermediate between type IV and I. This type of isotherm behavior is reported for the mesoporous systems having less thermal stability and less long-range order (Tiemann et al., 2001a; Luan et al., 1998a, 1998b). This may be due to the fact that after clacination the order of mesoporous network decreased. For all the samples (Cr-AlPO), the isotherms are similar, having an inflection around p/p_0= 0.2-0.4 characteristic of mesoporous materials. The BET surface area of the Cr-AlPO mesoporous material is ~ 500 m^2/g and that of Cr-MCM-48 is ~ 640 m^2/g. In all the cases, the pore size distributions calculated on the basis of BJH analysis from the desorption branch of the isotherms show a narrow distribution with a maximum around 29 Å.

Table 4.7. Physico-chemical properties of catalysts studied

Catalyst	$d_{10\,0}$ [uncalc] Å	$d_{10\,0}$ [calc] Å	a= Å	BET surface area m^2/g	Pore size Å	Pore volume cc/g
$AlPO_4$	34.5[1]	33.0[1]	38.10[3]	685	28	0.65
Cr-$AlPO_4$	35.0[1]	33.4[1]	38.56[3]	490	29	0.51
MCM-48	33.7[2]	32.9[2]	80.5[4]	1,020	29	0.99
Cr-MCM-48	35.9[2]	33.6[2]	82.4[4]	640	29	0.70

where [1]—d_{100}, [2] --d_{211}

[3]----$a= 2d_{100}/ \sqrt{3}$

[4]----$a= d_{211}. \sqrt{(h^2+k^2+l^2)}$

4.7.3 Thermal analysis

The thermogram of as-synthesized mesoporous AlPO (Fig. 4.13a) shows two weight loss regions, one corresponding to loss of physi-sorbed water below 373 K and the second and the main weight loss in the temperature range 450-550 K corresponding to loss of organic template. The mesoporous Cr-AlPO is stable up to 1073 K. Similar features are also observed for chromium substituted cubic silicate analogue whose thermogram is given in Fig. 4.13b for comparison.

4.7.4 Temperature programmed desorption of ammonia

The presence of acidic sites and the distribution of the acid sites have been monitored through temperature programmed desorption measurements. For this purpose weak base like ammonium was chemisorbed and its desorption profile was monitored as a function of temperature. Figure 4.14 represents temperature programmed desorption of ammonia in the temperature range 323 – 823 K. A broad desorption pattern indicates a large distribution of different types of acid sites. Deconvolution of the profile results in three distinct peaks in the range 323- 623, 473- 723 and 573- 823 K. The three desorption peaks can be assigned to weakly acidic, moderately acidic and strongly acidic groups respectively.

4.7.5 UV-VIS nujol

The presence of the heteroatom with in the framework as well as on the extra framework can be seen through UV-VIS spectroscopy. Extensive literature is available on chromium-substituted zeolites, microporous aluminophosphates and mesoporous silica based materials (Weckhuysen et al., 1996; Sheldon et al., 1998; Hartmann et al., 1999, Biz et al., 1998). In all these cases, as mentioned earlier, chromium is present on the extra framework in the case of as-synthesized material as stabilization of chromium (III) in tetrahedral co-ordination is difficult to achieve. However, on calcination, partial or complete oxidation of chromium (III) to higher oxidation states facilitates the substitution of Cr (V) or Cr (VI) in tetrahedral co-ordination as the presence of the later in tetrahedral coordination is known in dichromate or chromate like species (Sakthivel et al., 2001b; 2002a; 2002b; Wang et al., 2002a;2002b; Mahalingam et al., 1999). Based on the literature data, the presence of the heteroatom as extra framework Cr (III) species results in band around 440 nm (Ulagappan et al., 1996a; Sakthivel et al., 2002a). This band is

due to the forbidden d-d transitions arising from the d^3 electronic configuration. However, on calcination, a new band around 370 nm is observed confirming the presence of Cr (VI) with in the framework. This band is due to charge transfer transition from ligand oxygen to metal chromium, which is present as d^0 configuration (Sakthivel et al., 2002a; 2002b).

Figure 4.15 represents UV-VIS spectra of as-synthesised and calcined mesoporous Cr-AlPO and Cr-MCM-48 samples recorded in nujol mode. As-synthesised mesoporous Cr-AlPO shows bands around 610 and 440 nm. These bands are characteristic of trivalent chromium in octahedral co-ordination and occupying extra framework sites rather than being substituted at tetrahedral framework sites. This could be due to a large difference in LFSE between these two geometries (West, 1988). On calcination, a new charge transfer band centred at 370 nm is observed, along with a shoulder at 440 nm. This CT band could be due to O (2p) $\rightarrow$ Cr^{+6} ($3d^0$) and/or Cr^{+5} ($3d^1$) charge transfer transitions viz., chromate-or dichromate-like species in tetrahedral environment. The assignment of the observed bands for Cr-MCM-48 is given in chapter 3.

4.7.6 ESR spectroscopy

ESR spectra provide information regarding the presence of the ESR active moieties in different environments. In literature reported chromium substituted systems, the presence of a broad band around g= 1.98 was assigned to the presence of Cr (III) in extra framework species (Ulagappan et al., 1996a; Sakthivel et al., 2002a). The UV-VIS band around 440 nm further supports this observation. On calcination, the signal intensity decreased, indicating the oxidation of the Cr (III) species to higher oxidation states like

Cr (V) and Cr (VI). Since Cr (VI) is a d^0 configuration, the spectrum is only due to the ESR active Cr (V) (Sakthivel et al., 2002a; 2002b, Ulagappan et al, 1996a; Mahalingam et al.,1999). In addition to this decrease in intensity, a narrow signal with g=1.97 confirms the presence of chromium in +5 oxidation state. ESR spectra of as-synthesised and calcined mesoporous Cr-AlPO are shown in Fig. 4.16.

As- synthesised material shows a broad singlet with g value of 1.98, indicating Cr^{+3} ions in octahedral co-ordination. The ESR spectrum of calcined mesoporous Cr-AlPO shows a signal at a g value at 1.97, characteristic of pentavalent chromium in tetrahedral or distorted tetrahedral co-ordination. In a similar way, in as-synthesised Cr-MCM-48 material, the presence of a broad signal around g~1.98 suggests the presence of trivalent chromium in octahedral coordination. On calcination, the signal intensity partially decreased, resulting in a narrow signal centered at g ~1.97 which is characteristic of pentavalent chromium in tetrahedral co-ordination.

4.7.7 Gas phase selective oxidation of toluene on Cr-containing mesoporous catalysts

Gas phase oxidation of toluene was studied over mesoporous Cr-AlPO and Cr-MCM-48. Molecular oxygen diluted in argon was employed as oxidant. The detailed experimental procedure was given in earlier sections. TPR patterns of the studied catalysts in the temperature range 323-973K are shown in Fig. 4.17. The TPR pattern of mesoporous Cr-AlPO shows the presence of a single peak at about 713 K, whereas a broad reduction peak, which is centred at 730 K, is observed for Cr-MCM-48. the activation energy

values for the oxidation of toluene are 54 and 49 kJ/ mol on mesoporous Cr-AlPO and on Cr-MCM-48, respectively. Scheme 4.3 represents the probable reaction sequence through which toluene oxidation might take place. Typical results on toluene oxidation in the temperature range 523-648K over mesoporous Cr-AlPO and Cr-MCM-48 are given, respectively in Tables 4.8 and 4.9. Benzaldehyde, benzene, CO_2 and CO are the reaction products observed on Cr-AlPO. On the surface of the mesoporous Cr-AlPO, both oxidation and dealkylation reactions take place simultaneously, leading to benzaldehyde and benzene as main products, whereas the redox nature of the Cr-MCM-48 governs the oxidation of toluene, giving aldehyde as the main product. The formation of benzene as a result of dealkylation reaction predominates on acid (Al^{+3}) sites, whereas on redox sites ($Cr^{+5/+6}$) oxidation of toluene is taking place, leading to benzaldehyde. The absence of the coupled products indicate that the reaction is not taking place in radical pathway, rather it takes place in a concerted manner where adsorption of toluene takes place parallel to the lattice. Oxygen atoms are adsorbed on the sites adjacent to the site holding the carbon atom of the methyl group. One of these sites donates its oxygen to the carbon atom of the methyl group, leading to the formation of carbon monoxide. Another oxygen atom reacts with hydrogen atoms of the methyl group, giving rise to water. Donation of hydrogen atoms from the acidic sites to the ring carbon completes the reaction with the formation of benzene.

Table 4.8 Catalytic activity of mesoporous Cr-AlPO for the oxidation of toluene with molecular oxygen (reaction condition: 2% toluene diluted in argon)

Temperature (K)	Conversion of Toluene (%)	Product selectivity (%)		
		Benzaldehyde	Benzene	(CO_2+ CO)
523	0.7	91.0	2.4	6.6
548	0.9	83.5	2.6	13.9
573	1.4	60.4	3.0	36.6
598	2.2	50.6	6.1	43.3
623	4.8	42.4	8.2	49.4
648	9.1	25.3	12.4	62.3

Table 4.9.Catalytic activity of Cr-MCM-48 for the oxidation of toluene with molecular oxygen(reaction condition: 2% toluene diluted in argon)

Temperature (K)	Conversion of Toluene (%)	Product selectivity (%)	
		Benzaldehyde	(CO_2+ CO)
523	0.9	75.3	24.6
548	1.2	61.5	38.4
573	2.2	44.7	55.2
598	3.4	33.9	66.1
623	6.8	20.6	79.3
648	11.3	16.0	84.0

At lower temperatures, redox properties of mesoporous Cr-AlPO influence the reaction, leading to the formation of benzaldehyde in larger quantity. As the temperature is

increased, the selectivity to benzaldehyde drops down whereas the selectivity towards benzene increases, indicating the influence of acidity. The conversion of toluene increased with increase in temperature. At higher temperatures, CO_x products may be formed mainly through consecutive reaction of oxidation of primary products.

In contrast, Cr-MCM-48 acts as a pure redox catalyst, giving rise to only benzaldehye as oxidation product. Further oxidation of benzaldehyde gives CO_2 and H_2O. No significant amount of benzoic acid was detected on either of the catalysts. This confirms that aldehyde is formed in a slow and rate-determining step and that further oxidation takes place at a faster rate. The catalyst was reused after calcination in air for 5 h at 673 K. Table 4.10 represents the results on the catalytic activity of Cr-AlPO for the oxidation of toluene with respect to number of cycles. It was observed that there was loss of catalytic activity in subsequent cycles.

Table 4.10. Catalytic activity of mesoporous Cr-AlPO for toluene oxidation at 648 K after recycling

Cr-AlPO at 648 K	Conversion of Toluene (%)	Product selectivity (%)	
		Benzaldehyde	(CO_2+ CO)
Cr-AlPO	11.33	16.0	84
Cr-AlPO	10.47	19.5	80.5
Cr-AlPO	9.33	18.4	81.6

In addition to the vapour phase oxidation of toluene, catalytic activity of the mesoporous Cr-AlPO was also tested for liquid phase oxidation of aromatics like ethylbenzene and benzylalcohol with 70 % TBHP, since side chain oxidation products of these substrates are important as precursors for various fine chemicals. Data on the catalytic activity of

Cr-AlPO in comparison with Cr-MCM-48 for the oxidation of ethylbenzene and benzyl alcohol with 70 % TBHP are given in Tables 4.11 and 4.12. Initially, the catalytic activity was tested without solvent and later acetone and acetonitrile were used as solvents. The results in Table 4.11 indicate that both Cr-AlPO and Cr-MCM-48 are active for conversion of ethylbenzene selectively to acetophenone. In order to examine the catalytic activity due to leached metal ions, in a separate experiment, the reaction mixture was filtered after 2 h in hot condition and the experiment was continued with the filtrate. Increase in conversion was not observed, indicating homogeneous catalysis is not taking place under the reaction conditions. It was observed that Cr-AlPO exhibits slightly higher activity when compared to Cr-MCM-48. This could be due to the stabilization of the active species ($Cr^{+5/+6}$) in aluminophosphate network than in aluminosilicate network. Acetone appears to be a better solvent than acetonitrile.

The catalytic activity data of benzyl alcohol over mesoporous Cr-AlPO and Cr-MCM-48 are given in Table 4.12. Oxidation of benzyl alcohol produces a mixture of benzaldehyde and benzoic acid as main products. When the experiment was carried out with out solvent, conversion of the substrate was less indicating the need of solvents. Both Cr-AlPO and Cr-MCM-48 show higher activity in acetone when compared to acetonitrile. This may be due to the fact that initially formed viscous products are readily soluble in acetone compared to in acetonitrile and thereby facilitating the substrate to approach the active site.

Table 4.11. Oxidation of ethyl benzene with 70 % TBHP over mesoporous Cr-AlPO& Cr-MCM-48

Solvent	Conv. (%)	Product selectivity (%)	
		Acetophenone	Others
Cr-AlPO			
None	9.8	94.6	3.0
Acetonitrile	23.2	97.0	2.3
Acetone	28.5	97.7	5.4
Cr-MCM-48	7.6	93.7	6.3
None	18.9	97.6	2.4
Acetonitrile	20.4	98.2	1.8
Acetone			

Reaction conditions: Substrate: 70%TBHP: Solvent = 0.0282: 0.0282 : 0.141 (moles);Weight of the catalyst = 100mg; T= 333 K ; t= 6 h

Table 4.12. Oxidation of benzyl alcohol with 70 % TBHP over mesoporous Cr-AlPO& Cr-MCM-48

Solvent	Conv. (%)	Product selectivity(%)		
		Benzaldehyde	Benzoic acid	Others
Cr-AlPO				
None	29.1	74.5	21.3	4.2
Acetonitrile	38.9	58.8	37.5	3.7
Acetone	43.1	69.2	29.5	1.4
Cr-MCM-48				
None	26.3	67.1	29.0	3.9
Acetonitrile	38.0	60.0	36.1	3.9
Acetone	39.8	56.5	40.6	2.9

Reaction conditions: Substrate: TBHP: Solvent = 0.0277 : 0.0277 : 0.138 (moles); Weight of the catalyst =100mg;T= 333 K ; t= 6 h

4.8 CONCLUSIONS

Hexagonal mesoporous aluminophosphates containing chromium could be successfully synthesized with better crystallinity. The system retains its morphology even after the removal of surfactant. Mesoporous Cr-AlPO exhibits both acidic and redox properties by promoting dealkylation and oxidation in a concerted manner, whereas under the same experimental conditions, Cr-MCM-48 promotes only oxidation. On mesoporous Cr-AlPO it is observed that, at lower temperatures, oxidation of toluene is favoured, whereas at higher temperatures dealkylation reactions govern the final products formed. Cr-AlPO is also a promising catalyst for the liquid phase oxidation of ethylbenzene and benzyl alcohol with 70 % TBHP

4.9 MESOPOROUS Fe-AlPO

4.9.1 Introduction

With the success of the redox catalyst titanosilicate, TS-1 various successful attempts have opened new directions for the production of fine chemicals in an environmentally benign manner. The intellectual challenge involved in catalysis is to devise strategies for such environmentally desirable objectives as the development of one-step processes and /or solvent-free chemical conversions and design of oxidation catalysts that use air or oxygen as the oxidant. One way of designing the solid redox catalyst is to incorporate the heteroelements into the framework structures. In the case of microporous solids, the largest two sub-families are the aluminosilicates and aluminophosphates. Ions such as Ti^{+4}, Co^{+2}, Mn^{+2} and Fe^{+3} are known to exhibit powerful catalytic properties. Out of these, Co^{+2} and Mn^{+2} are easy to be incorporated into the framework of AlPOs and they are convertible to Co^{+3} and Mn^{+3} during the calcination (Raja et al., 2000). These catalytic systems are known to produce oxidation products by utilizing air/ molecular oxygen as oxidant. Use of molecular oxygen or air will always be an advantage in the sense that they are cheaper and environmentally benign.

In this sequence, incorporation of iron into the framework sites of both zeolites and AlPOs are known and the resulting systems are promising catalysts for various selective reactions (Thomas, 1999; Thomas et al., 2001; Goldfrad et al., 1994; Park et al., 1992; Das et al., 1992). These catalysts have been mainly employed for the oxidation of saturated hydrocarbons. Saturated hydrocarbons are among the most abundant of all naturally occurring organic molecules and they are the most difficult to oxyfunctionalize

at lower temperatures in a controlled manner. Microporous aluminophosphates containing transition metal ions in their framework have been employed as catalysts for selective oxyfunctionalization of alicyclic hydrocarbons. Recently, microporous aluminophosphates containing Fe^{+3}, Mn^{+2} and Co^{+2} in their framework have been used for oxidation of cyclohexane and adipic acid (Thomas et al., 2001). Selective oxyfunctionalizing alicyclic hydrocarbons such as cyclohexane and adamantine are similarly demanding task because of the importance of the oxidation products (cyclohexanol and cyclohexanone in the case of cyclohexane). These products are important in the production of Nylon-6 and Nylon-6, 6. Currently, this particular oxidation reaction has been carried out through homogeneous catalysis, where some hazardous chemicals have been used. Recently, catalysts like Cytochrome P-450, iron based oxidases and iron substituted microporous aluminophosphates were employed as catalysts for this purpose (Thomas et al., 2001). Over these systems, in addition to conventional oxidants like hydrogen peroxide, alkyl hydroperoxides and iodosyl benzene, molecular oxygen was also employed as an oxidant. In the present study, synthesis and characterization of iron incorporated mesoporous aluminophosphate (Fe-AlPO) are discussed. Results on the catalytic activity of Fe-AlPO for the aerial oxidation of cyclohexane will also be discussed.

4.10 EXPERIMENTAL

4.10.1 Synthesis of mesoporous Fe-AlPO

Mesoporous iron incorporated aluminophosphates (Fe-AlPO) were synthesized by using CTAB as the structure-directing agent. Aluminium hydroxide and 85 % phosphoric acid

were employed as the aluminium and phosphorous sources, respectively. Ferric nitrate nonahydrate was used as iron source. In a systematic procedure, to an aqueous solution of phosphoric acid, aluminium hydroxide was added under vigorous stirring. To this mixture, aqueous solution of ferric nitrate was added and stirring was continued further in order to attain homogeneous mixture. To this mixture, surfactant CTAB solution was added and stirred for half an hour. At this stage, tetramethylammonium hydroxide was added drop wise to maintain the pH around 9.5. The homogeneous gel thus obtained was found to have the gel composition of 0.95 Al_2O_3: 0.05 Fe_2O_3: 1.00 P_2O_5: 0.50 CTAB: 300 H_2O. pH of the synthetic gel was maintained at 9.5 with tetramethylammoniumhydroxide. Like in previous cases, when NaOH and NH_4OH were used to maintain the pH only amorphous materials resulted indicating the need of mild base. The homogeneous gel was stirred at room temperature for 24 h and autoclaved at 423 K for 24 h. The product was separated, washed with water and oven dried. Calcination was performed in air at 773 K to remove the organic surfactant. The systematic procedure for the synthesis of mesoporous Fe-AlPO is given in Scheme 4.4.

4.10.2 Characterization and catalytic activity of Fe-AlPO

Low angle X-ray diffraction is the suitable technique to confirm the formation of mesophase. The low angle X-ray diffraction pattern of the sample was recorded on Siemens D 500 (θ/2θ) using monochoromatised Cu Kα radiation (λ = 1.5406 Å) with a scan speed of 1^o/ min over the range $2<2\theta<10^o$. In order to observe the nature of the surfactant and its removal, thermal analysis was used. Thermal analyses of the samples were made with thermal analyzer (Perkin Elmer model TGA 7) at a heating rate of 20 ^oC/min. N_2 adsorption–desorption measurements provided information regarding the presence of mesopores with in the system and it also provided the BET surface area and average pore size of the material synthesized. N_2 adsorption–desorption measurements at 77 K were made using CE instruments, Sorptomatic 1990. The presence of the heteroatom with in the framework was confirmed through various spectroscopic techniques like UV-VIS DRS and ESR spectroscopy. Diffusive reflectance UV-VIS spectroscopy was carried out on Cary 5E UV-VIS-NIR spectrophotometer. ESR spectra were recorded with Varian E–112 spectrometer at room temperature. Oxidation of cyclohexane was performed in a high-pressure stainless steel reactor lined with teflon and dry air was used as oxidant. A pressure of 20 or 30 bar of air was used and the temperature was maintained at 403 K. The duration of the reaction was 24 h. Product identification was done with authentic samples and qualitative analysis was done using Nucon-4765 gas chromatograph with SE-30 column. The same reaction was tested over Fe containing silicate analogue Fe-MCM-48. In order to ensure the possible mechanism, the reaction was carried out in the presence of small quantity of radical initiator TBHP and radical inhibitor HQ and the reaction was continued further.

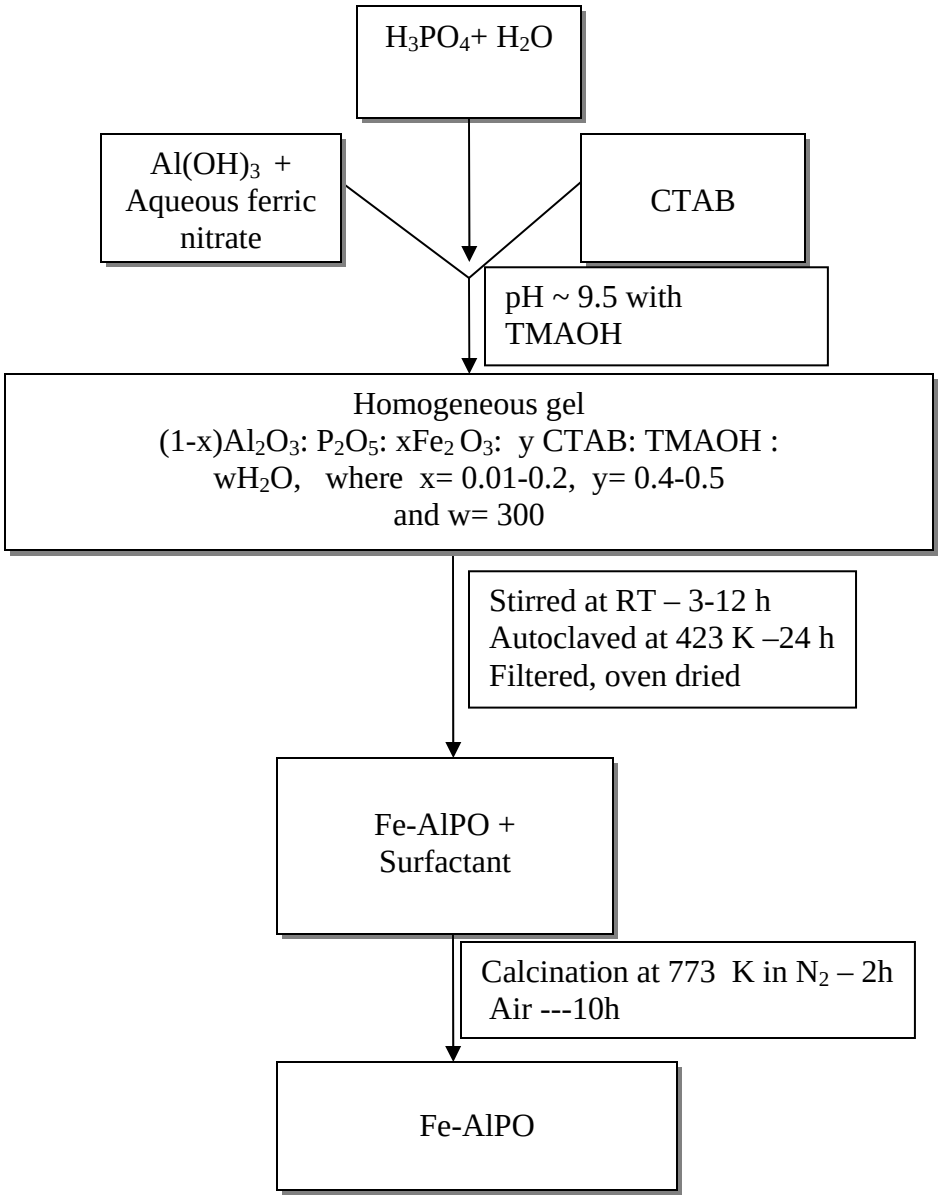

Scheme 4.4. Systematic procedure for the synthesis of mesoporous Fe-AlPO

4.11 RESULTS AND DISCUSSION

4.11.1 XRD

Low-angle XRD patterns confirm the formation of the mesophase of the materials synthesized. Figures 4.18 and 4.19 represent the XRD patterns of the as-synthesised and calcined Fe-AlPO materials respectively. As-synthesized mesoporous Fe-AlPO shows a maximum intense peak with d-spacing value 35.8 Ǎ, which corresponds to the 100 reflection. Up on calcination in air, a decrease in the d100 spacing from 35.8 to 34.7 Ǎ was observed (Table 4.13). This decrease is due to the contraction of the unit cell during the calcination. This type of decrease in d spacing values is known for mesoporous materials (Beck et al., 1992; Corma et al., 1994a). However, the peak intensity remains the same confirming that even after calcination, the materials retained their XRD pattern. These patterns can be indexed to uni-dimensional hexagonal lattice characteristic of MCM-41 type structure. In addition to the maximum intense peak, weakly resolved peaks corresponding to 110 and 200 reflections are also observed. These reflections are typical of a hexagonal lattice of MCM-41 type and characteristic of mesoporous materials.

The pH of the gel was maintained at 9.5 with TMAOH as the lower pH amorphous materials were obtained. It was observed that mild basic conditions are required to produce the hexagonal aluminophosphates (Zhao et al., 1997). Mesoporous AlPO resulted only at a pH > 9.0. For the reaction conditions, a modified S^{+}--I^{-} ion-pair process is likely to be operative.

Table 4.13. Physico-chemical data of Fe-substituted mesoporous materials

Catalyst	d [uncalc] (Å)	d [calc] (Å)	a= (Å)	BET surface area (m^2/g)	Pore size (Å)	Pore volume (cc/g)
AlPO	33.2	32.1	37.47[1]	695	28	0.65
Fe-AlPO	35.8	34.74	40.56[1]	820	28	0.61
MCM-48	33.7	32.9	80.50[2]	1,020	29	0.99
Fe-MCM-48	34.7	33.1	81.07[2]	840	28	0.91

1----a= $2d_{100}/\ 3$

2----a= $d_{211}.\ \sqrt{(h^2+k^2+l^2)}$

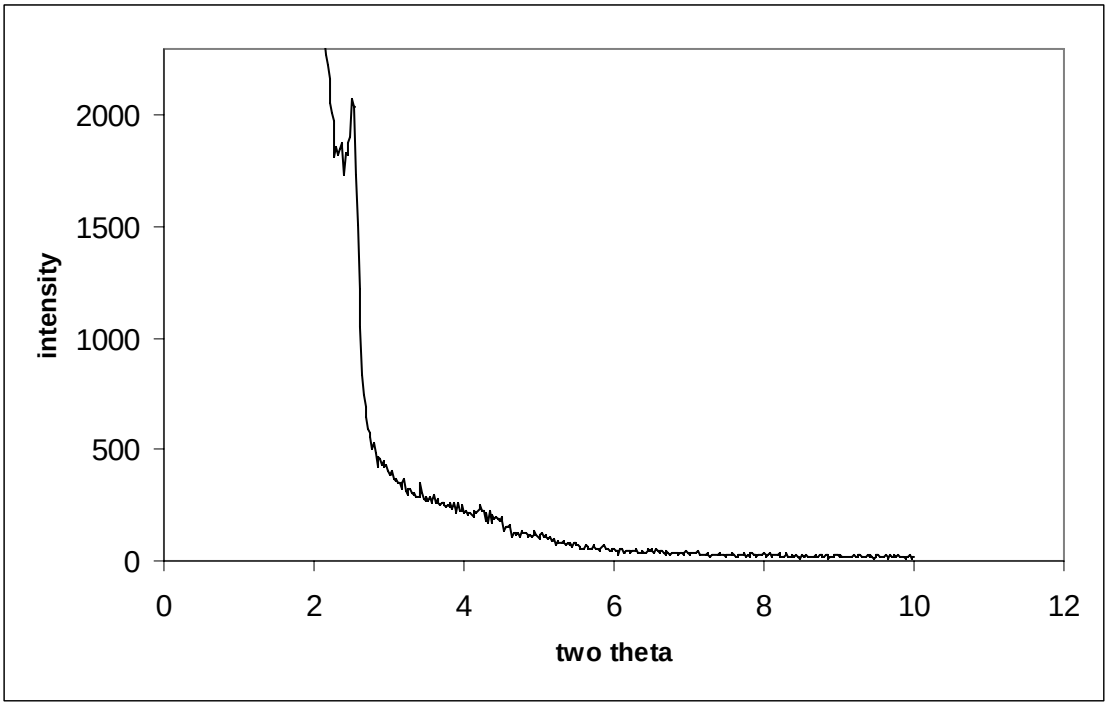

Fig.4.18. XRD pattern of mesoporous Fe-AlPO (uncalcined)

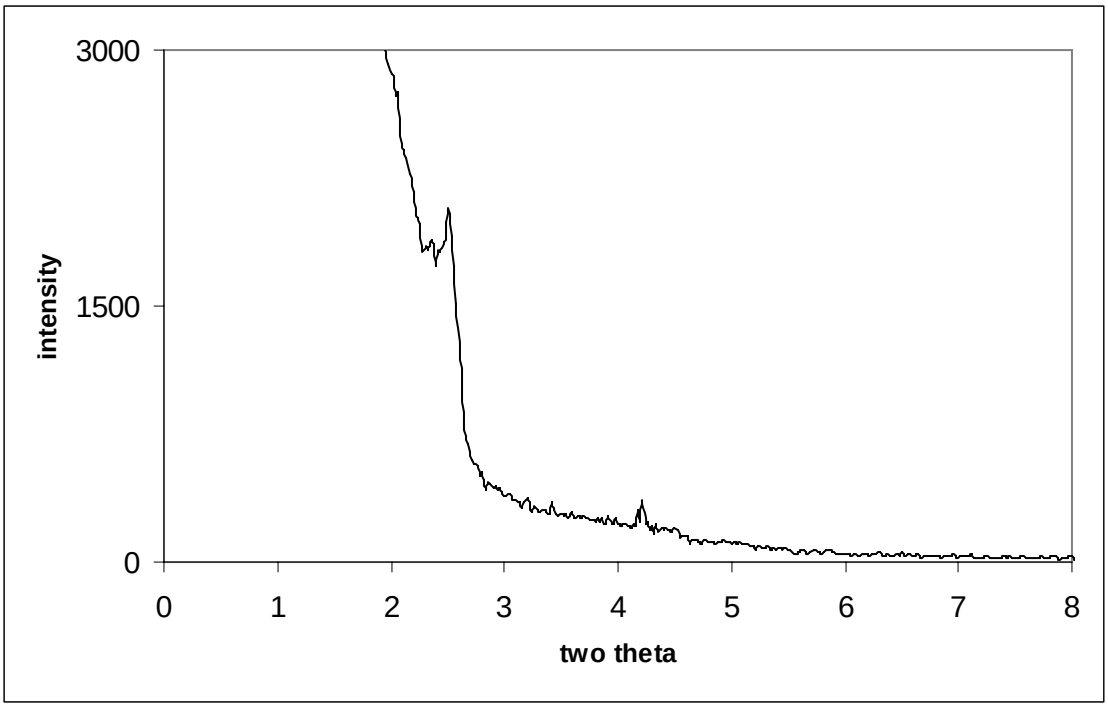

Fig.4.19. XRD pattern of mesoporous Fe-AlPO (calcined)

4.11.2 N_2 adsorption

Nitrogen adsorption- desorption data provide information regarding the porous nature and the surface area of the materials prepared. Figure 4.20 represents the nitrogen adsorption-desorption isotherms of mesoporous iron substituted analogue recorded at liquid nitrogen temperature (77 K). Fe-AlPO has a BET surface area of 830 m^2/g with an average pore size ~26 Å. It was observed that Fe-AlPO exhibits type IV isotherm with a hysteresis loop in the region p/p_0 =0.2-0.4 indicating mesoporous nature of the catalyst. This hysteresis loop is due to the capillary

condensation. The value of BET surface area along with pore size distribution is given in Table 4.13 from which it can be seen that the surface area of mesoporous aluminophosphates is less compared to analogous silicate materials indicating the less degree of thermal stability.

4.11.3 Thermal analysis

In the case of mesoporous aluminophosphates, unlike microporous aluminophosphates, caution should be taken during the removal of the surfactant as removal of the same leads to collapse of the structure. This is because removal of organic template through calcination in air is a combustion reaction. Since these mesoporous solids are weakly crystalline with less periodicity, the excess heat that is generated during the combustion can lead to amorphous materials after removal of the surfactant. Thermal analysis provides information regarding the removal of the surfactant and total weight loss after removal of the surfactant. Thermogram of mesoporous Fe-AlPO is given in Fig. 4.21 which also shows three weight loss regions in the temperature range <373, 373-623 and above 623 K that corresponds to loss of physisorbed water, loss of surfactant and loss of water due to the condensation of hydroxyl groups respectively. In order to examine the thermal stability of mesoporous Fe-AlPO, calcination was performed at various temperatures and it was observed that mesoporous Fe-AlPO shows high thermal stability up to 973 K.

4.11.4 UV-VIS nujol

The location of the metal ions in different environments can be identified through UV-VIS spectroscopy. Mohapatra et al (Mohapatra et al., 2002a) recently reported the synthesis of mesoporous Fe-AlPO, where in they have observed two prominent bands at 290 and 230 nm which they have assigned to the charge transfer transitions arising from oxygen to metal iron. Similar observations have also been reported in the literature for microporous ferrite and other iron substituted aluminophosphates (Goldfrab et al., 1994; Park et al., 1992, Das et al., 1992, Badamali et al., 1998a; 1998b; Dapurkar et al., 2001; Selvam et al., 2001; Mohapatra et al., 2002a) and in all these cases the band at 230 –250 nm is assigned to the ligand to metal charge transfer band. In all the cases, the absence of the forbidden d-d transitions in the range 330-380 nm was taken into consideration for the absence of extra framework iron.

UV-VIS spectra of as-synthesized and calcined mesoporous Fe-AlPO recorded in nujol mode are given in Fig 4.22. As-synthesized mesoporous Fe-AlPO shows only a band around 240 nm. Based on the earlier reports, this band was assigned to the ligand oxygen to metal iron charge transfer transition, indicating the presence trivalent iron in framework tetrahedral positions. On calcination, the same band was retained indicating the presence of iron in the framework of mesoporous Fe-AlPO. Interestingly, in both the cases unlike many silicate and aluminosilicate based systems, broadening of the bands were not observed. On calcination bands corresponding to the extra framework iron oxide species were absent indicating the presence of the iron in the network of mesoporous Fe-AlPO.

4.11.5 ESR spectroscopy

Since ferric iron is paramagnetic in both the low-spin and high –spin electronic configurations, ESR spectroscopy should be a good method for characterizing the iron sites in zeolites and related materials like aluminophosphates. The interpretation of the ESR spectra is difficult due to the complications associated with in homogeneous broadening arising from the zero field splitting and over lapping signals (Goldfrab et al., 1994). The X-band ESR spectrum usually consists of three major signals at g= 4.3, 2.2-2.4 and 2.0. The commonly accepted assignments of these signals are as follows: framework iron, iron in interstitial oxide or hydroxide phases and iron in cation-exchange sites, respectively. The appearance of the signal at g= 4.3 has often been taken as evidence for the framework substitution in zeolites and AlPO's (Badamali et al., 1998a; Goldfrab et al., 1994; Park et al., 1992; Wang et al., 2002b; Szegedi et al., 2001; Zhang et al., 2001; Xu et al., 2001).

ESR spectra of as-synthesized and calcined mesoporous Fe-AlPO are shown in Fig. 4.23. As-synthesized material at room temperature shows ESR spectrum with signals at g= 4.3 and 2.0. Based on the literature data, the first signal with g=4.3 is assigned to Fe(III) in tetrahedral environment and the other signal at 2.0 is attributed to the presence of high spin Fe(III) in distorted tetrahedral/octahedral environments (Mohapatra et al., 2002a). The increase in intensity of g=4.3 signal with decrease in temperature suggests that Fe (III) is in isolated tetrahedral location. Calcined Fe-AlPO also shows similar signals at g=4.3 and 2.0. Interestingly, upon calcination, dislodgement of the iron from the framework was not observed indicating the absence of extra framework ferric oxide species after

calcination. The assignment of the signals is also the same like the uncalcined sample. In the case of calcined samples also, increase in intensity of the signals at 77 K was observed suggesting the presence of Fe (III) in isolated tetrahedral environment.

4.11.6 Catalytic activity

Oxidation of cyclohexane over mesoporous Fe-AlPO

Typical results on the aerial oxidation of cyclohexane over mesoporous Fe-AlPO and Fe-MCM-48 are given in Table 4.14. Liquid phase aerial oxidation of cyclohexane was carried out under high-pressure conditions (20, 30 bar) in a stainless steel autoclave at 403 K and the results indicate that Fe-AlPO is active for the cyclohexane oxidation and selective towards cyclohexanol. Under the reaction conditions employed mesoporous Fe-AlPO shows conversion of 7.5 % with selectivity of ~87 % towards cyclohexanol. In order to check whether the reaction proceeds by a radical mechanism, a small amount (< 3 wt %) of radical initiator (70 % TBHP) was added. Conversion of cyclohexane has increased to 14.2 % retaining the same selectivity towards cyclohexanol. This increase in the conversion indicates that oxidation of cyclohexane is taking place through radical mechanism. In order to confirm this further, the reaction was carried out with radical inhibitor hydroquinone (HQ). The decrease in the cyclohexane conversion to 1.3 % further confirms the radical initiated mechanism. Based on these observations, a reaction mechanism has been proposed. Scheme 4.5 represents the probable reaction sequence in which there is an initial attack of oxygen on hydrocarbon giving rise to peroxo radical. This unstable species, once formed, quickly reacts with dissolved oxygen to form peroxo radicals. Such peroxo radicals are stabilized in different ways, for

example, by formation of a hydroperoxide. The main role of the metal ions is to catalyze the homolytic decomposition of the intermediate hydroperoxide (ROOH) (Hartmann et al., 2000; Sheldon, 1996; Sheldon et al., 1998). As a result of this decomposition, metal ions generate chain-initiating radicals, which form alcohols as oxidation products. However, this reaction will be facilitated only by those metal ions, which are capable of existing in two oxidation states with comparable stability (Hartmann et al., 2000).

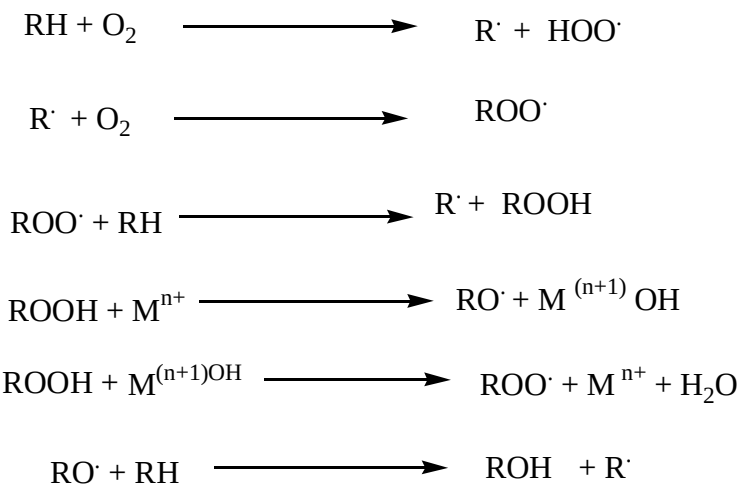

Scheme 4.5 Possible reaction mechanism of cyclohexane oxidation over Fe-AlPO

Table. 4.14. Catalytic activity of mesoporous Fe-AlPO for oxidation of cyclohexane

Catalyst	Conversion (%)	Product selectivity (%)		
		cyclohexanol	cyclohexanone	Others
Fe-AlPO	7.5	86.6	7.0	6.4
Fe-AlPO + 3 wt% TBHP	14.2	92.0	3.7	4.3
Fe-AlPO + 3 wt % HQ	1.4	68.0	29.6	--
Fe-MCM-48				
Fe-AlPO*	1.3	> 99	--	--

	7.7	87.2	6.1	6.7

Reaction conditions: Pressure = 20 bar, T = 403 K, t= 24 h; * P= 30 bar

4.12 CONCLUSIONS

Mesoporous Fe-AlPO analogous to uni-dimensional hexagonal MCM-41 was synthesized. The formation of hexagonal mesoporous aluminophosphate and the presence of iron with in the framework have been established using various physico-chemical techniques. Catalytic activity of synthesized mesoporous Fe-AlPO was tested for the aerial oxidation of cyclohexane under high-pressure conditions. The results indicated that the Fe-AlPO is an active catalyst for the oxidation of cyclohexane and the reaction is taking place through radical mechanism.

CHAPTER 5

COATINGS OF M41S ON STAINLESS STEEL GRID

5.1 INTRODUCTION

During the past decade, there has been growing interest in catalytic reactor engineering based on structured catalytic beds. Structured reactors offer several advantages over the conventional fixed-bed and slurry reactors (Cybulski et al., 1998, Kiwi-Minsker et al., 1999). Their open macrostructures allow for high flow rates with low-pressure drops. The flow dynamics is better controlled, leading to improved heat and mass transfer. Catalytic materials prepared via zeolite coatings on metal grids have recently been reported as novel structured catalysts (Jansen et al., 1992; 1994; 1998; Calis et al., 1995; Shan et al., 2000; Valtchev et al., 1995; Mintova et al., 1996; Yan et al., 1995). Despite the increasing interest in zeolitic coatings, only a few practical applications have been reported (Jansen et al., 1998; van Bekkum et al., 1994). In literature, ZSM-5 crystals grown on stainless steel grids were tested for the gas-phase hydroxylation of benzene to phenol by N_2O (Louis et al., 2000; 2001). This industrially important reaction has been chosen because it is exothermic and the use of a metallic-based structured catalytic bed allows for better heat distribution. This avoids hot spot and runaway problems. However, the pore size of microporous solids may impose diffusional limitations if the substrate dimensions are greater than their pore openings. The increasing demand for new and selective catalysts with larger molecular dimensions led to the discovery of M41S, mesoporous catalytic materials. Even though M41S materials are potential systems for various reactions, their applications are limited in large-scale industrial processes mainly due to their poor cystallinity. MCM-41 catalysts are used in catalytic fixed beds,

randomly packed by powdered micro-granules or extruded pellets with a few millimeters in size. The main disadvantage of randomly packed bed is the limited heat and mass transfer, high-pressure drop and maldistribution of flow, all of which leading to poor reactor performance.

Amorphous nature of these catalysts, in addition to fine particle nature, limits their potential use in industrial catalysis. However, it is possible to over come this problem by supporting these materials on inert materials like quartz, carbon, stainless steel etc., In this connection, attempts have been made to support zeolites and MCM-41 on inert stainless steel supports (Louis et al., 2000; 2001). In the present study, syntheses and characterization of hexagonal MCM-41 and cubic MCM-48 on stainless steel grids are reported.

5.2 EXPERIMENTAL

5.2.1 Support pre-treatment

Figure 5.1 represents the photograph of the stack of the stainless steel grid employed for the preparation of mesoporous materials. The structured packing consists of a stainless steel grid (AISI 316 type, wire diameter of 250 μm, mesh size of 800 μm) as a support for mesoporous coatings, arranged by superposition of 7 plates separated from each other by steel rings of 4 mm length. For the effective formation of mesoporous materials on the grid, pre-treatment of the gird plays an important role. Perhaps this pretreatment is to create sticking sites or in other sense defect sites, where the growth of the mesoporous material takes place. To emphasize this particular aspect, initial attempts have been made without any pretreatment. In all these cases after ultrasonication, which facilitates removal of loosely bound particles, very less amount of the final material got deposited

on the grid. The whole packing was pre-treated in boiling toluene and in hydrochloric acid solution to remove surface contaminations (van Bekkum et al., 1994). Even when the gird was pretreated in acidic solution followed by basic solutions, mesoporous solids were not effectively produced on the grid. This might be due to the difference in the synthetic procedures involved in the synthesis of zeolites and mesoporous solids. During the procedure adopted in the present study, after ultrasonication in distilled water, the support was immersed in 0.1 M cetyltrimethylammonium bromide (CTAB) solution for 1 hour at room temperature. The CTAB adsorbs on the grid surface guiding the synthesis of mesoporous network selectively on the support. Similar treatment was given for the synthesis of MCM-48 coatings on stainless steel grid, however the synthetic gel composition was different, which will be dealt in subsequent sections.

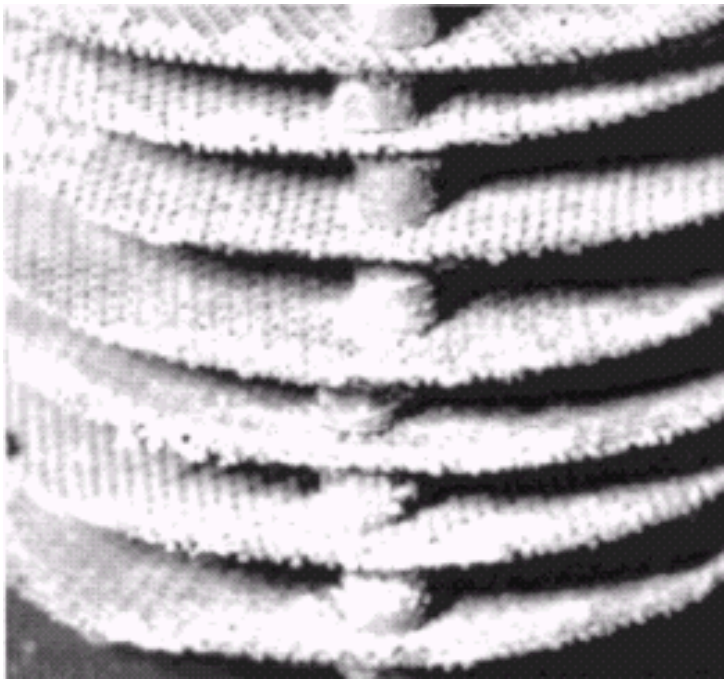

Fig. 5.1. Photograph of the grid used for M41S coatings

5.2.2. Characterization

The X-ray diffraction (XRD) patterns were acquired on D500 Siemens powder diffractometer (θ / 2θ) using monochromatised Cu-Kα radiation (λ=1.5406 Å) in the 2θ range of 0.5-10° with the steps of 0.04° and a step time of 8 s.

The specific surface area (SSA) of the catalysts was measured using N_2 adsorption-desorption at 77 K by Sorptomatic 1990 (Carlo Erba) instrument. Samples before the measurements were heated in vacuum at 523 K for 2h. The SSA values of the samples were calculated employing the BET method while the BJH method was applied for the calculation of pore volume and pore-size distribution (PSD).

Scanning electron microscopy (SEM) and high-resolution transmission electron microscopy (HRTEM) were employed to study the morphology of mesoporous silica formed on the support. HRTEM measurements were carried out on Philips CM300UT FEG with 300 kV field emission gun. SEM images were recorded using JEOL JSM-6300F electron microscope operating at a voltage of 5 kV.

Thermal analyses of the samples were made with Perkin Elmer thermal analyser (model TGA 7) at a heating rate of 20 ^{o}C/min

5.2.3 MCM-41 coating on stainless steel grid

The chemicals tetraethylorthosilicate (TEOS, 98%, Merck-Suchardt), ethanol (EtOH, 96%, Fluka), NaOH (98%, Fluka), cetyltrimethylammonium bromide (CTAB, 99%, Merck) were used as received. Deionised water was used for the synthesis. MCM-41 molecular sieves were prepared *via* S^{+}/I^{-} templating route as described elsewhere (Beck et al., 1992). Schematic representation of the procedure adopted in the present study is given in Scheme. 5.1. TEOS (10.5ml) was mixed with a solution containing CTAB (11.6

g) and NaOH (1.6 g) in H_2O (74.88g) and ethanol (3.6 ml) as co-solvent (Gallis et al., 1998). The homogenous gel thus obtained was found to have the gel composition $1SiO_2$: 0.68 CTAB: 0.88 Na_2O: 2 EtOH: 88.65 H_2O, where ethanol is a co-solvent (Gallis et al., 1998). After ageing for 3 h under vigorous stirring, the gel was poured into a teflon-lined (100 ml) autoclave containing a vertically positioned stainless steel support. The temperature was increased within one hour to 423 K and the synthesis was continued for another 24 h under autogeneous pressure. Afterwards, the packing was kept in an ultrasonic bath (45kHz) for 20 min to remove loosely attached particles and dried overnight at 400 K. The catalytic packing was calcined in air at 823 K for 10 h to burn out the organic template. The yield of the synthesis is defined as the ratio between the amount of Si incorporated into MCM-41 and the initial amount of Si present in the synthesis gel.

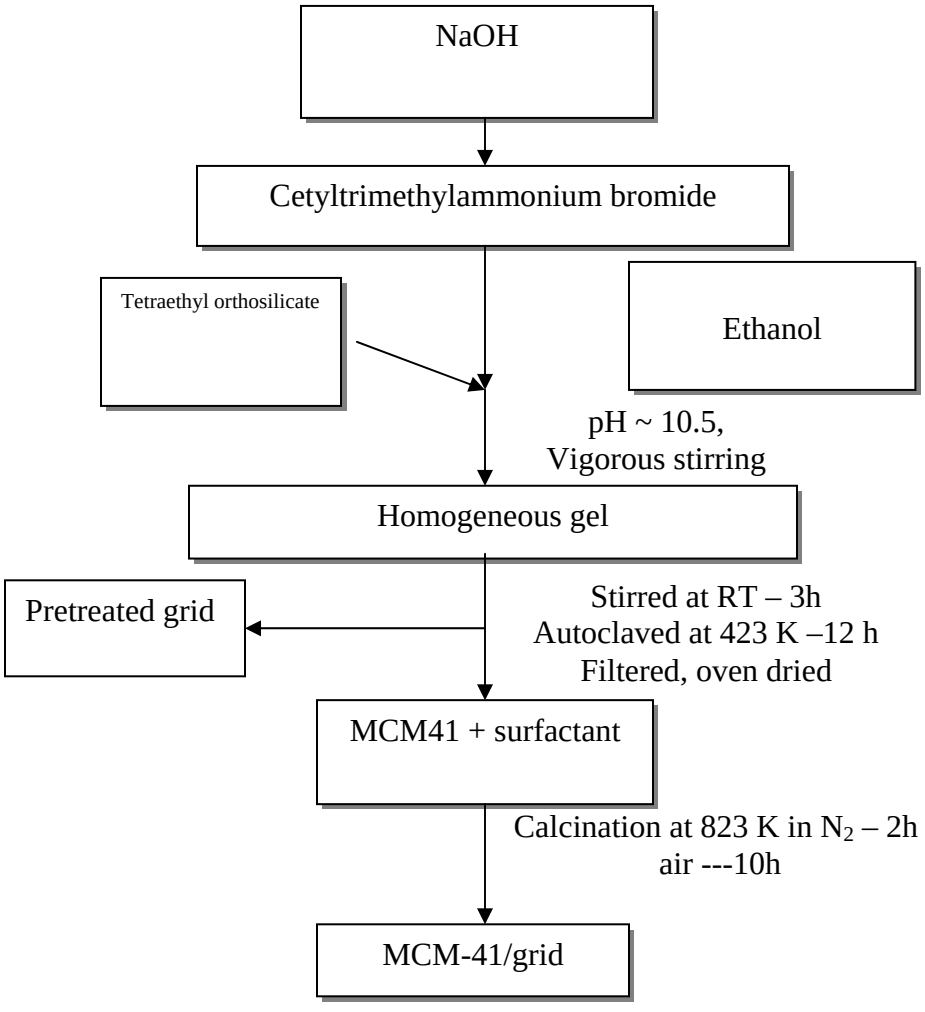

Scheme 5.1 Schematic representation of the synthesis of MCM-41/ stainless steel grid

5.3 RESULTS AND DISCUSSION

5.3.1 XRD

A yield of 54% was achieved in the synthesis of MCM-41. The selectivity of the coating, defined as the % mass of MCM-41 coated on the grid with reference to the total mass of MCM-41 formed (attached to the grid and present in the solution), was about 24%. The grid coverage was found to be ~100 g of MCM-41/m^2grid. In the earlier reported work of ZSM-5 deposition on metal grid (Louis et al., 2000), it was made possible to attain this coverage only after a three-step synthesis. Figures 5.2 & 5.3 represent the X-ray diffraction patterns of the as-synthesized and calcined MCM-41/stainless steel grid. Both samples exhibit a single broad d_{100} reflection in the 2θ range of 2-3°, characteristic of the MCM-41 phase. The higher order reflections are barely resolved in the X-ray pattern of coated material (powder scratched from the grid). Weak reflections are also observed in the 2Θ range from 4 to 6° confirming less long-range order. It is important to note the shift of the reflection maximum in the patterns of these two samples. In other words, the uncalcined coated MCM-41 has a spacing of 37 Å, which upon calcination decreased to 35.2 Å. This decrease in the d spacing value is due to the contraction of the pore structure, which is taking place during the process of calcination. It can be seen that in addition to the maximum intense 100 peak, weak reflections arising from 110 and 200 planes in the 2θ range 4-6. These reflections can be indexed to a hexagonal lattice. When

the same synthetic procedure was employed without pretreatment, only a lesser quantity of the material was formed on the support. Moreover, upon ultrasonication, no material was present on the grid indicating the essence of the pretreatment conditions. Previous studies on zeolite coatings on metal surfaces have demonstrated the influence of the support pretreatment on the crystal morphology and on the density of the

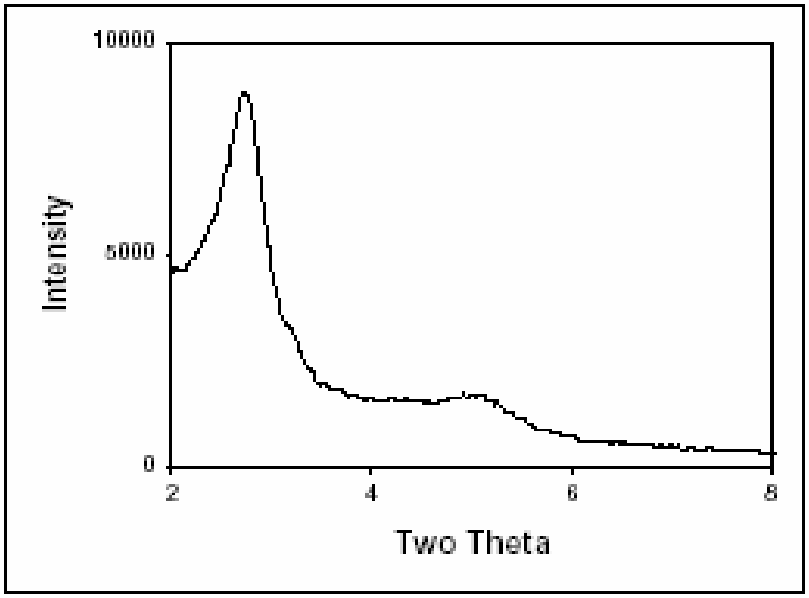

Fig. 5.2. XRD patterns of MCM-41/ stainless steel grid (As-synthesized)

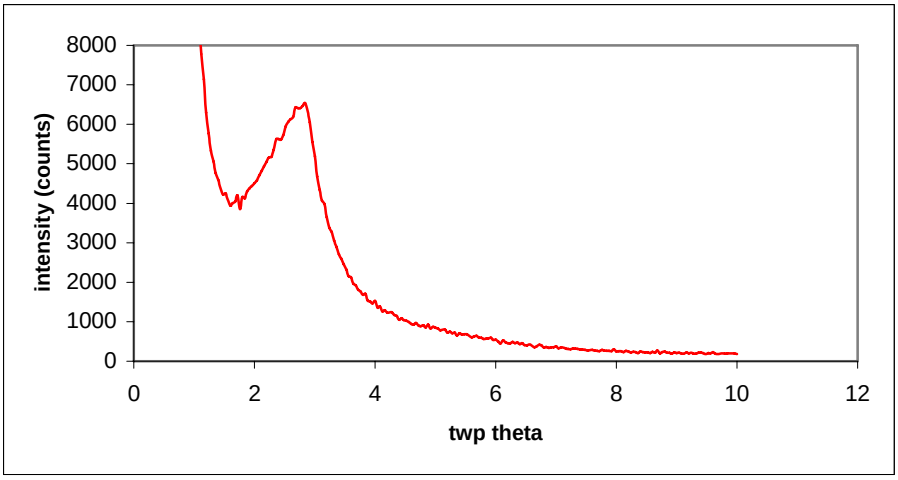

Fig. 5.3. XRD patterns of MCM-41/ stainless steel grid (calcined)

coating film (Louis et al., 2000). The zeolite coatings had much higher density as compared to the grains formed in the bulk volume due to the preferential growth of crystals from the surface nucleation sites. Mesoporous materials are formed through complementary electrostatic interactions between charged surfactant and inorganic Si-containing species. Under highly basic conditions (pH~ 10.5) used during the MCM-41 synthesis, the mesoporous sieves were successfully supported on metal grid via *in-situ* hydrothermal synthesis. After a one-step synthesis, the support is completely covered by a dense layer with a thickness of ~80 μm with the negatively charged OH-groups forming a electric double layer in the vicinity of the support. The self-arrangement of the micelles in a two-dimensional scale is affected by this induced electric field reducing the critical diameter of the surfactant micelles. Therefore, a more compact mesoporous structure with a less long-range crystalline material was formed.

5.3.2 N_2 adsorption

The nitrogen adsorption-desorption isotherms with the pore-size distribution calculated on the basis of BJH analysis are represented in Figure 5.4. MCM-41 material exhibits typical type IV isotherms with a hysteresis loop characteristic of mesoporous materials. The initial formation of a monolayer at lower relative pressures is followed by an inflection around p/p_0 0.2-0.3. This inflection around p/p_o= 0.2-0.3 is indicative of mesoporous solids where adsorption is taking place within mesopores (Kresge et al., 1992; Patarin et al., 2002; Conner et al., 1998). The adsorption-desorption isotherms are typical for well-defined mesoporous materials. BET surface area of ~ 550 m^2/g was observed along with uniform porous framework of~30 Å diameter, characteristics of MCM-41 type mesoporous materials.

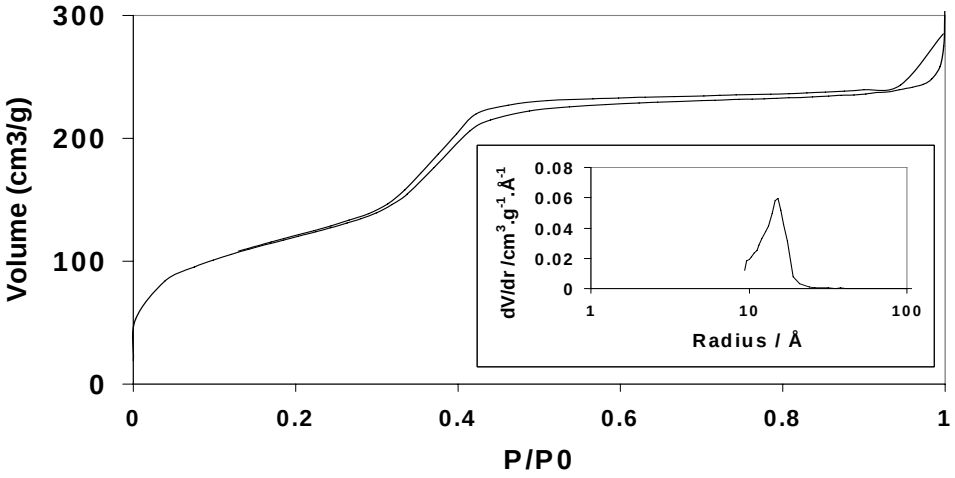

Figure 5.4.N_2 adsorption-desorption isotherms and pore size distribution **of MCM-41/ stainless steel grid.**

5.3.3 Thermal analysis

One of the important points to be considered in the preparation of M41S on stainless steel grid is to preserve the crystallinity of these materials, i.e. removal of the surfactant in a controlled manner. This was proved to be a crucial step for the successful preparation of mesoporous materials, since removal of the surfactant is an exothermic process. Fig. 5.5 represents the thermogram of as-synthesized MCM-41 material (powder scratched from the grid) which shows three weight loss regions. The first one corresponds to the loss of physi-sorbed water, the second and main weight loss in the temperature range

423-673 K corresponds to weight loss due to the removal of the surfactant and the final weight loss beyond 673 K is due to the loss of water from the condensation of the silanol groups. More interestingly, the material remains intact on the grid even after calcination.

5.3.4 SEM studies

Figures 5.6 and 5.7 represent SEM images of the grid after synthesis of MCM-41. When pretreatment with CTAB solution was not applied to the grid, coverage was not complete after ultrasonication. On the contrary, a complete coverage by the MCM-41 is seen after the CTAB treatment with a layer thickness of 80 μm. Therefore, it can be concluded that such a treatment with CTAB induces the formation of the mesoporous material on the metal grid. Surfactant molecules containing hydrophilic head and hydrophobic tail seems to provide spatial distribution by minimizing the interaction between incompatible substances. Relatively high selectivity (24%) of the coatings on the grid suggests increased affinity of the support for the micelle formation. This is probably due to creation of “sticking sites” by the template adsorption during the course of pretreatment on the metal surface. Figure 5.6 represents the coverage of the material on the grids where as Figure 5.7 confirms the layer morphology and the uniform size of grains ~ 4-5μm.

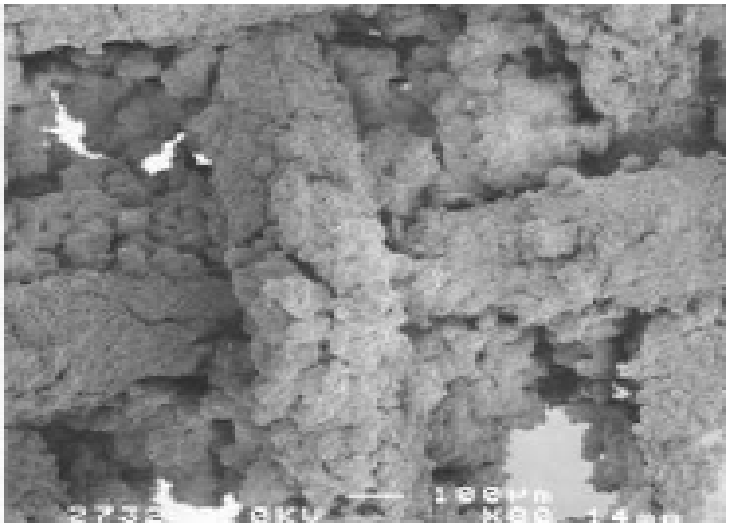

Fig. 5.6. SEM image of MCM-41/ stainless steel grid (low resolution)

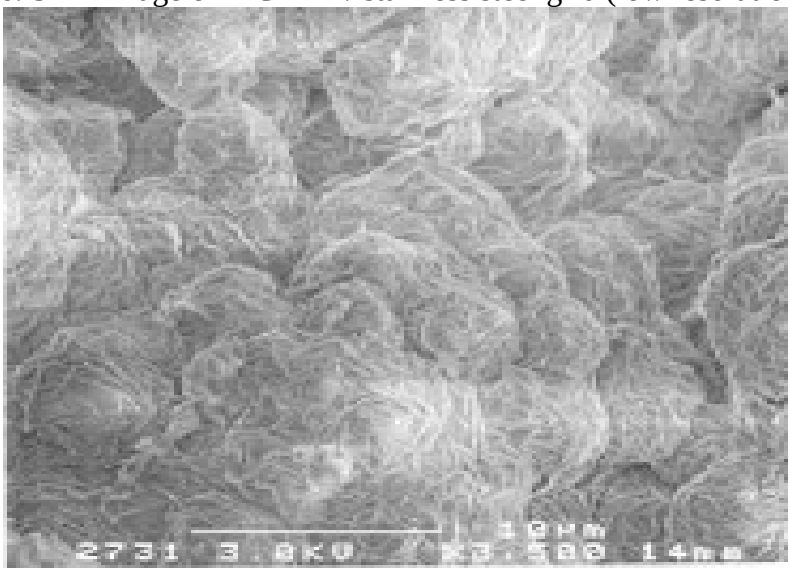

Fig. 5.7. SEM images of MCM-41/stainless steel grid (high resolution)

5.3.5 TEM studies

The ordered structure is clearly seen on HRTEM image presented in Fig. 5.8. Well-distributed pores with an average pore diameter of around 3 nm confirm the earlier observation made with N_2 adsorption studies. The hexagonal structure, known to be the main characteristic of MCM-41 is observed in a suitable orientation of the sample in the electron beam.

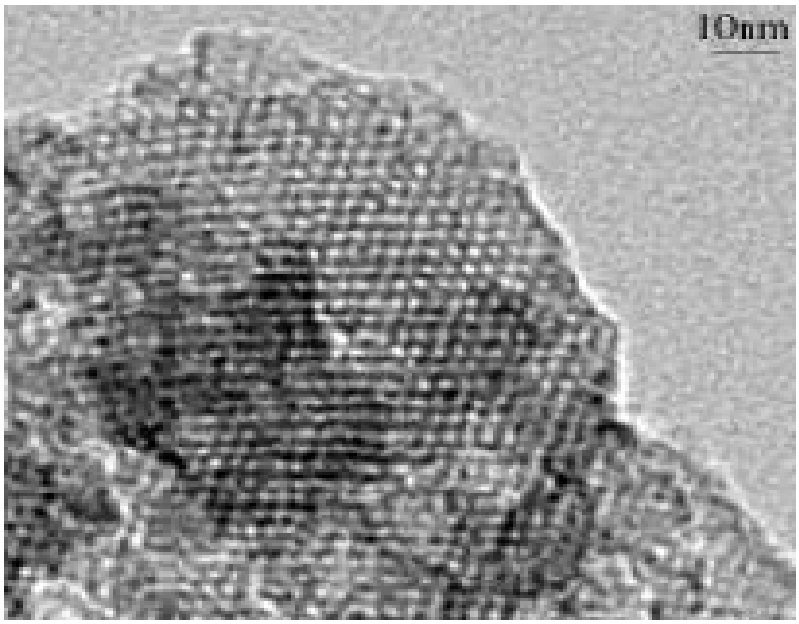

Fig. 5.8. TEM image of MCM-41/ stainless steel grid

5.4 MCM-48 COATING ON STAINLESS STEEL GRID

5.4.1 Synthesis

The pretreatment conditions employed for the synthesis of MCM-48/stainless steel grid are the same as that of MCM-41 coatings. MCM-48 materials have been prepared under hydrothermal synthesis conditions using cetyltrimethylammonium bromide as structure directing template and tetraethylorthosilicate as the silica source. TEOS (12.7ml) was mixed with a solution containing CTAB (2.5g) and NaOH (0.57g) in H_2O (100g) and ethanol (3.5 ml) as co-solvent (Gallis et al., 1998). The homogeneous gel was found to have the composition 2 SiO_2: 0.24 CTAB: 0.5 NaOH: 1-3 EtOH: 195 H_2O. This

homogeneous gel after ageing at room temperature for 3 hours then transferred into a static autoclave and the pretreated stack of the grid was introduced vertically into the autoclave, hydrothermally treated at 423K for 10-15 h. After removing from the oven, the solid obtained was washed with water and oven dried. The packing was then kept in an ultrasonic bath for 30 min to remove loosely attached particles and dried overnight at 400 K. The catalytic packing was calcined in air at 823K for 12h to remove the template. During the initial calcinations period nitrogen atmosphere was maintained in order to preserve the structure.

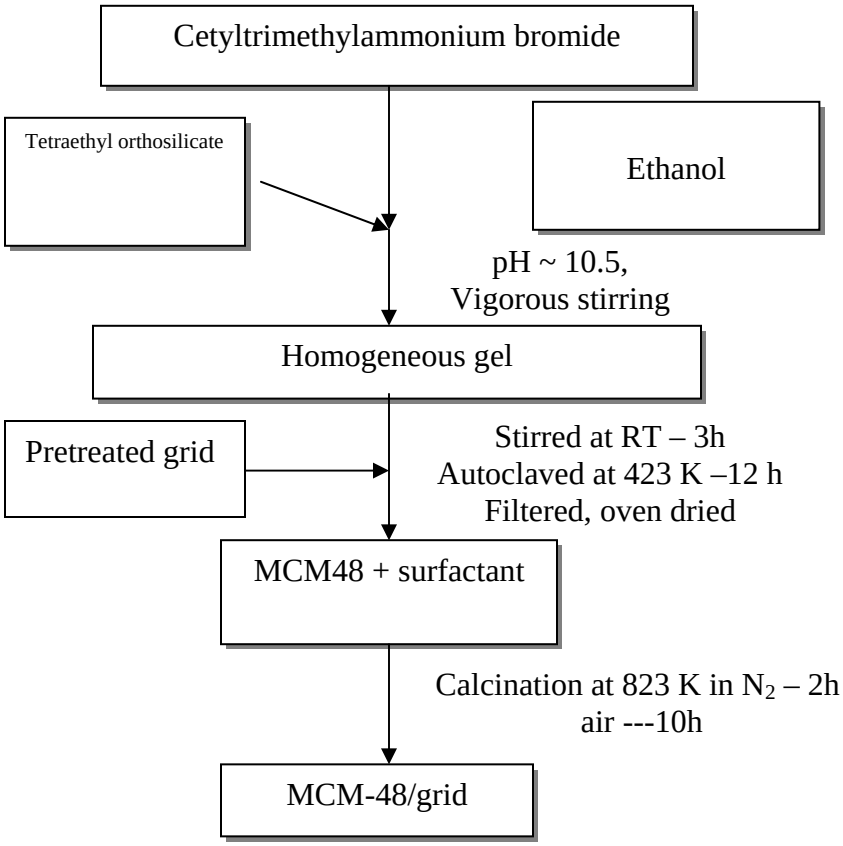

Scheme 5.2. Schematic representation of the synthesis of MCM-48/ stainless steel grid

5.5 RESULTS AND DISCUSSION

5.5.1 XRD

The powder X-ray diffractograms of the as-synthesized and calcined (powder scratched from the grid packing) MCM-48 samples are shown in Fig. 5.9& 5.10. It can be seen that ordered MCM-48 mesoporous material consistent with an *Ia3d* cubic symmetry is formed. In the procedure adopted in the present study, the synthesis of MCM-48 was achieved at low surfactant to silicon ratio unlike the synthesis reported by Mobil researchers, where higher ratios are mandatory to obtain the cubic structure (Beck et al.,1992; Alfredsson et al., 1996). As-synthesized material shows a maximum intense peak that corresponds to 211 reflection at a d spacing of 33.9Å. In addition to the maximum intense 211 reflection, weaker but clearly visible peaks corresponding to 220 and 321 reflections are also seen, which can be indexed to a cubic MCM-48 lattice. The calcined MCM-48 material exhibits a maximum intense peak with d_{211} value of 31.5 Å. This decrease in the d spacing upon calcination is due to the contraction of the unit cell during the process of calcination. Moreover, in addition to 211 reflection, less intense peaks corresponding to (220), (321) and (400) reflections were also observed. After the calcination at 823 K in air, the cell calculated parameter was found to be 81.2 Å.

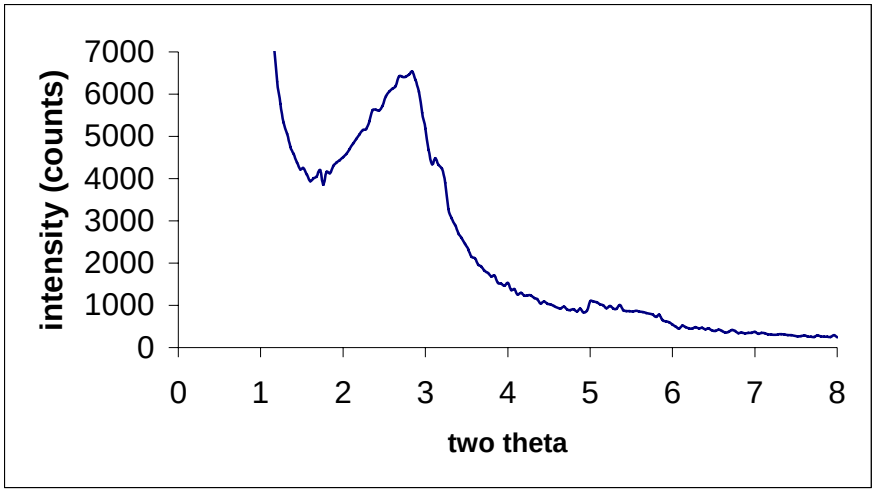

Fig. 5.9. XRD patterns of MCM-48/ stainless steel grid (uncalcined)

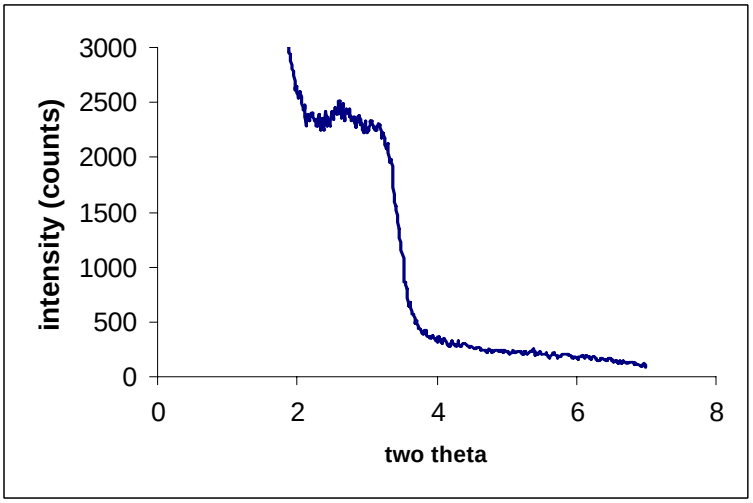

Fig. 5.10. XRD patterns of MCM-48/ stainless steel grid (calcined)

5.5.2 N_2 adsorption-desorption

The N_2 adsorption-desorption isotherms for MCM-48 material are shown in Fig. 5.11. MCM-48 catalyst exhibits typical type IV isotherm with a hysteresis characteristic of mesoporous materials. The isotherm is similar to the one observed for MCM-41 coating. It clearly shows the initial formation of monolayer at lower relative pressures, an inflection around p/p_0 0.2-0.3 indicative of mesoporous nature and an inflection at higher relative pressures, which is due to the macropore filling region. The BET surface area of the material is found to be 740m^2/ g with an average pore size distributed around 28 A^o.

5.5.3 Thermal Analysis

Thermogram of the MCM-48/ stainless steel grid is shown in Fig. 5.12, which shows mainly three weight loss regions, corresponding to the loss of physi-sorbed water (below 373 K), removal of template (473-523 K) and loss of water from condensation of silanol groups (above 550 K). It has been observed that these catalysts are stable up to 1073K.

5.5.4 SEM studies

Scanning electron microscopic images were recorded to observe the formation and morphology of the MCM-48 on the stainless steel grid. Figures 5.13 and 5.14 represent the scanning electron microscopic images of MCM-48 calcined materials on the grid at low and high resolutions, respectively. In order to use these metal catalytic supports as structure beds, there should be a complete coverage of the sample on the grid in order to avoid the participation of the metal supports in catalysis. Figure 5.13 represents the SEM recorded at low resolution confirms the converge of the material on the gird where as Fig. 5.14 recorded at high resolution confirms the layer morphology of the materials on the grid with uniform particle size of grains ~ 4-5μm. It was observed that formation of

MCM-48 was uniform on the grid. More interesting aspect is that even after the thermal treatment at 823 K for 12 h, the material was retained on the grid. This is probably due to creation of “sticking sites” by the template adsorption during the course of pretreatment on the metal surface.

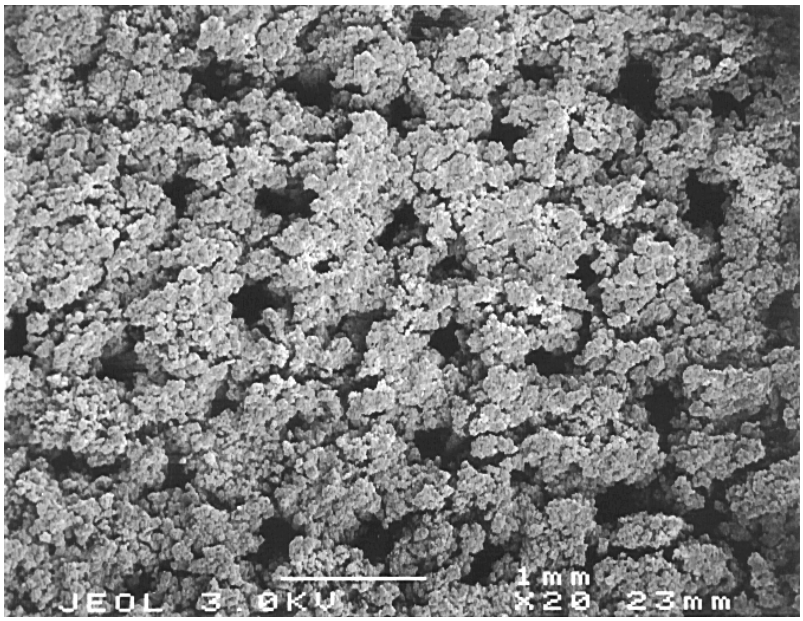

Fig. 5.13. SEM image of MCM-48/ stainless steel grid (low resolution)

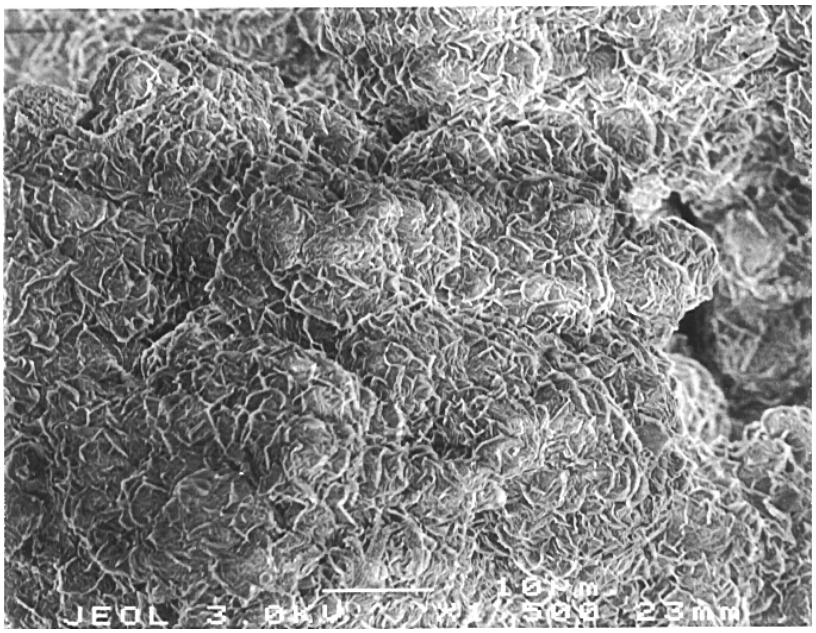

Fig. 5.14. SEM image of MCM-48/ stainless steel grid (high resolution)

5.5.5 TEM studies

Transmission electron microscopy gives information about the particle morphology and pore size of the MCM-48 material prepared in the presence of stainless steel grid. TEM image shown in the Figure 5.15 confirms the presence of mesopores with average pore size of ~ 3 nm, which is in agreement with the nitrogen adsorption-desorption studies where an average pore size of 28 Å was observed.

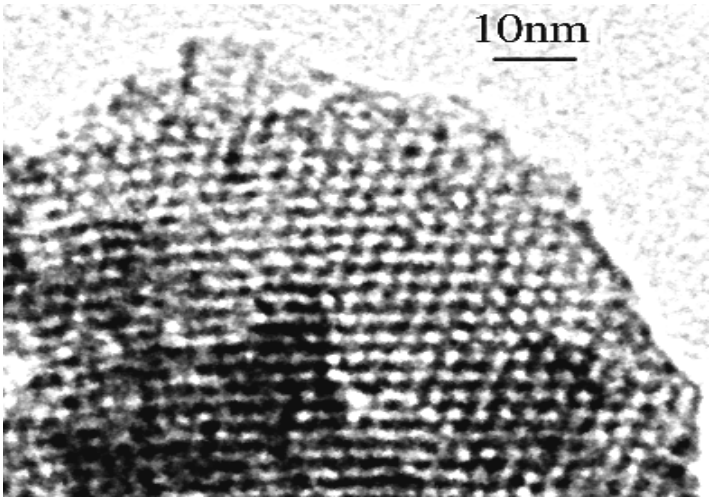

Fig. 5.15. TEM image of MCM-48/ stainless steel grid

5.6 CONCLUSIONS

The MCM-41 and MCM-48 mesoporous sieves were successfully synthesized on stainless steel grid via *in-situ* hydrothermal synthesis. After a one-step synthesis, the support is completely covered by a dense layer with a thickness of ~80 μm. This method opens the route for applications of mesoporous materials in the form of structured catalytic packing. The successful use of stainless steel grid as support for M41S materials may eliminate mass as well as heat transfer limitations in industrial processes.

CHAPTER 6

SYNTHESIS AND CHARACTERIZATION OF THERMALLY STABLE MESOPOROUS TITANIA

6.1 INTRODUCTION

Since the discovery of M41S materials by Mobil researchers (Beck et al., 1992) most of the works have been devoted only to the synthesis, characterization and catalytic exploitation of silica based mesoporous materials. Even though it has been realized initially that non-silica based materials can also be prepared by the same mechanistic pathways, the first successful attempt to prepare transition metal oxide; mesoporous titania was made only in 1993 (Monnier et al.1993). However, for these materials it had not been possible to remove the template by preserving the mesoporous nature and thus only mesostructured materials resulted after removal of the surfactant and not the mesoporous materials. With the first report on non-silica based mesoporous material titania in 1995 (Antonelli et al.,1995), steady developments started in this direction. Despite, the field of non-siliceous ordered mesoporous materials has found considerably less attention compared to that of mesostructured silica. Based on a number of alternative surfactant-assisted synthetic approaches, non-silicate mesoporous metal oxides were synthesized using low molecular weight surfactants. Some of the examples are titania (Antonelli et al., 1995; 1999); niobia (Stone et al.,1998); alumina (Bagshaw et al.,1996); tin oxide (Ulagappan et al.,1996b); ceria (Yang et al.,1998); and zirconia (Yang et al.,1998); vanadium oxide (Yang et al.,1998); aluminophosphates and vanadophosphates (Tiemann et al.,2001a; 2001b) were reported. However, these mesoporous transition metal oxides are somewhat less satisfactory than M41S in terms of

thermal stability and textural properties. For the synthesis of these non-silica based materials various mechanisms were proposed based on the existing interactions between the structure directing template or the inorganic precursor, where the surfactant can be cationic, anionic or neutral. Bagshaw et al., (1996) used non-ionic surfactants to synthesize mesoporous alumina in neutral media and suggested that the resulting mesoporous materials with wormhole-like channels are assembled by hydrogen-bonding interaction of the inorganic species with the surfactant molecules. Antonelli and Ying (1995) prepared the mesoporous TiO_2 using a modified sol–gel method, in which titanium alkoxide was hydrolyzed in the presence of an alkylphosphate surfactant. The authors reasoned that the hydrolysis and condensation rates were controlled using a chelating agent such as acetylacetone. BET surface area of about $200m^2/g$ was achieved. However, it was observed that phosphorus from the surfactant was bound so strongly to the molecular sieve that it could not be removed either by calcination or by solvent extraction. Later studies proved that the residual phosphorus might poison the catalytic surface sites. This limits the use of these materials as catalysts and catalyst supports. Moreover, calcination of as-synthesized material resulted only in amorphous material, which indicates that these materials can sustain only low temperatures. So, later studies aimed at the synthesis of mesoporous titania through surfactants other than phosphorus and with inorganic precursors such as titanocines and soluble peroxytitanates as the source of titanium. With these materials, it is possible to get the hexagonal mesoporous TiO_2 after calcination at 300 ^oC, however the pores are not uniform. Other than titanium various attempts have also been made to synthesize transition metal oxides in mesoform. Suib et al. (1997) prepared mixed-valent semiconducting mesoporous manganese oxides

with hexagonal and cubic structures and showed that these materials are catalytically active. For the syntheses of these materials, the redox state of manganese has to be carefully adjusted to allow the formation of the mesostrcture, similar to that observed by the same group for the syntheses of so-called octahedral molecular sieve (OMS) type materials. They started the synthesis with Mn^{+2} , which in solution forms $Mn(OH)_2$ which then reacts with CTAB, the template. They claimed that the final material can also be achieved with Mn(IV) precursor, however, reducing atmosphere is a prerequisite. Zirconium oxide contains both weakly acidic and basic surface sites providing high activity in reactions requiring acid–base bi-functional catalysts. Several synthetic routes, leading to mesostructured zirconia were described, which were based on two main synthesis pathways, a templating and a scaffolding mechanism. The main difference is that the templated materials are distinguished by their ordered pore system, while the ones made via scaffolding mechanism have a disordered pore arrangement, further, the materials have been found to collapse upon calcination (Yang et al., 1998). Furthermore, it was reported that ordered mesostructured zirconia could be thermally stabilized by the existence of an appreciable amount of sulfate or phosphate groups. In addition, these mesoporous solids have a sponge like mesoporous zirconia with some degree of pore wall crystallinity and on calcinations, resulted in the collapse of the mesoporous structure. Stable and well-defined mesoporous zirconia was also prepared through a one-pot synthesis with anionic and cationic surfactants which depended highly, however, on the nature of the head group (Yang et al.,1998). It was noted that the introduction of dopants such as phosphates and sulfates not only improved in the thermal stability of the zirconia but also resulted in higher acid strength and acidity for acid catalyzed reactions.

For example, phosphated zirconia is mildly acidic and sulfated zirconia is strongly acidic or even super acidic.

Even though a broad spectrum of mesoporous solids have been reported, they are associated with severe problems like surfactant removal which in turn reflected on the thermal stability of the final material. In most of the cases, it has been observed that after the removal of the surfactant the pore looks worm-like rather cylindrical (Schuth, 2001; Yang et al., 1998).

Most important aspect to be considered for the successful synthesis of mesoporous material is the removal of the surfactant. Moreover, compositions other than silica are often more susceptible to hydrolysis, redox reactions or phase transformations, accompanied by thermal breakdown of the structural integrity, which makes it more difficult to remove the template (Schuth, 2001).

6.1.1 Strategies for the synthesis of mesoporous titania

Majority of the synthetic routes for the production of non-siliceous mesoporous oxides involve either the use of organic species, which will form liquid crystals, or the amphiphilic block copolymers as structure directing agents. A co-operative templating mechanism has been speculated in all these systems, which is sensitive to synthetic parameters like template concentration, aging time and also the hydrothermal synthesis conditions. Among the non-siliceous mesoporous oxides, special attention has been paid mainly to synthesize titania in mesoporous form. A recent review suggested (Gratzel, 1999) that mesoporous titania can also be effectively used in advance applications like solar cells. The objective of the present investigation is to synthesize

thermally stable titania in mesoporous form and to study its physico-chemical properties using various techniques.

An initial report on the synthesis of mesoporous titania appeared in 1995 (Antonelli et al., 1995) by modified sol-gel route with phosphate surfactants that combined the principals of liquid crystal templating and the sol-gel procedure. In this procedure, it was observed that acetylacetone was required to delay the condensation process of the titanium precursor so that enough time is allowed for a suitable interaction with the phosphate head groups in aqueous media. Even though as-synthesized materials show well-ordered hexagonal structures, calcination of these materials yielded solids with low BET surface area values (~ 200 m^2/g). Further studies which revealed the collapse of the ordered structure with the retention of the surfactant, invoked the need to achieve an adequate balance between the rate of hydrolysis of titanium precursor and condensation process. Like wise, a few attempts have also been made to prepare thermally stable titania where anionic (Stone et al., 1998; Antonelli, 1999) and cationic surfactants were used(Cabrera, 2000). In a similar fashion, neutral surfactants have also been tried to prepare mesoporous titania. However, in all these methods, either removal of surfactant caused structural collapse or the final material has a BET surface area that was less than 100 m^2/g.

The possible synthesis of mesoporous titania by extending the existing mechanisms, as such is not successful due to the high rate of hydrolysis of titanium precursors. In the synthesis of mesoporous TiO_2, a combination of a surfactant and an inorganic precursor is being used. The synthesis of mesoporous titania is governed by the controlled precipitation of titanium precursor, specific temperature for the synthesis

and the easy removal of the surfactant. By achieving an adequate balance between the rate of hydrolysis and condensation process, it is possible to synthesize thermally stable mesoporous titania.

Due to faster rate of hydrolysis of the titanium precursor, there is a need to optimize the hydrolysis rate so as to achieve a stable homogeneous gel. In this connection, Antonelli et al (1995) used acetylacetone in acidic medium to obtain a stable gel. The use of anionic surfactant dodecylphosphate was also reported (Putnam et al., 1997) where pH was maintained in the range 4-6 with dilute HCl. Inspite of the initial success, it was observed that the removal of the surfactant was not complete, which was confirmed by the ICP-AES analysis. Though they have claimed the formation of mesoporous titania, their results have been questioned by several groups. Moreover, the use of acetylacetone in basic medium is not promising as the titanium acetylaceotone is stable only in acidic medium (Ying et al., 1999). Among the other known complexing agents, water-soluble triethanolamine was used to control the hydrolysis rate (Cabrera et al., 2000). However, removal of such species proved to be an important factor, as in this case attempts to remove the surfactant resulted in the collapse of the structure. Moreover, the presence of the heteroatom plays an important role as nitrogen might be present as an impurity in the final material. But, water soluble polymers with lower molecular weights can serve this purpose, especially polyethylene glycol (400) (PEG 400) which can be easily removed by simple calcination under mild conditions (250-400 ^{o}C) depending on the matrix in which it is present. In the present study, PEG 400 was used as hydrolysis retarding agent. This is due to its miscibility with Ti-precursors. In this approach the removal of polyethylene glycol was achieved by calcination process.

In the present study, thermally stable mesoporous titania was prepared by using cetyltrimethylammonium bromide as template and tetrabutylorthotitanate as titanium precursor. Polyethylene glycol (400) was employed as complexing agent to control the hydrolysis of the titanium precursor. As-synthesized and calcined materials were characterized by using low angle XRD, N_2 adsorption and thermal analysis to ensure the complete removal of the surfactant and the polymer.

6.2 SYNTHESIS OF MESOPOROUS TITANIA

The synthesis is based on the use of a cationic surfactant (CTAB)as a structural directing agent and a complexing agent polyethylene glycol as hydrolysis retarding agent. In the typical synthesis 0.0066 mole of CTAB (2.43 g) was dissolved in 60 ml of water. Tetramethylammonium hydroxide was added to this solution to maintain pH between 10.5 and 11.0. 0.0198 mole of titanium n-butoxide was added to 0.0066 mole of polyethylene glycol, stirred well and then this mixture was added to CTAB solution slowly by maintaining pH between 10.5 and 11.0 with tetramethylammonium hydroxide .The solution was stirred for three hours in nitrogen atmosphere. Then it was loaded in a stainless steel autoclave and hydrothermally treated at 423K for 24 h. The mixture was filtered and washed with ethanol + water mixture and oven dried. Calcination was carried out at 823 K in N_2 atmosphere for 2h followed by air for 10 more hours. For the synthesis of mesoporous TiO_2 in the present study, tetramethylammonium hydroxide was used as base source to maintain pH around 10.5 as other sources resulted in amorphous materials. This may be due to high rate of hydrolysis of Ti-alkoxides in the presence of strong base. Schematic representation of the synthetic procedure is given in Scheme 6.1.

When the synthesis was carried out with out any modification of the procedure, only amorphous materials resulted. This was due to the rapid hydrolysis of Ti-precursor. To confirm this point, the synthesis of titania was attempted without the complexing agent which probably hinders the rate of hydrolysis. Moreover, when the synthesis was carried out only in polymer (PEG-400), then also it resulted in amorphous material, which rules out the possibility preparing the material with simple polymers like PEG-400. These results indicate that there should be an optimum concentration of the polymer with respect to inorganic precursor. As mentioned earlier, by achieving an adequate balance between hydrolysis and condensation process it is possible to produce mesoporous TiO_2.

Though, syntheses of inorganic solids especially, mesoporous solids were reported with polymeric surfactants (Bagshaw et al., 1996), there has been no report on the formation of such network with the surfactant used in the present study i.e. PEG-400. This is due to the fact that PEG-400 cannot form micellar arrangement in water medium. For the formation of the micelles in solution, there should be different moieties with hydrophilic/ hydrophobic difference. Polymers like tri-block polyethyleneoxide, polypropyleneoxide etc. are known to form such a network in proper combination of solvents.

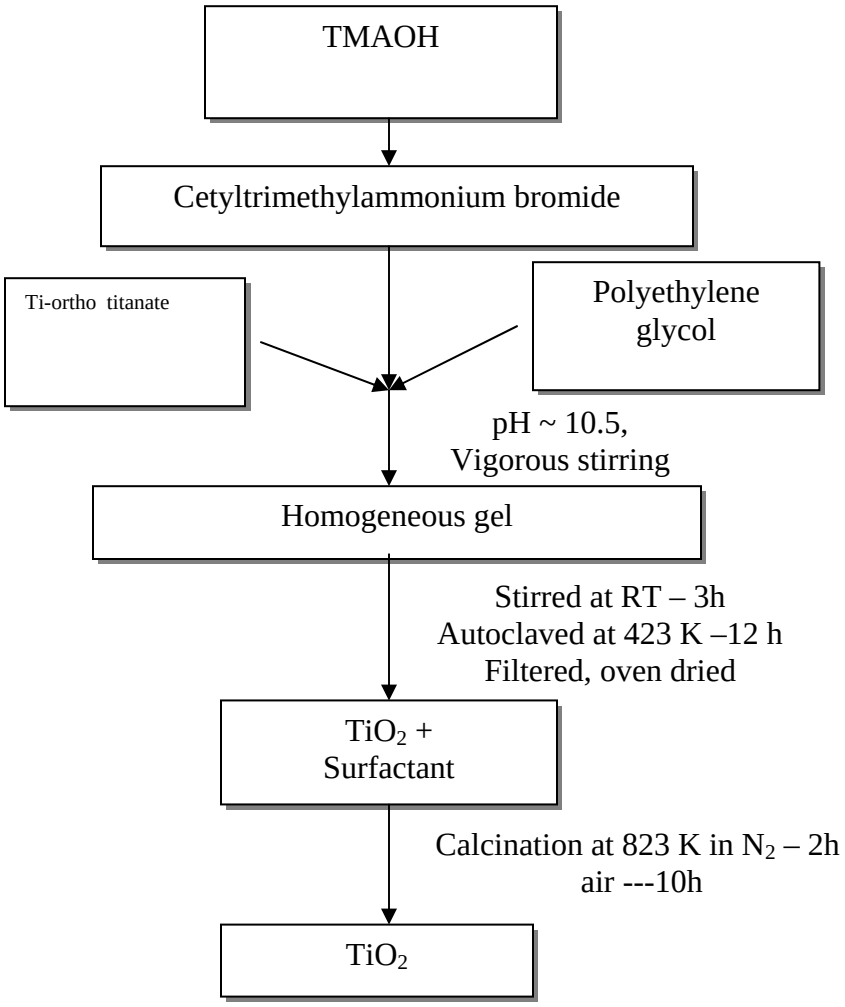

Scheme 6.1 . Schematic representation of preparation of TiO_2 by CTAB

6.3 RESULTS AND DISCUSSION

6.3.1 XRD

XRD patterns of the uncalcined and calcined mesoporous titania are shown in figures 6.1, 6.2, 6.3 and 6.4. As-synthesized material shows XRD pattern with a maximum intense peak in addition to peaks, which are not well resolved. The observed pattern can be indexed to d_{100}, d_{110} and d_{200} reflections of a hexagonal unit cell, which is characteristic of mesoporous solids (Beck et al., 1992). As-synthesized material shows a d_{100} spacing of 3.35 nm, which upon calcination decreases to 3.20 nm indicating less long-range crystallographic order. The as-synthesized TiO_2 also shows weaker but clear peaks corresponding to (110) and (200) reflections that can be indexed to a hexagonal lattice. pH of the synthesis gel was adjusted to 10.5 with tetramethylammonium hydroxide. As stated earlier, when NaOH or NH_4OH was used as a base instead of tetramethylammonium hydroxide, only amorphous material was obtained. This clearly indicates the need to maintain the pH of the synthesis gel with a milder base like TMAOH. The function of the organic ammonium cation of TMAOH is probably to modify the strength of the electrostatic interactions between the inorganic precursor species and the cationic surfactant micelle assembly to form a stable gel. If either NaOH or NH_4OH is used, the smaller cations Na^+, NH_4^+ compete with the TiO^- species and thus restrict the interaction with the positively charged cationic surfactant. However, it can be clear from the XRD pattern of the calcined material that upon calcination, the higher order reflections are absent. This is due to partial disorder of the structure. However, the d_{100} peak is still retained and this peak is shifted slightly to higher d-value confirming the partial disorder of titania after calcination. It has been observed that the titania prepared in this procedure exhibits thermal stability up to 973K unlike the materials reported in the literature where, upon the removal of the surfactant the ordered structure

collapses and becomes non porous. The high thermal stability of the mesoporous titania might be due to the formation of stable homogeneous gel that facilitates sufficient condensation process. To examine the thermal stability of the mesoporous titania, as-synthesized material has been calcined at various temperatures in order to remove the surfactant. Figures 6.3 and 6.4 represent the X-ray diffractograms of the mesoporous titania calcined at 973K and 1023 K. It can be seen that the mesoporous titania is stable up to 973 K. The material calcined at 973 K shows low angle diffraction peaks indicating that the mesoscopic order has been preserved in the sample.

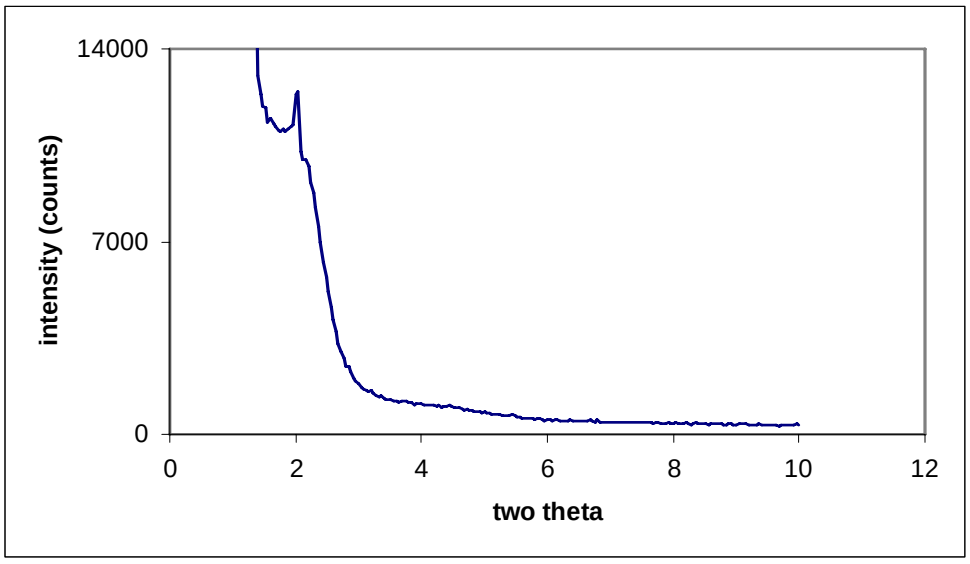

Fig. 6.1. XRD pattern of mesoporous TiO_2 synthesized with CTAB

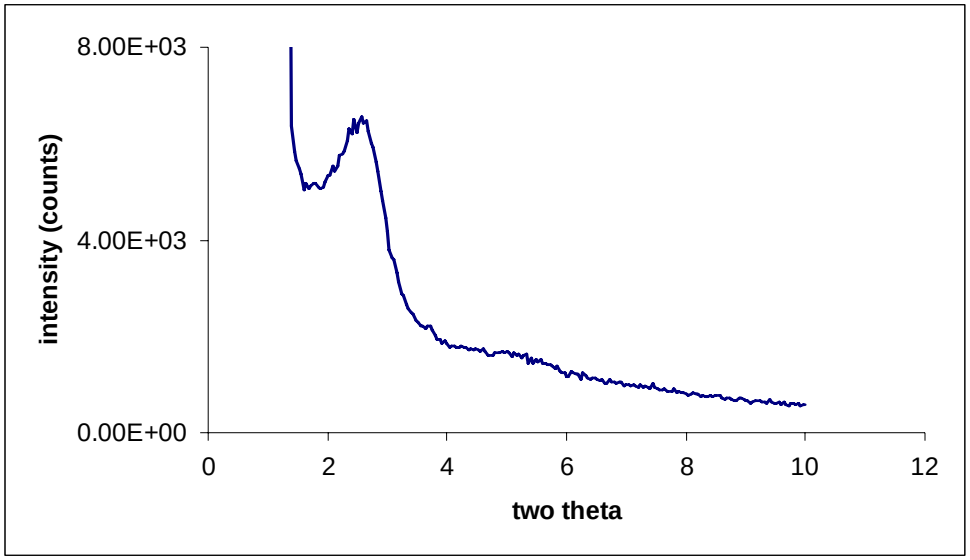

Fig. 6.2. XRD pattern of mesoporous TiO_2 synthesized with CTAB (calcined at 823 K)

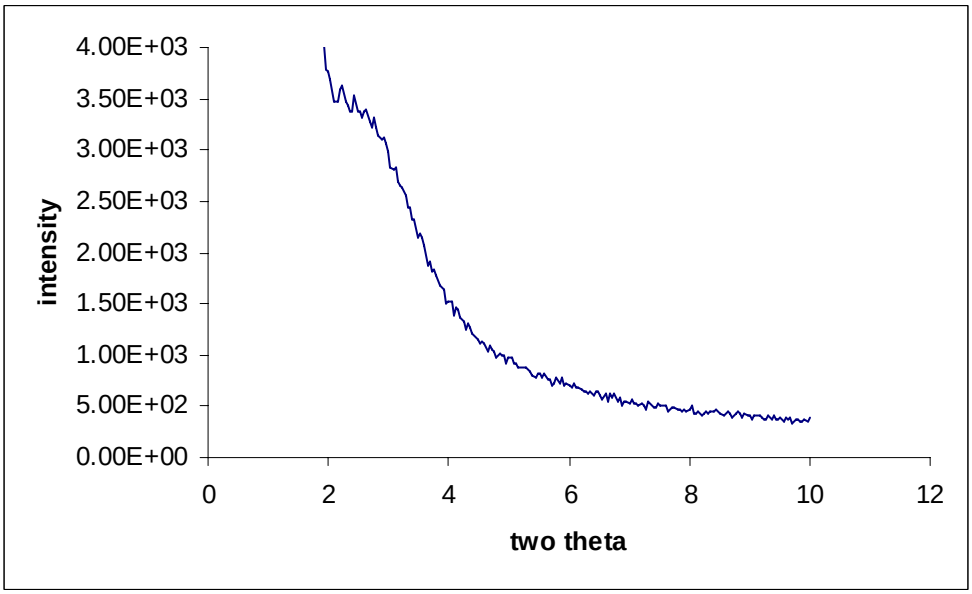

Fig. 6.3. XRD pattern of mesoporous TiO_2 synthesized with CTAB (calcined at 923 K)

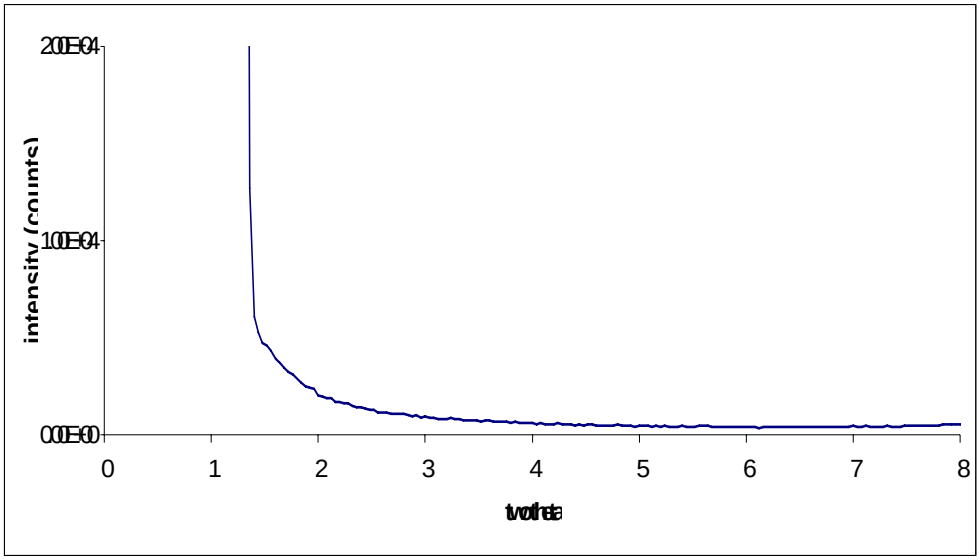

Fig. 6.4. XRD pattern of mesoporous TiO_2 synthesized with CTAB (calcined at 1023 K)

For titania prepared at higher concentrations of polyethylene glycol (PEG/T > 0.3) , XRD is not well resolved, and still in as-synthesized form MCM-41 like hexagonal structure was observed. Figures 6.5, 6.6, 6.7 and 6.8 represent the x-ray patterns of the materials prepared at higher concentrations of the polyethylene glycol-400. These materials are not thermally stable like the material prepared with (PEG/Ti~ 0.3-0.4). This may be due to the difficulty in the removal of PEG at higher concentration of surfactant. During the removal of surfactant by calcination process, the excess of heat generated because of exothermic process (combustion of carbon) may lead to the collapse of the mesostructure and impart less thermal stability to the final material.

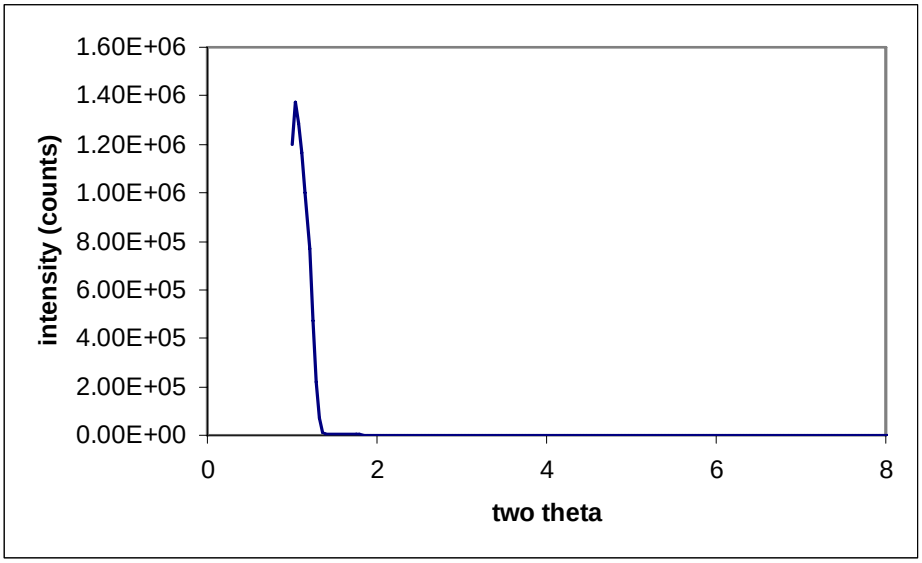

Fig. 6.5. XRD pattern of the mesoporous TiO_2 synthesized at PEG/Ti=0.5

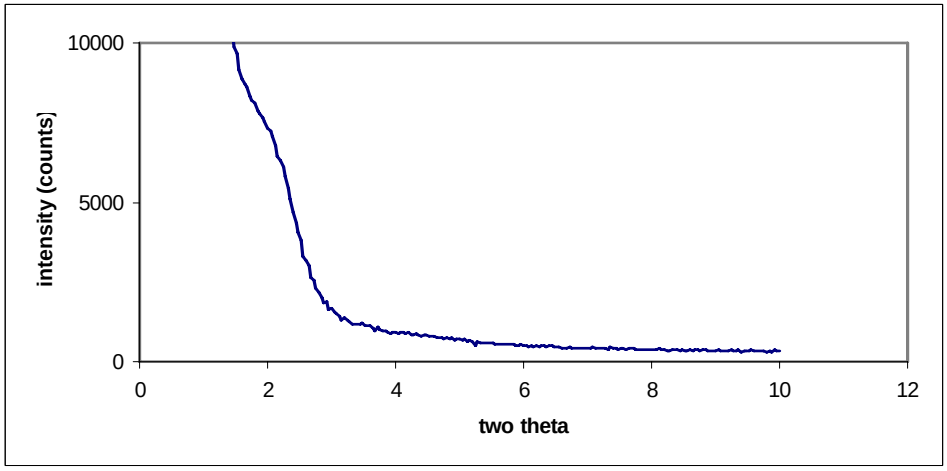

Fig. 6.6. XRD pattern of the calcined mesoporous TiO_2 synthesized at PEG/Ti=0.5

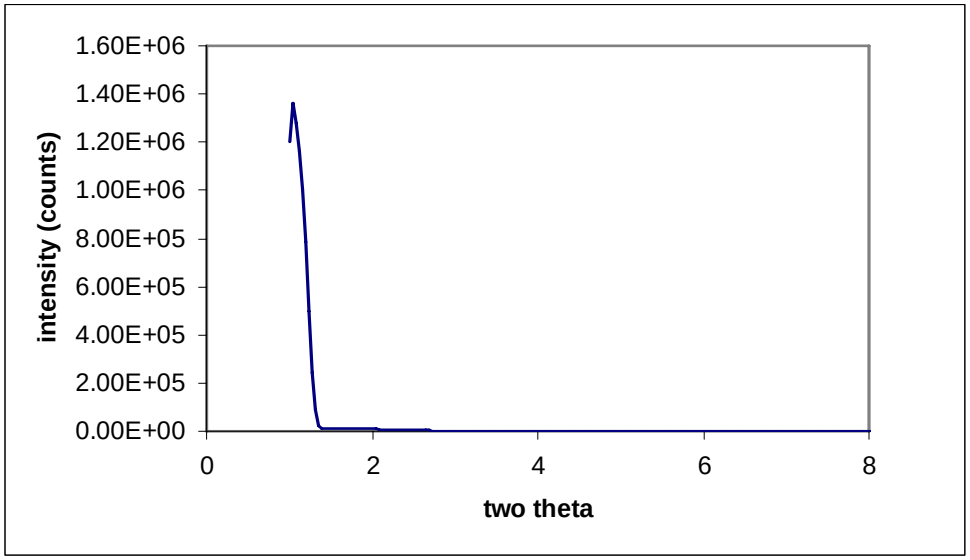

Fig. 6. 7. XRD pattern of the mesoporous TiO_2 synthesized at PEG/Ti=0.7

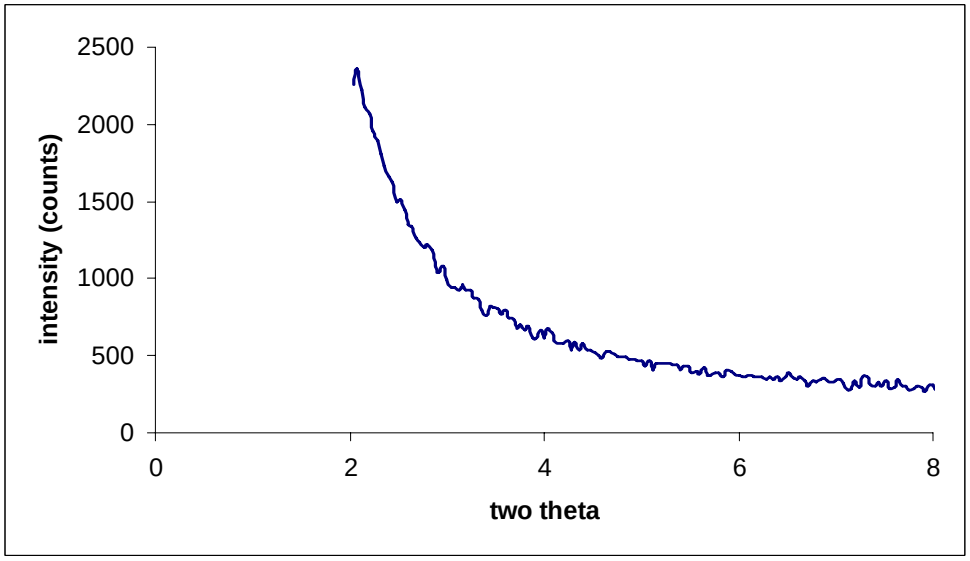

Fig. 6.8. XRD pattern of the calcined mesoporous TiO_2 synthesized at PEG/Ti=0.7

6.3.2 N_2 adsorption

Nitrogen adsorption-desorption isotherms of mesoporous titania calcined at 823 K shown in Fig.6.9. The isotherms provide information on the texture and porosity of the material. Mesoporous titania shows an isotherm which is some what similar to type IV isotherm with a small and distinct hysteresis loop, which is due to the capillary condensation taking place in side the mesoporous. The observed isotherms can be explained as follows: adsorption at lower relative pressures ($p/p_0 < 0.3$) is due to monolayer adsorption of nitrogen molecules on the walls of mesoporous titania. Thus, a thin layer of adsorbed nitrogen gas on the pore walls was observed at lower relative pressures, which was followed by a sharp inflection (~ 0.3), characteristic of capillary condensation within the walls. This hysteresis loop is due to the capillary condensation which takes place in narrow cylindrical pores of mesoporous titania. In general, for mesoporous materials the presence of hysteresis loop was taken as the confirmation for the presence of mesopores in the material. The mesoporous titania samples exhibited another sharp inflection at higher relative pressures ($p/p_0 > 0.9$), which can be attributed to macropore filling or to the filling of inter particles. In the case of mesoporous siliceous materials, this observation was explained as due to the formation of macropores during the process of calcination (Luan et al.,1995). In our present study, closer to type IV isotherm was observed, even though possibilities of different types of isotherms for mesoporous titania were dealt in literature by various groups (Zhang et al.2001a; Putnam et al., 1997; Ulagappan et al., 1996b; Yang et al., 1998; Antonelli, 1995). This ambiguous observation based on the poor crystalline nature may be due to the partial collapse of the semicrystallinity of these materials as a result of the thermal treatment at higher temperatures. The BET surface area of the titania is found to be 674 m^2/g. The pore size

distributions calculated on the basis of BJH analysis from the desorption branch of the isotherms show an average pore size distributed around 29 A^{o}.

6.3.3 Thermal analysis

Thermal analysis gives an idea on the removal of the surfactant as well as thermal stability of the materials prepared. Fig. 6.10 represents the thermogram of as-synthesized mesoporous titania, which shows mainly four weight loss regions, the first one corresponding to the loss of physi-sorbed water below 373K. In general, loss of surfactant CTAB can be observed in the temperature range 373- 623 K depending on the matrix (Beck et al.,1992; Antochshuk et al., 1998; Montes et al., 1998; Firouzi et al., 1997). In the case of silica based materials, the weight loss due to the removal of surfactant can be observed in the temperature range 473-573 K. Based on these observations, the second weight loss region in the range 373-550 K can be attributed to the loss of surfactant. The third weight loss above 550 K is due to the removal of the polymer polyethyleneglycol. The final weight loss above 650 K corresponds to the loss of water due to condensation of Ti-OH groups resulting in Ti-O-Ti linkages. It has been observed that titania has thermal stability up to 923K which is an improvement over the earlier reports where the thermal stability is only up to 773 K. This high thermal stability could be mainly due to the optimized synthesis conditions in an modified procedure.

6.3.4 Conclusions

Mesoporous titania was synthesized using the modified synthetic conditions using CTAB. The synthetic gel was modified with a simple polymer PEG-400. During the

approach adopted in the present study, mesoporous titania was synthesized at lower concentrations of the surfactant and the polymer. Mesoporous titania shows thermal stability up to 923 K unlike the earlier reports. This high thermal stability might be attributed to the optimization of the rate of hydrolysis and the condensation processes, which proved to play a vital role in the successful synthesis of the final material.

CHAPTER 7

SUMMARY AND CONCLUSIONS

Cubic analogous of M41S series have been prepared at low concentrations of the surfactant CTAB. Incorporation of heteroatoms like Al, Ti, V, Cr, Mn and Fe was done by adopting the liquid crystals of the surfactant CTAB. The textural properties of as synthesized materials were studied using low angle XRD and N_2 adsorption studies. The nature of binding of the surfactant with the mesoporous matrix was studied by thermal analysis. The presence of heteroatoms was ensured by various spectroscopic techniques, which not only confirmed their presence but also their oxidation states. Acidity of H-Al-MCM-48 and H-Fe-MCM-48 was measured by TPD of ammonia. Alkylation of naphthalene with alcohol was used as a probe reaction for acid catalysis. Redox properties of the catalysts were tested for liquid phase hydroxylation of phenol over Ti, V, Cr and Mn-substituted cubic MCM-48 with 30 % H_2O_2 as oxidizing agent.

Mesoporous aluminophosphates were also synthesized at low concentrations of the surfactant. Incorporation of vanadium, chromium and iron was done in order to synthesize redox catalysts. Catalytic activity of mesoporous V-AlPO was tested for the partial oxidation of toluene with 70 % TBHP and 30 % H_2O_2 in a variety of solvents and the results compared with V-MCM-48 and other literature reported systems for the same reaction.

Mesoporous chromium AlPO was synthesized and characterized. Catalytic activity of this catalyst was tested for partial oxidation of toluene in vapour phase and the results

compared with chromium substituted cubic analogue (Cr-MCM-48). Liquid phase oxidation of aromatics was also carried out over these systems.

Iron incorporated mesoporous aluminophosphates were synthesized and characterized with various physico-chemical techniques. Liquid phase oxidation of cyclohexane was performed as a test reaction at high-pressure conditions. Results were compared with that obtained with Fe-MCM-48 and a possible reaction mechanism was also proposed.

Since the application of mesoporous solids is limited because of their poor cystallinity and poor thermal stability, it imposes mass transfer limitations in industrial applications. To overcome this problem, stainless steel grids were employed as support materials for M41S materials. An in-situ synthetic approach was developed based on which MCM-41 and MCM –48 have been synthesized and characterized.

Mesoporous titania was synthesized under hydrothermal synthesis conditions where CTAB was employed as the surfactant. Various physico-chemical techniques confirmed the formation of mesoporous titania analogous to hexagonal MCM-41.

The major conclusions that evolved out of the present studies are

- All synthesized mesoporous aluminosilicates were found to be semicrystalline in nature with cubic lattice typical of MCM-48 materials. The crystallinity of these materials decreased with the incorporation of heteroatoms

- TGA analyses of as-synthesized samples revealed that strong interactions existed between the cationic surfactants and anionic inorganic matrices.

- N_2 adsorption studies at 77 K on all the calcined samples resulted in type IV isotherms accompanied with hysteresis, typical of mesoporous solids. They have high surface area (> 1000 m^2/g) with an average pore size distribution centered on 28 Å.

- Due to the less acidic nature these acid catalysts, catalytic selectivity of these systems towards monosubstituted products was high. Extent of oligomerization of primary alcohols was less on these mesoporous acid catalysts at high temperatures compared to the conventional zeolites. Thus, naphthalene conversions on these materials were higher compared to zeolites.

- Among the catalysts examined for alkylation of naphthalene with alcohols, H-Al-MCM-48 showed higher activity compared to H-Fe-MCM-48 or H-Al-MCM-41.

- Ti-MCM-48 exhibited higher activity for phenol hydroxylation when compared to other catalytic systems and water proved to be a better solvent for this reaction.

- Mesoporous aluminophosphates were synthesized under hydrothermal synthesis conditions at lower concentrations of surfactant and were systematically characterized with various physico-chemical and spectroscopic techniques. V, Cr and Fe- substituted mesoporous aluminophosphates were also synthesized and characterized by various physico-chemical techniques, which confirm the formation of mesophase and the presence of heteroatoms within the framework.

- Mesoporous aluminophosphates were found to be less crystalline compared to aluminosilicates and were also thermally less stable.

- Mesoporous V-AlPO was found to be active for liquid phase toluene oxidation with both 70 % TBHP as well as 30% H_2O_2 and were more selective for side chain oxidation products. Mesoporous V-AlPO was found to be more active than V-MCM-48 and acetone was found to be a better solvent.

- Molecular oxygen/air have been employed as an oxidant over mesoporous Cr-AlPO, which exhibited both acidic and redox properties where as Cr-MCM-48 was purely a redox catalyst. Both mesoporous Cr-AlPO and Cr-MCM-48 showed selectivity towards side chain oxidation.

- Results on the liquid phase oxidation of side chain aromatics over Cr-substituted mesoporous solids also suggested that Cr-AlPO is more active when compared to Cr-MCM-48.

- Mesoporous Fe-AlPO promoted aerial oxidation of cyclohexane and showed selectivity towards cyclohexanol through a radical route. Interestingly under the same reaction conditions, Fe-MCM-48 had not shown any significant activity.

- *In-situ* synthesis of M41S on stainless steel grids have been done and various characterization techniques confirmed the formation of mesoporous materials on the grids. Scanning electron microscopic analysis confirmed the complete coverage of the material on the grids and transmission electron microscopic analysis confirmed the well distributed uniform pores within the material.

- Synthesis of thermally stable mesoporous titania had been carried out under hydrothermal synthesis conditions by using CTAB as the template. Various

characterization techniques confirmed the formation of mesoporous material with a BET surface area ~ 675-m^2/g and pore size distribution of around 30 Å.

These mesoporous solids, though could be synthesized, exhibited lesser thermal stability and lower acidity compared to conventional zeolites. Mesoporous aluminophosphates seem to be promising materials over which natural oxidants can successfully be employed as oxidants. However, the successful synthesis of M41S materials on stainless grids will surely open new directions for the potential applications of these materials. It is hoped that further scope exists for exploring these materials with suitable modifications and reaction conditions.

REFERENCES

1. **Ahn, W.S., D. H. Lee, T. J. Kim, J. H. Kim, G. Seo and R. Ryoo (**1999) Post-synthetic preparations of titanium-containing mesoporous molecular sieves**.** *Applied Catalysis A: General, **181**, 39-49.*
2. **Alexandridis P., U. Olsson and B. Lindman** (1998) A Record Nine Different Phases (Four Cubic, Two Hexagonal, and One Lamellar Lyotropic Liquid Crystalline and Two Micellar Solutions) in a Ternary Isothermal System of an Amphiphilic Block Copolymer and Selective Solvents (Water and Oil). *Langmuir, **14**,* 2627-2638.
3. **Alfredsson, V., M. Keung, A. Monnier, G.D. Stucky, K.K.Unger and F. Schuth** (1994) High resolution transmission electron microscopy of mesoporous MCM-41 type materials. *Journal of chemical society, chemical communications*, 921-922.
4. **Alfredsson, V. and M.W. Anderson** (1996) Structure of MCM-48 revealed by transmission electron microscopy. *Chemistry of Materials*, **8**, 1141-1146.
5. **Anderson, M.W.** (1997) Simplified description of MCM-48, *Zeolites*, **19**, 220-225.
6. **Anderson, M. W., C.J. Jackson and D.P. Luigi** (1999) Structure and synthesis of MCM-48. *Proceedings of the International Zeolite Conference,* **1**, 697-704.
7. **Antochshuk, V. and M. Jaroniec** (1998) Thermogravimetric studies of alkyl-modified ordered mesoporous materials. Proceedings of the Conference of the North American Thermal Analysis Society, **13-15,** 247-252.

8. **Antonelli, D.M**. (1999) Synthesis of phosphorus-free mesoporous titania via templating with amine surfactants. *Microporous and Mesoporous Materials,* **30**, 315- 319.
9. **Antonelli, D.M and J.Y. Ying** (1995) Synthesis of a stable hexagonally packed mesoporous niobium oxide molecular sieve through a novel ligand-assisted templating mechanism. *Angewandte Chemie Internation Edition in English,* **35**, 426-430.
10. **Armengol, E., M.L. Cano, A. Corma, H. Garcia and M.T . Navarro** (1995) Mesoporous aluminosilicate MCM-41 as a convenient acid catalyst for Friedel-Crafts alkylation of a bulky aromatic compounds with cinnamyl alcohol. *Journal of Chemical Society, Chemical Communications*, 519-520.
11. **Armengol, E., A. Corma, H. Garcia and J. Primo** (1997) Acid zeolites as catalysts for inorganic reactions. Tert-butylation of anthracene, naphthalene and thianthrane. *Applied catalysis A*, **149,** 411-423.
12. **Arneds, I.W.C.E., R.A. Sheldon, M. Wallan and U. Schuchardt** (1997) Oxidative transformations of organic compounds mediated by redox molecular sieves. *Angewandte Chemie International Edition in English,* **36,** 1144-1163.
13. **Ashtekar, S., S.V.V. Chilikuri and D.K. Chakraborty** (1994) Small pore molecular sieves SAPO-34 and SAPO-44 with chabazite structure: a study of silicon incorporation. *Journal of Physical Chemistry*, **98**, 4878-4888.
14. **Athilakshmi** (1996**)** Ph.D thesis IIT Madras.
15. **Attard, G.S., J.C. Glyde and C.G. Goltner** (1995) Liquid-crystalline phases as templates for the synthesis of mesoporous silica. *Nature*, **378**, 366-368.

16. **Aufdembrink, B.A., A.W. Chester, J.A. Herbst and C.T. Kresge,** US patent, 5, 258, 114, 1993

17. **Auvray, X., C. Patipas, R. Anthore, I. Rico and A. Lattes** (1989) X-ray diffraction study of mesoporous of cetyltrimethylammonium bromide in water, formamide and glycerol. *Journal of Physical Chemistry*, **93**, 7458-7464.

18. **Badamali, S.K., A. Sakthivel and P. Selvam** (1998b) Tertiary butylation of phenol over mesoporous H-Fe-MCM-41. *Catalysis Letters*, **65**, 153-157.

19. **Badamali, S. K and P. Selvam** (1998a) Synthesis and characterization of mesoporous ferrisilicate (FeMCM-41) molecular sieves**.** *Studies in Surface Science and Catalysis*, **113**, 749-758.

20. **Bae, J. Y., K.T. Ranjit, Z. Luan, R.M. Krishna and L. Kevan** (2000) Photoionization of N-Alkylphenothiazines in Mesoporous Metal Silicoaluminophosphate Molecular Sieves**.** *Journal of Physical Chemistry B,***104,** 9661-9669.

21. **Bagshaw, S.A., E. Prouzet and T.J. Pinanvaia** (1996) Templating of mesoporous molecular sieves by non-ionic polyethylene oxide surfactants. *Science*, **269**, 1242-1244.

22. **Beck, J.S., J.C. Vartuli, G.S. Kennady, C.T. Kresge, W.J. Roth and S.E. Schramm**. (1994) Molecular or supramolecular templating: Defining the role of surfactant chemistry in the formation of microporous and mesoporous sieves. *Chemistry of Materials*, **6**, 1816-1821.

23. **Beck, J.S., J.C. Vartuli, W.J. Roth, M.E. Leonowicz, C.T. Kresge, K.D. Schimtt, C.T.W. Chu, D.H. Olson, E.W. Sheppard, S.B. McCullen, J.B.**

Higgins and J.L. Schlenker (1992) A new family of mesoporous molecular sieves prepared with liquid crystal templates. *Journal of the American Chemical Society,* **114**, 10834-10843.

24. **Behrens, P., and G.D. Stucky** (1993) Ordered molecular arrays as templates: A new approach to synthesis of mesoporous materials, *Angewandte Chemie International Edition in English,* **32**, 696-699.
25. **Biz, S. and M. L. Occelli** (1998) Synthesis and characterization of mesostructured materials. *Catalysis Review Science and Engineering*, **40**, 329-407.
26. **Blackwell, C.S. and R.L. Patton** (1988) Solid state NMR of silicoaluminophosphate molecular sieves and aluminophosphate materials. *Journal of Physical Chemistry*, **92**, 3965-3970.
27. **Blasco T., A. Corma, M. T. Navarro and J. P. Pariente** (*1995)* Synthesis, Characterization, and Catalytic Activity of Ti-MCM-41 Structures, *Journal of Catalysis, **156**,* 65-74.
28. **Branton, P.J., P.G. Hall and K.S.W. Sing** (1993) Physisorption of nitrogen and oxygen by MCM-41, a model mesoporous adsorbent. *Journal of Chemical Society, Chemical Communications,* 1257-1258.
29. **Breck, D.W**. Zeolite molecular sieves, structure chemistry and use. John Wiley and Sons, New York, 1974.
30. **Cabrera, S., J. E. Haskouori, A. Beltran-Porter, D. B. Porter, M. D. Marcos and P. Amoros** (2000) Enhanced surface area in thermally stable pure mesoporous TiO_2, *Solid State Science,* **2**, 513-518.

31. **Cabrera, S., J. El Haskouri, C. Guillem, J. Latorre, A. Beltran-Porter, D. Beltran-Porter, M. D. Marcos and P. Amoros** (2000) Generalized syntheses of ordered mesoporous oxides: the atrane route. *Solid State Sciences* **2**, 405-420.

32. **Calis, H. P., A. W. Gerritsen, C.M. van den Bleek, C.H. Legein, J.C. Jansen and H. van Bekkum** (1995) Zeolites grown on wire gauze: A new structured catalyst packing for dustproof, low pressure drop DeNox processes. *Canadian Journal of Chemical Engineering*, ***73***, 120.

33. **Carlsson, A., M. Kaneda, Y. Sakamoto, O. Tersaki, R. Ryoo and S. H. Joo** (1999) The structure of MCM-48 determined by electron microscopy. *Journal of Electron Microscopy*, 48, 795-798.

34. **Carrington, A. and A.D. McLachalan** (1988) Introduction to magnetic resonance with applications to chemistry and chemical physics**.** Harper& Row, New York.

35. **Cavani, F., G. Centi, E. Feresti, F. Trifiro and G. Busca** (1988) Surface structure and reactivity of vanadium oxide supported on titanium dioxide V_2O_5 / TiO_2 (rutile) catalysts prepared by hydrolysis (1988) *Journal of Chemical society Dalton Transactions*, **84**, 237-241.

36. **Centi, G., S. Perathnor, F.Trifiro, A. Aboukais, C.F. Aissi and M. Guelton** (1992) Physicochemical characterization of V-Silicate, *Journal of Physical Chemistry*, **96,** 2617-2622**.**

37. **Chakraborty, B** (1998) Ph.D thesis, IIT Madras.

38. **Chakraborty, B., A.C. Pulikottil, S. Das and B. Viswanathan** (1997) Synthesis and characterization of mesoporous SAPO materials, *Journal of Chemical Society Chemical Communications*, 911-912.

39. **Chakraborty, B., A.C. Pulikottil and B. Viswanathan** (1996) Alkylation of naphthalene with alcohols over mesoporous MCM-41, *Catalysis Letters*, **39**,63-65.

40. **Chatterjee, M., T. Iwasaki, Y. Onodera, H. Hayashi, T. Ebina and T. Nagase** (2001) Vanadosilicate: cubic mesoporous molecular sieve, *Studies in Surface Science and Catalysis* **135,** 1163-1169.

41. **Chen, C.Y., H.X. Li and M.E. Davis** (1993) Studies on mesoporous materials. I. Synthesis and characterization of MCM-41. *Microporous Materials*, **2**, 17-26.

42. **Cheng, C.F., D.H. Park and J. Klinowski** (1997) Optimal parameters for the synthesis of mesoporous molecular sieve [Si]-MCM-41. *Journal of Chemical Society, Faraday Transaction*s, **93**, 193-197

43. **Chester, A. W., F.E. Daugherty, A.S. Fung, C.T. Kresge, H.K.C. Timken, J.C. Vartuli, R. Kumar, T. G. Roberie, and M. Ziebarth**, A catalytic cracking process using a modified mesoporous aluminophosphate material. US patent, 2001.

44. **Christian B., F. Giovanni, G. Matteo, M. Giuliano, P. Rinaldo and R. Nicoletta** (1998) A comparison between [Ti]-MCM-41 and amorphous mesoporous silica–titania as catalysts for the epoxidation of bulky unsaturated alcohols, *Microporous and Mesoporous Materials***, 44-45**, 595-602.

45. **Conner, W. C., M.A. Springuel-Huet, J. Fraissard, J. Bonardet, T. McMahon, L. Boudreau, and J. Masciadrelli** (1998) Hysteresis in physical sorption for MCM-41. *Studies in Surface Science and Catalysis*, **117**, 575-581.

46. **Corma A.** (1997) From microporous to mesoporous molecular sieve materials and their use in catalysis, *Chemical Reviews* , **97**, 2373-2419.

47. **Corma, A** (1998) Preparation and catalytic properties of new mesoporous materials. *Topics in Catalysis* , **4,** 249-260.

48. **Corma, A., V. Fornes, M.T. Navarro and J. Perez-Pariente** (1994) Acidity and stability of MCM-41 crystalline aluminosilicates. *Journal of Catalysis*, **148,** 569-574.

49. **Corma, A., M.T. Navarro and J.P. Pariente** (1994) Synthesis of an ultralarge pore titanium silicate isomorphous to MCM-41 and its applications as a catalyst for selective oxidation of hydrocarbons. *Journal of Chemical Society, Chemical Communications,* 147-148**.**

50. **Corma, A., Q. K. Qiubin and R. Fernando** (1998) Synthesis of Si and Ti-Si-MCM-48 mesoporous materials with controlled pore sizes in the absence of polar organic additives and alkali metal ions. *Chemical Communications*, 579-580.

51. **Cybulski, A. and J.A. Moulijn**, *The present and the future of structured catalysts -An overview. Structured catalysts and reactors*; Marcel Dekker: New York, 1998.

52. **Dapurkar, S.E., S. K. Badamali and P. Selvam** (2001) Nanosized metal oxides in the mesopores of MCM-41 and MCM-48 silicates, *Catalysis Today*, ***68****, 63-68.*

53. **D'Arbonneau, S., A . Tuel and A. Auroux** (1999) Calorimetric study of the acidity of a new family of mesoporous catalysts. *Journal of Thermal Analysis and Calorimetry* **56**, 287-296.

54. **Das, T. K., K. Chaudhari, E. Nandanan, A. J. Chandwadkar, A. Sudalai, T. Ravindranathan and S. Sivasanker** (1997) Cr-MCM-41-catalyzed selective oxidation of alkylarenes with TBHP. *Tetrahedron Letters,* **38,** 3631-3634.

55. **Das, J., C.V.V. Satyanarayana, D.K. Chakraborty, S.N. Piramanayagam and S.N. Shringi (1992)** Substitution of Al in the $AlPO_4$-5 and $AlPO_4$-11 frameworks by Si and Fe: A study by Mossbauer, Magic-angle-spinning nuclear magnetic resonance and electron paramagnetic resonance spectroscopies and chemical probes. *Journal of Chemical Society, Faraday Transactions***, 88,** 3255-3261.

56. **Davidson, A. and M.J. Che** (1992) Temperature induced diffusion of probe vanadium(IV) ions into the matrix of titanium dioxide ; An investigated by EPR technique, *Journal of Catalysis,* **96**, 99-109.

57. **Davis, M.E.** (1991) Zeolites and molecular sieves- not just ordinary catalysts. *Industrial Engineering and Chemical Research*, **30,** 1675-1683.

58. **Davis, M.E, C. Saldarriaga, C. Montes, J. Garces and C. Crowder** (1988) A molecular sieve with eighteen-membered rings. *Nature*, **331**, 698-699.

59. **Dejoz, M. L.; A. Fornes, F. Rey, M.I. Vazquez and J.M. Lopez Nieto** (2001) V-containing MCM-41 and MCM-48 catalysts for the selective oxidation of propane in gas phase. *Applied Catalysis, A: General* **209,** 155-164.

60. **Dellarocca, V., M.L. Pena, R. Rey, A. Corma, S. Coluccia and L. Marchese** (2001) Ti-MCM-48 with different titanium loading: synthesis, spectroscopic

characterization and catalytic activity. *Studies in Surface Science and Catalysis*, **135,** 4841-4848.

61. **Escalante, D., L. Giraldo, M. Pinto, C. Pfaff, V. Sazo, M. Matjushin, B. Mendez, C.M. Lopez, F.J. Machado, J. Goldwasser and M.M. Ramirez de Agudelo** (1997) A study of the feasibility of incorporation of chromium into the molecular sieve framework: The transformation of 1-butene over Cr-silicoaluminophosphate molecular sieves. *Journal of Catalysis***, 169**, 176-187.
62. **Feng, P., Y. Xia, J. Feng, X. Bu and G. D. Stucky** (1997) Synthesis and characterization of mesostructured aluminophosphaes using the fluoride route. *Chemical Communications*, 949-950.
63. **Firouzi, A., D. Kumar, L.M. Bull, T. Besier, P. Sieger, Q. Huo, S.A. Walker, J.A. Zasadzonki, C. Glinka, J. Nicol, D. Margolese, G. D. Stucky and B.F. Chmelke** (1995) Cooperative organization of inorganic-surfactant and biomimetic assemblies. *Science*, **267**, 1138-1143.
64. **Firouzi, A., S. Tolbert, G.D. Stucky and B.F. Chmelka** (1997) Orientational ordering of silicate-surfactant mesophases. Book of Abstracts, 213th ACS National Meeting, San Francisco, April 13-17 .
65. **Flanigen, E. M.** (2001) Zeolites and molecular sieves: An historical perspective. *Studies in Surface Science and Catalysis* , 137, 11-35.
66. **Flanigen, E.M., B.M. Lok, R.L. Patton and S.T. Wilson** (1986) Incorporation of transition elements into to the framework of $AlPO_4$: in Proceedings of 7^{th} International Zeolite Conference, 103-111.

67. **Frenkel, D., M. Cherniavsky, B. Ittah and M. Levy** (1986) Shape-selective alkylation of naphthalene and methyl naphthalene with methanol over H-ZSM-5 zeolite catalysts , *Journal of Catalysis*, **101**, 273-283.

68. **Galanos, E., K. Kolonia, D. Petrakis, M. Hudson and P. Pomonis** (1998**)** Influence of vanadium and cerium additives in development of porosity and surface acid catalytic properties of mesoporous aluminophosphates. *Studies in Surface Science and Catalysis*, **118,** 911-920.

69. **Gallis, K. W. and C. C. Landry** (1997) Synthesis of MCM-48 by a phase transformation process, *Chemistry of Materials*, **9**, 2035-2038.

70. **Gallis, K. W. and C.C. Landry** (1998) Low temperature phase transformations of M41S materials. *Preprints - American Chemical Society, Division of Petroleum Chemistry*, **43**, 317-319.

71. **Goldfrab, D., M. Bernardo, K.G. Strohmaier, D.E.W. Vaughan and H. Thomann B** (1994) Characterization of iron in zeolites by X-band and Q-band ESR, Pulsed ESR and UV-Visible spectroscopies. *Journal of American Chemical Society*, **116**, 6344-6353.

72. **Gratzel, M.** (1999) Mesoporous oxide junctions and nanostructured solar cells, *Current Opinion in Colloid & Interface Science*, **4**, 314-321.

73. **Goltner, C., H. Colfen and M. Antonietti** (1999) Nanostructuring of solids with amphiphilic polymers. *Chemie in Unserer Zeit* **33,** 200-205.

74. **Haanepen, M. J., A.M. Elemans-Mehring and J.H.C. van Hooff** (1997) VAPO as catalyst for liquid phase oxidation reactions. Part II: stability of VAPO-5 during catalytic operation. Applied Catalysis A: General, 152, 203-220.

75. **Hari, P. R., P. Rao and A.V. Ramaswamy** (1992) Oxyfunctionalization of alkanes with hydrogen peroxide catalyzed by vanadium silicates. *Journal of the Chemical Society, Chemical Communications*, 1245-1246

76. **Hartmann and L. Kevan** (1999) Transition-metal ions in aluminophosphate and silicoaluminophosphate molecular sieves: Location, interaction with adsorbates and catalytic properties.

77. **Hartmann, M and E. Stefan**. (2000) Selective oxidations of linear alkanes with molecular oxygen on molecular sieve catalysts-a breakthrough**?** *Angewandte Chemie, International Edition* **39**, 888-890.

78. **Hassan, M., Zahedi-Niaki, S. M. Javaid Zaidi and S. Kaliaguine** (2000) Comparative study of vanadium aluminophosphate molecular sieves VAPO-5, -11, -17 and -31**,** *Applied Catalysis A: General, **196**, 9-24.*

79. **Holderich, W.F. and H. van Bekkum** (1991) Zeolites in organic synthesis, *Studies in Surface Science and Catalysis*, **58**, 631-726.

80. **Holland, B.T., P.K. Isbester, C. F. Blanford, E. J. Munson and A. Stein** (1997), Synthesis of Ordered Aluminophosphate and Galloaluminophosphate Mesoporous Materials with Anion-Exchange Properties Utilizing Polyoxometalate Cluster/Surfactant Salts as Precursors., *Journal of the American Chemical Society* **119**, 6796-6803.

81. **Holland, B.T., P.K. Isbester, E.J. Munson and A. Stein**. (1999) Transformation of layered polyoxometalate cluster salts into mesoporous materials. *Materials Research Bulletin* **34**, 471-482.

82. **Hudson, M.J. and P. Trens** (2000) Studies on the formation and properties of some highly ordered mesoporous solids. *Studies in Surface Science and Catalysis*,**128,** 505-513.

83. **Huo, Q., D.I. Margolese, U. Ciesla, D.G. Demuth, P. Feng, T.E. Gier, P. Sieger, A. Firougi, B.F. Chmelka, F. Schuth and G.D. Stucky** (1994) Generalized synthesis of periodic surfactant/inorganic composite materials, *Nature*, **368**, 317-320.

84. **Hyde, S.T.** (1996) Bicontinuous structures in lyotropic liquid crystals and crystalline hyperbolic surfaces. *Current Opinion in Solid State & Materials Science*, **1**, 653-662.

85. **Jacobs, P.A. and C.F. Heylen** (1974) Active sites in zeolites III. Selective poisoning of Bronsted sites on synthetic Y zeolites. *Journal of Catalysis*, **34**, 267-274.

86. **Janicke, M. T., C. C. Landry, S.C. Christiansen, S. Birtalan, G. D. Stucky and B. F. Chmelka** (1999) Low Silica MCM-41 Composites and Mesoporous *Solids Chemistry of Materials,* **11,** 1342-1351.

87. **Janicke, M. T., C.C Landry, S.C. Christiansen, D. Kumar, G.D. Stucky and B.F. Chmelka** (1998) Aluminum Incorporation and Interfacial Structures in MCM-41 Mesoporous Molecular Sieves. *Journal of the American Chemical Society*, 120**,** 6940-6951.

88. **Jansen, J. C., D. Kashchiev and A. Erdem-Senatalar** (1994) Preparation of coatings of molecular sieve crystals for catalysis and separation. *Studies in Surface Science and Catalysis.*, ***85***, 215-219.

89. **Jansen, J. C., J.H. Koegler, H. van Bekkum, H.P.A. Calis, C.M. van den Bleek, F. Kapteijn, J.A. Moulijn, E.R. Geus and N. van der Puil** (1998), Zeolitic coatings and their potential use in catalysis. *Microporous Mater, **21***, 213-217.

90. **Jansen, J. C., W. Nugroho and H. van Bekkum,** (1992) Controlled growth of thins films of molecular sieves on various supports. *Proceedings of the 9th International Zeolite Conference*; July 5-10, Montreal, Canada; von Ballmoos, R., Higgins, J.B., Treacy, M. M. J., Eds.; Butterworth-Heinmann: Boston, MA, 1993.

91. **Jhung, S. H., Y. S. Uh and H. Chon** (1990) Synthesis and characterization of the vanadium-incorporated molecular sieve VAPO-5,*Applied Catalysis*, **62,** *61-72.*

92. **Jing, H., Z. Guo, H. Ma, D. G. Evans and X. Duan** (2002) Enhancing the Selectivity of Benzene Hydroxylation by Tailoring the Chemical Affinity of the MCM-41 Catalyst Surface for the Reactive Molecules, *Journal of Catalysis, **212**, 22-32.*

93. **Jing, H., W. Xu, D. G. Evans, X. Duan and C. Li** (2001) Role of pore size and surface properties of Ti-MCM-41 catalysts in the hydroxylation of aromatics in the liquid phase, *Microporous and Mesoporous Materials, **44-45**, 581-586*

94. **Jin- Yu Z., P. Jie-Bin, K.Y. Aiu and Y. Wei** (2001) Synthesis and characterization of mesoporous titania and silica-titania by urea templated sol-gel reactions, Microporous and Mesoporous Materials, **49**,195-195.

95. **Kamalakar, G., M.R.K. Prasad, S.J. Kulkarni, S. Narayanan and K.V. Raghavan** (2000) Vapour phase ethylation of naphthalene with ethanol over molecular sieve catalysts, *Microporous and Mesoporous Materials,* **38**, 135-141.

96. **Kamalakar, G., M.R.K. Prasad, S.J. Kulkarni and K.V. Raghavan** (2002) Vapour phase tert. Butylation of naphthalene over molecular sieves. *Microporous and Mesoporous Materials*, **52**, 151-158

97. **Kapoor, M. P. and A. Raj**. (2000) Synthesis of mesoporous hexagonal titanium aluminophosphate molecular sieves and their catalytic applications. *Applied Catalysis, A: General,* **203**, 311-319.

98. **Katayama, A., M. Toba, G. Tekeuchi, F. Mizukami, S. Niwa and S. Mitamura** (1991) Shape-selective synthesis of 2,6, diisopropyl naphthalene over H-mordenite catalyst. *Journal of Chemical Society, Chemical Communications*, 39-40.

99. **Keiko, A., K.A. Koyano and T. Tatsumi**, (1996) Synthesis of titanium-containing mesoporous molecular sieves with a cubic structure, *Chemical communications*, 145-146.

100. **Khimyak, Y.Z. and J. Klinowski** (2000a) Formation of mesoporous silicates using Triton XN surfactants in the presence of concentrated mineral acids**.** *Journal of Materials Chemistry* **10**, 1847-1855.

101. **Khimyak, Y.Z. and J. Klinowski** (2000b) Synthesis of mesostructured aluminophosphates using cationic templatings**.** *Physical Chemistry Chemical Physics* **2,** 5275-5285.

102. **Khimyak, Y. Z. and J. Klinowski** (2001) Incorporation of magnesium in mesostructured and mesoporous aluminophosphates. *Physical Chemistry Chemical Physics* **3**, 1544-1551.

103. **Khimyak, Y. Z. and J. Klinowski** (2002) Synthesis and characterisation of mesoporous aluminophosphates containing boron. *Journal of Materials Chemistry,* 12, 1079-1085.

104. **Kim, J. M.; S. K. Kim and R. Ryoo** (1998) Synthesis of MCM-48 single crystals. *Chemical Communications*, 259-260.

105. **Kimura, T., Y. Sugahara and K. Kuroda** (1997) synthesis of a hexagonal mesostructured aluminophosphate, *Chemistry Letters*, 983-984.

106. **Kimura, T., Y. Sugahara and K. Kuroda** (1998a) Synthesis of mesoporous aluminophosphates using surfactants with long alkyl chain lengths and triisopropylbenzene s a solubilizing agent. *Chemical Communications*, 559-560.

107. **Kimura, T., Y. Sugahara and K. Kuroda** (1998b) Synthesis of mesoporous aluminophosphates and their adsorption properties. *Microporous and Mesoporous Materials* **22**, 115-126.

108. **Kimura, T., Y. Sugahara and K. Kuroda** (1999a) Synthesis of mesoporous aluminophosphates using surfactants with long alkyl chains. *Proceedings of the International Zeolite Conference*, 12th, Baltimore, July 5-10, 1998 , 771-778.

109. **Kimura, T., Y. Sugahara and K. Kuroda**. (1999b) Synthesis and Characterization of Lamellar and Hexagonal Mesostructured Aluminophosphates Using Alkyltrimethylammonium Cations as Structure-Directing Agents. *Chemistry of Materials* ***11***, 508-518.

110. Kiwi-Minsker, L., I. Yuranov, V. Ho¨ller and A. Renken (1999). Supported glass fiber catalysts for novel multiphase reactor design. *Chemical Engineering Science*, ***54***, 4785-4792.

111. Klinowski, J (2002) .NMR study of porous materials**,** Solid-State NMR Spectroscopy, Blackwell Science Ltd., Oxford, UK, 437-482.

112. Komatsu, T., Y. Araki, S. Namba and T. Yashima (1994) Active formation of 2,6-dimethylnaphthalene from 2-methyl naphthalene on ZSM-5 and metallosilicates with MFI structure. *Studies in Surface Science and Catalysis*, Part C, **84**, 1821-1828.

113. Kosslick, H., G. Lischke, B. Parlitz, W. Storek, W amd R. Fricke (1999) Acidity and active sites of Al-MCM-41. *Applied Catalysis, A: General*, **184**, 49-60.

114. Koyano, K. A. and T. Tatsumi (1996) Synthesis of titanium-containing mesoporous molecular sieves with a cubic structure, *Chemical Communications*, 145-46.

115. Koyano, K. A. and T. Tatsumi, (1997) Synthesis of titanium-containing mesoporous molecular sieves with a cubic structure. *Studies in Surface Science and Catalysis* , **105A**, 93-100.

116. Kresge, C.T., M.E.Leonowicz, W.J. Roth, J.C. Vartuli and J.C. Beck (1992) Ordered mesoporous molecular sieves synthesized by a liquid crystal templating mechanism, *Nature*, **359**, 710-712.

117. **Kron, D.A., B. T. Holland, R. Wipson, C. Maleke and A. Stein** (1999) Anion Exchange Properties of a Mesoporous Aluminophosphate. *Langmuir* **15**, 8300-8308.

118. **Kruk, M., M.Jaroniec, R. Ryoo and S. H. Joo** (2000) Characterization of MCM-48 silicas with tailored pore sizes synthesized via a highly efficient procedure, *Chemistry of materials,* **12**, 1414-1421.

119. **Kumar, P., R. Kumar and B. Pandey** (1995) Oxidative organic transformations catalyzed by titanium- and vanadium-silicate molecular sieves, *Synthetic Letters*, 289-293.

120. **Lee, C. W., W.J. Lee, Y.K. Park and S.E. Park** (2000) Catalytic hydroxylation of benzene over vanadium-containing molecular sieves. *Catalysis Today* **61**, 137-141.

121. **Louis, B., L. Kiwi-Minsker, P. Reuse, and A. Renken** (2000) ZSM-5 Coatings on Stainless Steel Grids in One-Step Benzene Hydroxylation to Phenol by N_2O: Reaction Kinetics Study. *Industrial Engineering and Chemical Research*, **40**, 1454-1458.

122. **Louis, B., P. Reuse, L. Kiwi-Minsker and A. Renken** (2001), Synthesis of ZSM-5 coatings on stainless steel grids and their catalytic activity for partial oxidation of benzene by N_2O. *Applied Cataysi A: General*, ***210***, 103-111.

123. **Luan, Z., D. Zhao and L. Kevan** (1997a) Synthesis of thermally stable mesoporous hexagonal aluminophosphate molecular sieves, *Chemical Communications,* 1009-1010.

124. **Luan, Z., D. Zhao and L. Kevan**. (1998a) Electron spin resonance and optical spectroscopy of tubular aluminophosphate materials containing framework vanadium. *Microporous and Mesoporous Materials,* **20,** 93-99.

125. **Luan, Z., D. Zhao, J. Klinowski, and L. Kevan** (1997b) Electron Spin Resonance and Electron Spin Echo Modulation Spectroscopy of Aluminophosphate-Based Mesoporous Molecular Sieve Containing Framework Manganese, Journal *of Physical Chemistry B,* **101**, 6943-6948.

126. **Luan, Z., D. Zhao, H. He, J. Klinowski, and L. Kevan** (1998b) Characterization of Aluminophosphate-Based Tubular Mesoporous Molecular Sieves. *Journal of Physical Chemistry B,* **102**, 1250-1259.

127. **Luan, Z., D. Zhao, J. Klinowski and L. Kevan** (1998c) Tubular aluminophosphate mesoporous materials containing framework silicon, vanadium and manganese. *Studies in Surface Science and Catalysis,* 117, 103-110.

128. **Luan, Z., W. Zhou, C.F. Cheng, H. Zani and J. Klinowski** (1995) Thermal stability of structural aluminium in the mesoporous molecular sieve MCM-41, Journal of Physical Chemistry, **99**, 10590-10593.

129. **Mahalingam, R. J., S.K. Badamali and P. Selvam** (1999) Oxidation of phenols over mesoporous (Cr)MCM-41 molecular sieves *Chemistry Letters* **(11)**, 1141-1142.

130. **Maschmeyer, T.** (1998) Derivatized mesoporous solids. *Current Opinion in Solid State & Materials Science* **3**, 71-78.

131. **Masson, N. C and H. O. Pastore** (2001) Synthesis and characterization of tubular aluminophosphate mesoporous materials containing framework magnesium**.** *Microporous and Mesoporous Materials,* **44-45**, 173-183.

132. **Mathieu, M., M. Baltes, P. van der Voort and E.F. Vansant** (2000) Incorporated and supported VOx/MCM-48 catalysts: a comparative study, *Proceedings of the Pacific Basin Conference on Adsorption Science and Technology*,Brisbane, Australia, 643-647.

133. **Mathieu, M., E. Van Bavel, P. van Der Voort and E.F. Vansant** (2001a) Pore size engineering of MCM-48: The use of different additives as expanders. *Studies in Surface Science and Catalysis*, **135,** 938-945.

134. **Mathieu, M., P. van Der Voort, B.M. Weckhuysen, R. R. Rao, G. Catana, R.A. Schoonheydt and E.F. Vansant** (2001b) Vanadium-Incorporated MCM-48 Materials: Optimization of the Synthesis Procedure and an in-situ Spectroscopic Study of the Vanadium Species. Journal of Physical Chemistry B, 105, 3393-3399.

135. **Meir, W.M. and D.H. Olson** Atlas of zeolite structure types. Butter worth Heinemann, London, 1992.

136. **Mimoun, A., L. Saussine, E. Daire, M. Postel, J. Fischer and R. Weiss** (1983) Vanadium peroxo complexes. New versatile biomimetic reagents for epoxidation of olefins and hydroxylation of alkanes and aromatic hydrocarbons. *Journal of American Chemical Society*, **105**, 3101-3110.

137. **Mintova, S., V. Valtchev and L. Konstantinov** (1996) Adhesivity of molecular sieve films on metal substrates. *Zeolites*, ***17***, 462-468.

138. **Mohapatra, S. K., S. B . Sahoo; W. Keune and P. Selvam** (2002a) Synthesis, characterization and catalytic properties of trivalent iron substituted hexagonal mesoporous aluminophosphates. *Chemical Communications*, 1466-1467.

139. **Mohapatra, S. K., S. U. Sonavane, R. V. Jayaram and P. Selvam** (2002b) Heterogeneous catalytic transfer hydrogenation of aromatic nitro and carbonyl compounds over cobalt (II) substituted hexagonal mesoporous aluminophosphate molecular sieves. *Tetrahedron Letters* **43**, 8527-8529.

140. **Monnier, A., F. Schuth, Q. Huo, D. Kumar, D. Margolese, R.S. Maxwell, G. D. Stucky, M. Krishnamurty, P. Petroff, A. Firozuli, M. Janicke and B. F. Chmelka (1993)** A Charge Density Mechanistic Model for the Formation of Mesoporous Silicates. *Science*, **261**, 1299-1303.

141. **Montes, A., E. Cosenza, G. Giannetto, E. Urquieta, R.A. De Melo, N.S. Gnep and M. Guisnet** (1998) Thermal decomposition of surfactant occluded in mesoporous MCM-41 type solids. *Studies in Surface Science and Catalysis*, **117**, 237-242.

142. **Moraeau, P., A. Finiels, P. Geneste, F. Moreau and J. Solofro** (1992a) Shape selective synthesis of 2,6 dicyclohexane naphthalene over H-Y zeolites. *Journal of Organic Chemistry*, **57**, 5040-5041.

143. **Moraeau, P., A. Finiels, P. Geneste and J. Solofro** (1992b) Selective isopropylation of naphthalene over zeolites. *Journal of Catalysis*, **136**, 487-492.

144. **Morey, M., A. Davidson and G. D. Stucky** (1996) A new step toward transition metal incorporation in cubic mesoporous materials: preparation and characterization of Ti-MCM-48. *Microporous Materials*, **6**, 99-104.

145. **Morey, M. S., S. O'Brien, S. Schwarz and G. D. Stucky** (2000), Hydrothermal and Postsynthesis Surface Modification of Cubic, MCM-48, and Ultralarge Pore SBA-15 Mesoporous Silica with Titanium. *Chemistry of Materials* , **12**, 898-911.

146. **Moudrakovski, I., A. Sayari, C.I. Ratcliffe, J.A. Ripmester and K.F. Preston** (1994) Vanadium modified zeolite with the structure of ZSM-12; EPR and NMR study, *Journal of physical chemistry*, **96** 10895-10902.

147. **Müller, C.A., M. Schneider, T. Mallat and A. Baiker** (2000) Amine-modified titania–silica hybrid gels as epoxidation catalysts, Applied Catalysis A: General, **201** (2000) 253–261.

148. **Nieto, J and M. Lopez** (2001) Microporous and mesoporous materials with isolated vanadium species as selective catalysts in the gas phase oxidation reactions. *Topics in Catalysis*, **15**, 189-194.

149. **Nishiyama, N., A. Koide, Y. Egashira and U. K. Yasuyuki** (1998) Mesoporous MCM-48 membrane synthesized on a porous stainless steel support *Chemical Communications*, 2147-2148.

150. **Notari, B.** (1991) Titanium Silicate: A New Selective Oxidation Catalyst, *Studies in Surface Science and Catalysis*, **60**, 243-256.

151. **Olah, G.O**. Friedel Crafts and related reactions Part I, Vol. II. Interscience, New York, 1964.

152. **Oye, G., J. Sjoblom and M. Stocker** (2000) Synthesis and characterization of the titanium containing mesoporous molecular sieve MCM-48. *Journal of Dispersion Science and Technology*, **2,** 229-243.

153. **Park, J.W and H. Chon** (1992) Isomorphous substitution of iron ions into aluminophosphate molecular sieve, $AlPO_4$-5. *Journal of Catalysis*, **133**, 159-169.

154. **Patarin, J., B. Lebeau and R. Zana** (2002) Recent advances in the formation mechanisms of organized mesoporous materials. *Current Opinion in Colloid & Interface Science* **7**, 107-115.

155. **Pena, M. L., V. Dellarocca, F. Rey, A. Corma, S. Coluccia and L. Marchese** (2001) Elucidating the local environment of Ti(IV) active sites in Ti-MCM-48: a comparison between silylated and calcined catalysts. *Microporous and Mesoporous Materials* , **44-45**, 345-356.

156. **Perego,G., G.Bellussi, C. Corno, M. Taramasso and F. Buonomo** (1986) Titanium-silicate: a novel derivative in the pentasil family, *Studies in Surface Science and Catalysis*, **2**8, 129-136.

157. **Perez, J.O., R.B. Borade and A. Clearfield** (1998) Synthesis of a mesoporous aluminophosphate. *Journal of Molecular Structure,* **470**, 221-228.

158. **Petrakis, D. E., M.J. Hudson, P. J. Pomonis, A. T. Sdoukos and T. V. Bakas** (1995) Synthesis and properties of some mesoporous aluminophosphates with acidic surface sites, *Journal of Materials Chemistry* **5**, 1975-83.

159. **Petrakis, D. E., I. Pasxalidis, C. R. Theocharis, M.J. Hudson, and P. J. Pomonis** (1997) Scaling dimensions of nitrogen adsorption characteristics in modulated mesoporous aluminophosphates**,** *Journal of Colloid and Interface Science,* **185**, 104-110.

160. **Putnam, R.L., N. Nakagawa, K.M. McGrath, N. Yao, A. Aksay, S.M. Gruner and A. Navrotsky** (1997) Titanium Dioxide-Surfactant Mesophases and Ti-TMS1**,** *Chemistry of Materials*, **9**, 2690-2693.

161. **Raja, R. and J.M. Thomas** (2000) Catalyst design strategies for controlling reactions in microporous and mesoporous molecular-sieves. *Journal of Molecular Catalysis A: Chemical*, **181**, 3-14.

162. **Rajesh, B., M. Palanichamy, V. Kazansky and V. Murugesan** (2001) Mesoporous aluminophosphate and silicoaluminophosphate molecular sieves: room temperature synthesis, characterization and catalytic performance. *Indian Journal of Chemistry, Section A:* **40A**, 1262-1268.

163. **Rana, R.K.** (1999) Ph.D thesis, IIT Madras.

164. **Rao, C. N. R** (1999) Porous materials: a case study of supramolecular organization in materials design. *Bulletin of Materials Science*, **22**, 141-151.

165. **Rao, P. R.P. H., A.V. Ramaswamy and P. Ratnasamy** (1992) Synthesis and catalytic properties of crystalline, microporous vanadium silicates with MEL structure. Journal of Catalysis, **137**, 225-231.

166. **Reddy, J.S., P. Liu and A. Sayari** (1996) Vanadium containing crystalline mesoporous molecular sieves Leaching of vanadium in liquid phase reactions. *Applied Catalysis: A General*, **148**, 7-21.

167. **Rigutto, M.S. and H. van Bekkum** (1993a) Synthesis and characterization of a thermally stable vanadium-containing silicalite**,** *Applied Catalysis***, 68,** *L1-L7.*

168. **Rigutto, M. S. and H. van Bekkum (**1993b) Vanadium site in VAPO-5: Characterization and catalytic properties in liquid-phase alkene epoxidation and benzylic oxidation**,** *Journal of molecular catalysis,* **81**, *77-98.*

169. **Ryoo, R., S.H. Joo, S. Jun, T. subakiyama and T. Terasaki**, (2001) Ordered mesoporous carbon molecular sieves by templated synthesis: the structural varieties. *Studies in Surface Science and Catalysis,* **135**, 1121-1128.

170. **Saji P. V., R. Chandra and P. Ratnasamy** (1998) Zeolite-encapsulated manganese(III) salen complexes; *Journal of Molecular Catalysis A: Chemical* **135** 295–306.

171. **Sakthivel, A., S.K. Badamali and P. Selvam** (2002b) Catalytic Oxidation of Alkylaromatics over Mesoporous (Cr)MCM-41. *Catalysis Letters,* **80**, 73-76.

172. **Sakthivel, A., S.E. Dapurkar and P. Selvam** (2001a) Mesoporous V-MCM-41: Zeo-type heterogeneous catalysts for liquid phase oxidation of cyclohexane, Advances in Environmental Materials, Vol. I, Pollution control materials (Editors T. White and D. Sun) , Materials Research Society, Singapore.

173. **Sakthivel, A., S.E. Dapurkar and P. Selvam** (2001b) Mesoporous (Cr)MCM-41 and (Cr)MCM-48 molecular sieves: promising heterogeneous catalysts for liquid phase oxidation reactions. *Catalysis Letters,* **77,** 155-158.

174. **Sakthivel, A. and P. Selvam** (2002a) Mesoporous (Cr)MCM-41: A Mild and Efficient Heterogeneous Catalyst for Selective Oxidation of Cyclohexane, *Journal of Catalysis* **211**, 134-143.

175. **Sayari, A.** (1996) Catalysis by Crystalline Mesoporous Molecular Sieves**,** *Chemistry of Materials,* **8,** 1840-1852.

176. **Schumacher, K., C. Du Fresne von Hohenesche, K.K. Unger, R. Ulrich, A. Du Chesne, U. Wiesner and H.W. Spiess** (1999) The synthesis of spherical mesoporous molecular sieves MCM-48 with heteroatoms incorporated into the silica framework. *Advanced Materials*, **11**, 1194-1198.

177. **Schuth, F.** (2001) Non-siliceous mesostructured and mesoporous materials, Chemitry of Materials, **13**, 3184-3195.

178. **Selvam, P., S. E. Dapurkar, S. K. Badamali, M. Murugasan and H. Kuwano** (2001) Coexistence of paramagnetic and superparamagnetic Fe(III) in mesoporous MCM-41silicates, *Catalysis Today*, **68**, *69-74.*

179. **Sen, T., M. Chatterjee and S. Sivasankar** (1995) Novel large-pore vanadium alumino-and boo silicates with BET structure, *Journal of Chemical Society Chemical Communications*, 207-208

180. **Sen, T., P.R. Rajamohan, S. Ganapathy and S. Sivasankar** (1996) The nature of vanadium in vanado-silicate (MFI) molecular sieves: influence of synthetic methods. *Journal of Catalysis*, **163**, 354-364.

181. **Shan, Z., W. E. J. van Kooten, O.L. Oudshoorn, J.C. Jansen, H. van Bekkum, C.M. van den Bleek and H.P.A. Calis** (2000) Optimization of the preparation of binderless ZSM-5 coatings on stainless steel monoliths by in-situ hydrothermal synthesis. *Microporous Materials*, ***34***, 81-88.

182. **Sheldon, R.A.** (1996) Selective catalytic synthesis of fine chemicals: opportunities and trends. *Journal of Molecular Catalysis A: Chemical*, **107**, 75-83.

183. **Sheldon, R.*A*., I.W.C.E. Arends and H.E.B. Lempers** (1998) Liquid phase oxidation at metal ions and complexes in constrained environments. *Catalysis Today*, **41,** 387-409.

184. **Singh, A.P. and T. Selvam** (1996) Liquid phase oxidation reactions over chromium silicalite-1 (CrS-1) molecular sieve. Journal of Molecular Catalysis A: Chemical, **131**, 489-497.

185. **Sivasankar, S** (1998) Where is the metal in metallosilicate molecular sieves? An examination of some vanadosilicates, *Studies in Surface Science and Catalysis*, **113,** 27-38.

186. **Song, M. K., Y. H. Yeom, S. J. Kim and Y. S. Uh** (1993) Vanadium oxide loading on aluminophosphate molecular sieve by vapor adsorption**,** *Applied Catalysis A: General, **102,**93-103.*

187. **Srinivas, N., V. Radha Rani, S.J. Kulkarni and K.V. Raghavan** (2002) Liquid phase oxidation of anthracene and trans-stilbene over modified mesoporous (MCM-41) molecular sieves, *Journal of Molecular Catalysis A: Chemical* **179**, 221-231.

188. **Steel, A., S.W. Carr and M.W. Anderson** (1994) ^{14}N NMR study of surfactant mesoporous in the synthesis of mesoporous silicates, *Journal of Chemical Society Chemical Communications*, 1571-1572.

189. **Stein, A. and B. Holland,** (1997) Cluster-based synthesis of mesoporous metallophosphates with anion-exchange properties., Book of Abstracts, 214th ACS National Meeting, Las Vegas, NV, September 7-11.

190. **Stockenhuber, M., M.J. Hudson and R.W.Joyner** (2000) Preparation, Characterization, and Unusual Reactivity of Fe-MCM-41. *Journal of Physical Chemistry B,* **104,** 3370-3374.

191. **Stockenhuber, M., R. W. Joyner, J. M. Dixon, M. J. Hudson and G. Grubert** (2001) Transition metal containing mesoporous silicas – redox properties, structure and catalytic activity, *Microporous and Mesoporous Materials,* **44-45**,367-375.

192. **Stone, V.F. and R. J. Davis** (1998) Synthesis, Characterization, and Photocatalytic Activity of Titania and Niobia Mesoporous Molecular Sieves, Chemistry of Materials, **10**, 1468-1474.

193. **Storck, S., H. Bretinger and W.F. Maier** (1988) Characterization of micro- and mesoporous solids by physisorption method. *Applied Catalysis, A: General*, **174**, 137-146.

194. **Suib, S.L. and J. Luo** (1997), Synthesis and characterization of mesostructured manganese oxide, *Chemical Communications,*1031-1132.

195. **Suji, Y. and M. Toba** (1994) Shape selective alkylation of polynuclear aromatics. *Catalysis Today*, **19**, 187-211.

196. **Sung H.J., Y.S.Uh and H.Chon** (1990) Synthesis and characterization of the vanadium-incorporated molecular sieve VAPO-5**,** *Applied Catalysis, **62**,61-72.*

197. **Szegedi, A., G. Pal-Borbely and K. Lazar** (2001) Comparison of the redox properties of iron incorporated in different amounts into MCM-41. *Reaction Kinetics and Catalysis Letters,* **74,** 277-287.

198. **Szostak, R.M**. Molecular sieves: Principles of synthesis and identification. Van Nostrand Reinhold, New York, 1989.

199. **Tanev, P.T., M. Chibwe amd T.J. Pinnavaia** (1994) Titanium containing mesoporous molecular sieves for catalytic oxidation of aromatic compounds. *Nature*, **368,** 321-323.

200. **Tanev, P.T. and T.J. Pinnavaia** (1995) A neutral templating route to mesoporous molecular sieves, *Science*, **267**, 865-867.

201. **Tatsumi, T.** (2000) Importance of hydrophobicity in the liquid phase oxidation catalyzed by titanosilicates. *Research on Chemical Intermediates*, **26**, 7-12.

202. **Tatsumi, T., K. A. Koyano, A. and N. Igarashi** (1998) Remarkable activity enhancement by trimethylsilylation in oxidation of alkenes and alkanes with H_2O_2 catalyzed by titanium-containing mesoporous molecular sieves. *Chemical Communications* , 325-326.

203. **Thomas, J.M** (1999) Design, synthesis, and in situ characterization of new solid catalysts. *Angewandte Chemie, International Edition* **38(24)**, 3589-3628.

204. **Thomas, J. M., O. Terasaki, P. L. Gai, W. Zhou and J. Gonzalez-Calbet** (2001) Structural Elucidation of Microporous and Mesoporous Catalysts and Molecular Sieves by High-Resolution Electron Microscopy.. *Accounts of Chemical Research* **34**, 583-594.

205. **Tiemann, M. and M. Froba** (2001a), Mesostructured aluminophosphates synthesized with supra molecular structure directors**,** *Chemistry of materials*, **13**, 3211-3217.

206. Tiemann M. and M. Froba (2002) Mesoporous aluminophosphates from a single-source precursor, *Chemical Communications,* 406-407.

207. Tiemann, M., M. Froba, G. Rapp and S. S. **Funari,** (2000) In-situ small angle X-ray scattering (SAXS) studies on the formation of mesostructured aluminophosphate/surfactant composite materials. *Studies in Surface Science and Catalysis,* **129** , 559-566.

208. Tiemann, M., S. Marcus, J. Christian and M. Froba (2001) Mesoporous Aluminophosphate Molecular Sieves Synthesized under Nonaqueous Conditions. *Chemistry of Materials,* 13, 2885-2891.

209. Ulagappan, N. and C.N.R. Rao (1996a) Synthesis and characterization of the mesoporous chromium silicates, Cr-MCM-41. *Chemical Communications*, 1047-1048.

210. Ulagappan, N. and C.N.R. Rao (1996b) Mesoporous phases based on SnO_2 and TiO_2. *Chemical Communications*, 1685-1686.

211. Umamaheswari, V., M. Palanichami and V. Murugesan (2002) Isopropylation of *m*-Cresol over Mesoporous Al–MCM-41 Molecular Sieves. Journal of Catalysis, **210**, 376-374.

212. Uphade, B. S., T. Akita, T. Nakamura and M. Haruta (2002) Vapor-Phase Epoxidation of Propene Using H_2 and O_2 over Au/Ti-MCM-48. *Journal of Catalysis* , **209,** 331-340.

213. Valtchev, V. and A. Mintova (1995) The effect of the metal substrate composition on the crystallization of zeolite coatings. *Zeolites*, ***15***, 171-177.

214. van Bekkum, H., E.R. Geus and H.W. Kouwenhoven (1994), Supported zeolite systems and applications. *Studied in Surface Science and Catalysis,* ***85***, 509-92.

215. Walker, J.V., M. Morey, H. Carlsson, A. Davidson, G.D. Stucky and A. Butler (1997) Peroxidative Halogenation Catalyzed by Transition-Metal-Ion-Grafted Mesoporous Silicate Materials. *Journal of the American Chemical Society*, **119**, 6921-6922.

216. Wang, Y., Q. Zhang, Q. Guo, T. Chen, H. Wan, Y. Ohishi, T. Shishido and K. Takehira (2002a) UV Raman spectroscopy for characterization of chromium species on Cr-MCM-41**.** *Chemistry Letters*, 1152-1153.

217. Wang, Y., Q. Zhang, T. Shishido and K. Takehira (2002b) Characterizations of Iron-Containing MCM-41 and Its Catalytic Properties in Epoxidation of Styrene with Hydrogen Peroxide. *Journal of Catalysis,* **209,** 186-196.

218. Ward, J.W. (1970) The nature of active sites in zeoliets I. The decationated Y zeolite. *Journal of Catalysis*, **9**, 225-236.

219. Wark. M., A. Brückner, T. Liese and W. Grünert (1998) Selective Catalytic Reduction of NO by NH_3over Vanadium-Containing Zeolites**,** *Journal of Catalysis, **175,** 48-61.*

220. Weckhuysen, B.M., I. E. Wachs and R.A. Schoonheydt (1996) Surface chemistry and spectroscopy of chromium in inorganic oxides. *Chemical Reviews*, **96**, 3327-3349.

221. Wilson, S.T. (1991) Synthesis of $AlPO_4$ based molecular sieves, *Studies in Surface Science and Catalysis*, **58**, 137-151.

222. **Wilson, S.T., B.M. Lok, C.A Messina, T.R. Cannan and E.M. Flanigen** (1982) Aluminophosphate molecular sieves: A new class of microporous crystalline inorganic solids. *Journal of American Chemical Society*, **104,** 1146-1147.

223. **West, A. R.** Basic solids state chemistry, Wiley: Chichester, 1988.

224. **Xu, J. and L. Kevan** (2001) Electron spin resonance and electron spin echo modulation studies of Fe-containing mesoporous MCM-48 molecular sieves. *Applied Magnetic Resonance*, **20,** 3-15.

225. **Xu, J., Z. Luan, M. Hartmann and L. Kevan** (1999) Synthesis and Characterization of Mn-Containing Cubic Mesoporous MCM-48 and AlMCM-48 Molecular Sieves. *Chemistry of Materials,* **11,** 2928-2936.

226. **Xu, J., Z. Luan, T. Wasowicz and L. Kevan** (1998), ESR and ESEM studies of Mn-containing MCM-41 materials , *Microporous and Mesoporous Materials*, **22,** 179-191.

227. **Yan, Y. and T. Bein** (1995) Zeolite thin films with tunable molecular sieve function. *Journal of American Chemical Society*, ***117***, 9990.

228. **Yang, P., D. Zhao, D.I. Margolose, B. F. Chmelka and G. D. Stucky** (1998) Generalized syntheses of large-pore mesoporous metal oxides with semicrystalline frameworks, *Nature*, **396**, 152-155.

229. **Ye, W., Q. Zhang, Q. Guo, T. Chen, H. Wan, Y. Ohishi, T. Shishido and K. Takehira** (2002) UV Raman spectroscopy for characterization of chromium species on Cr-MCM-41**.** *Chemistry Letters*, 1152-1153.

230. Ying, J.Y., C. P. Mehnert and S. Wong (1999) Synthesis and applications of supramolecular-templated mesoporous materials. *Angewandte Chemie International Edition in English,* **38**, 56-77

231. Yuan, Z. Y., T. Chen, Z. Jing Li and X. He (2001) Synthesis and characterization of silicon and cobalt substituted mesoporous aluminophosphates. *Colloids and Surfaces, A:* **179,** 253-259.

232. Zhang W. and T.J. Pinnavaia (1996) Transition metal substituted derivatives of cubic MCM-48 mesoporous molecular sieves*; catalysis Letters***, 38,** 261-265**.**

233. Zhang, Q., Y. Wang, S. Itsuki, T. Shishido and K. Takehira (2002) Manganese-containing MCM-41 for epoxidation of styrene and stilbene. *Journal of Molecular Catalysis A: Chemical,* **188,** 189-200.

234. Zhang, Q., Y. Wang, S.Itsuki, T. Shishido and K. Takehira (2001) Fe-MCM-41 for selective epoxidation of styrene with hydrogen peroxide *Chemistry Letters*, 946-947.

235. Zhang, W., J. Wang and T.J. Pinnavaia (1996) Catalytic hydroxylation of benzene over transition metal substituted hexagonal mesoporous silicas, *Journal of Chemical Society Chemical Communications*, 979-980.

236. Zhao, D and D. Goldfarb (1995) Synthesis of mesoporous manganosilicates: Mn-MCM-41, Mn-MCM-48 and Mn-MCM-L. Journal *of the Chemical Society, Chemical Communications* , 875-876.

237. Zhao, D., Z. Laun and L. Kevan (1997) Synthesis of thermally stable mesoporous hexagonal aluminophosphate molecular sieves, *Chemical Communications*, 1009-1010.

238. Zhao, W., Y. Luo, P. Deng and Q. Li. (2001) Synthesis of Fe-MCM-48 and its catalytic performance in phenol hydroxylation. *Catalysis Letters,* **73,** 199-202.

239. Zhao, X. S and G. Q. Lu (2001) Aluminophosphate-based mesoporous molecular sieves: synthesis and characterization of TAPOs. *Microporous and Mesoporous Materials*, **44-45**, 185-194